UNIVERSITÀ DEGLI STUDI FIRENZE

DOTTORATO DI RICERCA IN SCIENZE CHIMICHE

CICLO XXVIII

COORDINATORE Prof. ANDREA GOTI

FROM CONVENTIONAL TO NOVEL Pt-BASED ANTINEOPLASTIC AGENTS:MECHANISTIC ASPECTS AND BIOLOGICAL EFFECTS

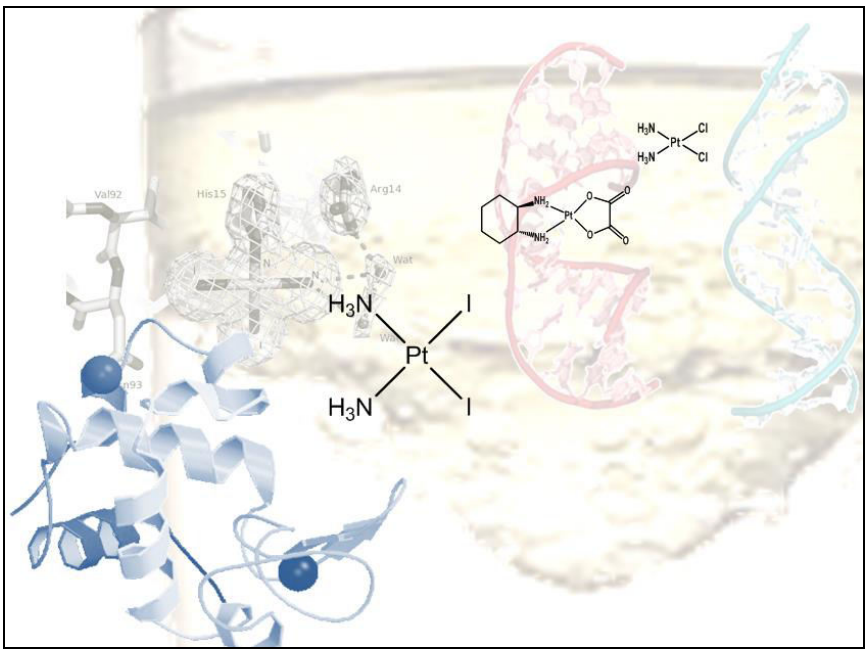

Dottorando
Dott. Tiziano Marzo

Tutore
Prof. Luigi Messori

UNIVERSITÀ
DEGLI STUDI
FIRENZE

DOTTORATO DI RICERCA IN SCIENZE CHIMICHE

CICLO XXVIII

COORDINATORE Prof. ANDREA GOTI

FROM CONVENTIONAL TO NOVEL Pt-BASED ANTINEOPLASTIC AGENTS: MECHANISTIC ASPECTS AND BIOLOGICAL EFFECTS

Settore Scientifico Disciplinare CHIM/03

Dottorando
Dott. Tiziano Marzo

Tutore
Prof. Luigi Messori

Coordinatore
Prof. Andrea Goti

Anni 2012/2015

A mio Padre, mia Sorella e Mara.

A mia Madre, sempre accanto a me.

CONTENTS

1

INTRODUCTION

1. INTRODUCTION

Metal ions are essential for many metabolic pathways; their homeostasis is crucial for life and, remarkable, are involved in many important processes including respiration, nitrogen and carbon cycling, gene regulation, replication and repair of DNA, antioxidant defense, neurotransmission.[1] Scarce bioavailability of some metal ions may determine diseases. Well known examples include pernicious anemia resulting from iron deficiency, growth retardation arising from insufficient dietary zinc, and heart disease in infants owing to copper deficiency. Metal ions can also induce toxicity in humans, classic examples being heavy-metal poisons such as mercury and lead. Even essential metal ions can be toxic when present in excess; iron is a common household poison worldwide as a result of accidental ingestion, usually by children, of the dietary supplement ferrous sulfate. Despite their important biological role is today commonly known, conversely, it is less known the role and the potential that metal ions have in medicine.[2]

The medicinal properties of metals have been known and used since very ancient times. Silver's association with anti-bacterial properties has long been established. Phoenicians knew enough to keep water, wine and vinegar in silver vessels to ensure freshness. The ancient Egyptians also knew how to sterilize water with copper.

The field of inorganic chemistry in medicine may usefully be divided into two main categories: firstly, ligands as drugs which target metal ions in some form, whether free or protein-bound; and secondly, metal-based drugs and imaging agents where the central metal ion is usually the key feature of the mechanism of action.[3] Our attention will be focused on this latter category. Research of new efficient metal-based drugs, has attracted growing attention in the last decades for their potential applications in different fields of medicine and, the efforts carried out, have produced a series of metal-based drugs in widespread use, being today an important arsenal in therapy and diagnosis of many diseases. Significant examples of metal-based drugs currently in clinic are Auranofin (Ridaura™), introduced since 1985 for the treatment of progressive rheumatoid arthritis resistant to conventional therapy,[4] silver sulfadiazine (Flamazine™) used for prophylaxis and treatment of infection in burn wounds, arsenic trioxide (Trisenox™), effective against acute promyelocytic leukemia.[3,5] A more detailed list of some inorganic compounds used for medical purposes is shown as table 1.

Element	Compound	Uses	Trade names
Li	Li_2CO_3	Manic depression	*Camcolit, Lithane*
Fe	$[Fe(NO)(CN)_5]^{2-}$	Vasodilation	*Nipride*
Ga	$Ga(NO_3)_3$	Hypercalcemia	*Ganite*
As	As_2O_3	Anticancer agent	*Trisenox*
Ag	$AgNO_3$ Ag (sulfadiazine)	Disinfectant Antibacterial	*Flamazine, Silvadene*
Sb	Sb^{3+} (tartrate)	Antiparasitic, leishmaniasis	*Stibophen*
Pt	Cis-$[Pt(amine)_2X_2]$	Anticancer agents	*Platinol, Paraplatin, Eloxatine*
Au	$Au(Pet_3)$(acetyl-thioglucose)	Rheumatoid arthritis	*Ridaura*
Bi	Bi(sugar)polymers	Antiulcer, antacid	*Pepto-Bismol, Ranitidine Bismutrex, De-Nol*
Hg	Hg-organic compounds	Antibacterial	*Thiomersal, mercurochrome*

Table1 Medical uses of inorganic compounds (Table from ref. 3)

In addition, gadolinium-based contrast agents are successfully used today to improve the quality of MRI and X ray images, so that it is possible to succeed in early stage diagnosis for different diseases; also, many patients, receive injections of a ^{99m}Tc compounds for radiodiagnostic purposes.[2]

Figure 1 Barnett Rosenberg and Loretta Van Camp April 24, 1969.

In any case, and despite the important role of these complexes in the modern medicine, the best known example of a small molecule metal-containing drug, is cisplatin (*cis*-$PtCl_2(NH_3)_2$, also known as *cis*-DDP). Cisplatin, originally known as Peyrone's chloride, was first prepared in its presently used form by Italian chemist Michele Peyrone in 1844.[6] It later played a central role in the Nobel prize-winning work of swiss chemist Alfred Werner (1866-1919) on isomerism in inorganic complexes. The cytostatic activity of cisplatin was first reported by Barnett Rosenberg (1926-2009) and co-workers in 1965,[7,8] and it progressed rapidly into the clinic until its approval by FDA in 1978 for the treatment of ovarian and testicular cancer.[9] To date cisplatin (with its second generation analogues carboplatin and oxaliplatin) is used in almost 50% of clinical protocols for cancer treatment.[10]

Despite its great curative success in testicular cancer, cisplatin is not universally effective against cancer and induces a number of important side effects. In fact, not all cancers are responsive to cisplatin therapy (intrinsic resistance), some other instead, become resistant to cisplatin during the treatment, especially if prolonged (acquired resistance).

To overcome these problems, new platinum complexes have been pursued and investigated for their antitumor properties. Although well over a thousand complexes have been prepared and tested thus far, only two other platinum drugs are approved for clinical use worldwide (i.e. carboplatin and oxaliplatin), and few additional compounds are approved for regional use in Asia. These complexes, operate with a mechanism of action similar to that of cisplatin, which involves DNA binding and transcription inhibition.[11] Hence, there is the urgent need to develop new antineoplastic agents able to circumvent these drawbacks and active toward those forms of cancer resistant to conventional platinum-based drugs. This doctoral thesis, hopefully, will contribute to the research in the field of platinum antineoplastic agents, to reach the goal of new and more effective treatments. To this end, interaction of cisplatin, carboplatin and oxaliplatin with model proteins will be tested and mechanistic considerations will be made. Starting from the observation made for these drugs, new likely drug candidates will be studied comparatively, their antiproliferative effect determined and possible further development discussed.

1.1 Cisplatin and its analogues, Pt-drugs used in clinical protocols and new candidates

Cisplatin (Figure 2, structure **(1)**) is a highly effective chemotherapeutic drug. Since its approval in 1978, its application has expanded to several types of cancer, administered either alone or in combination with other drugs/treatments. Currently, cisplatin is approved for the treatment of several cancers such as ovarian, testicular, cervical, non-small cell lung, head and neck, bladder and malignant mesothelioma.[12-15] Although this success there are, as already mentioned, severe limitations to its use and effectiveness. Some cancer is resistant to cisplatin and in other cases resistance arise during treatment and there are dose-limiting side effects such as nephrotoxicity, neurotoxicity, emetogenesis, ototoxicity and bone marrow suppression during and after therapy. These aspects led to development of "second-generation" platinum-based drugs (Figure 2).

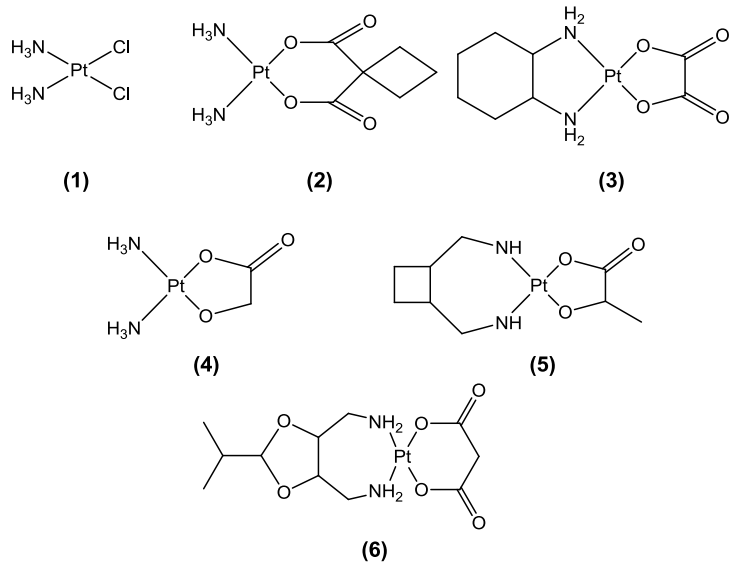

Figure 2 Structures of platinum anticancer drugs in clinical use.

Carboplatin ([Pt(cbdca-*O*,*O*')$(NH_3)_2$]; where cbdca is cyclobutane-1,1-dicarboxylate and O and O' are the ligand donor atoms) (Figure 2, structure **(2)**), was reported by Cleare and Hoeschele in 1973[16,17] and entered the clinic in 1998 (Paraplatin™) principally in response to the necessity to reduce the toxic side effects of the parent drug. Despite its lower toxicity (especially oto and neprotoxicity), carboplatin is essentially active in the same set of tumors as cisplatin and a broader spectrum of

activity is not indicated.[18] In addition, for some tumors, cisplatin appears to be therapeutically more effective than carboplatin (germ cell tumors, head and neck, and bladder) whereas for lung cancer and ovarian cancer effectiveness is comparable.[3]

Since the advent of cisplatin in the clinic, the three main goals for drug development have been improvement of toxicity profile, circumvention of resistance, and expansion of the cancer cells sensitive to treatment by cisplatin. The importance of circumventing resistance was recognized very early on and reports of the activity of complexes containing 1,2-diaminocyclohexane (dach) in murine L1210 resistant to cisplatin date back to 1978.[3,19] Oxaliplatin ([Pt(ox-*O*,*O*') ((1*R*,2*R*)-dach-*N*,*N*')]), where ox is oxalate and dach is 1,2-diaminocyclohexane (Figure 2, structure **(3)**), is a platinum anticancer drug which gained approval for clinical use in the European Union in 1999 and in the United States in 2002.[20-22]

Oxaliplatin is especially effective against colorectal cancer (CRC), where it is widely used in the adjuvant chemotherapy that mainly relies on fluoropyrimidine compounds combined with oxaliplatin. Indeed, either the FOLFOX (5-FU, leucovorin, and oxaliplatin) or CapeOx (capecitabine and oxaliplatin) regimens are used most often. Remarkably oxaliplatin is much less nephro- and ototoxic than cisplatin and can be used to treat cisplatin-resistant tumors, also, it is less myelosuppresive than carboplatin. An important limitation of oxaliplatin is that the drug induces peripheral neuropathy (nerve damage), the result is sensation to cold which for acute (brief) exposure, occurs quickly after administration and is reversible.[23] Since Ca^{2+} ions are important in the neuronal signaling system, this form of neuropathy may be caused by the complexation of the oxalate ligand released from the drug, with Ca^{+2}. In chronic (continual) exposure to oxaliplatin, the drug-induced neuropathy is not totally reversible. This form of nerve damage is thought to be related to accumulation of the drug in the cells located in the dorsal root ganglion of the spinal system and the subsequent decrease in cellular metabolism.[20]

Cisplatin, carboplatin and oxaliplatin are the only three Pt-drugs approved worldwide.

Other cisplatin analogues have gained regional approval, some are to date, in clinical trials in different countries.

Among these, Nedaplatin (cis-diammineglycolatoplatinum(II)) (Figure 2, structure **(4)**) is currently used in Japan to treat ovarian and cervix carcinomas, head and neck tumors, esophageal and bladder cancer.[24] Nedaplatin is in some ways similar to carboplatin in that it does not appear to use organic cation transporters for entering the cell and it is

myelosuppresive, which limits the dose that can be administered to the patient.[25,26]

Lobaplatin (D-19466; 1,2-diammino-methyl-cyclobutaneplatinum(II)-lactate) (Figure 2, structure **(5)**) has been approved in China for treatment of different cancers (e.g. the treatment of SCLC, chronic myelogenous leukaemia, and inoperable metastatic breast cancer).[20,27] Even lobaplatin exhibits few of the side effects of cisplatin.

At variance, heptaplatin (Figure 2, structure **(6)**) has been approved in South Korea and often used in protocols for gastric cancer treatment and, in combination with paclitaxel, against head and neck squamous cancers.[20] Also this compound presents important side effects such as mild hepatotoxicity and myelosuppression while its nephrotoxicity is dose-limiting. Overall, the choice of the most appropriate analogue is a function of the cancer being treated, treatment intention (palliative or curative), and other component drugs used in combination.[3] Beyond these complexes, that have received global or local approval for their use in clinic, other platinum complexes have been or still are in clinical trials. Among these, an interesting complex is satraplatin (Figure 3, structure **(1)**), a Pt(IV) entered in clinical trials in the United States for treatment of lung non-small cells cancer, resistant prostate cancer and other malignancies, with the very favourable feature of oral administration. To date was not approved due to its performances, very similar to those of established drugs.[27]

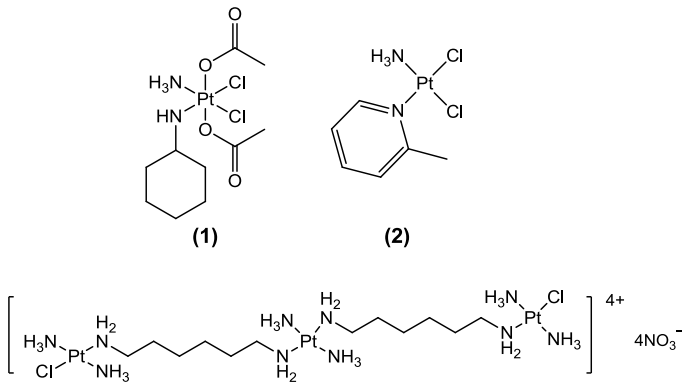

Figure 3 Structures of platinum anticancer drugs in clinical trials.

Picoplatin (Figure 3, structure **(2)**) reached clinical phase III. This drug is active against cisplatin-resistant cell lines and cell lines that have enhanced mechanisms for removing platinum from the cell, complexing platinum to cellular thiols or removing platinum from DNA.[28] Picoplatin appears to have good bioavailability when given orally, and this represents an interesting feature. The side effects of picoplatin include nausea, vomiting, anorexia and a transient metallic taste, but there is no or very little nephro- or neurotoxicity with the agent.[20,29]
BBR3464 (Figure 3, structure **(3)**) is a trinuclear complex developed by Farrell and coworkers, that reached clinical phase II. In clinical trials in the United States, BBR3464 is showing activity against melanoma, and against metastatic pancreatic and lung cancers. The dose-limiting toxicities with BBR3464 are determine by bone depression, and diarrhea.[20]

1.2 Chemistry and biology of conventional Pt-based antineoplastic agents: how these drugs work?

Almost 40 years after its approval, studies on cisplatin and analogues, still continue in an effort to understand exactly how these drugs work.[30]
It is commonly accepted that the primary target of cisplatin is DNA. After intravenous administration cisplatin enters in the bloodstream and once reached the cells is internalised. Cellular environment allows cisplatin activation due to the low concentration of Cl^- ions (~ 4 mM against ~ 103 mM of blood plasma).[31] The resulting platinum(II) aqua complexes are potent electrophiles that readily react with a number of biological ligands with loss of the bound water molecules. The purine bases of nucleic acids are strongly nucleophilic at the N7 position. Thus, cisplatin binds readily to DNA, forming primarily bifunctional adducts with loss of both chloride ligands.[11]
Overall the mechanism of cisplatin action (as well as for other clinical Pt-based drugs) is a multi-step process that includes: (i) cisplatin accumulation, (ii) activation and (iii) cellular processing.[32]

1.2.1 Accumulation

The mechanism by which cisplatin and its analogues enter cells is still under debate.[32,33] To date is not completely recognised whether cisplatin enters cells in an active or passive way, both mechanisms are most probably involved in platinum uptake process and play an important role

in the cell resistance mechanisms.[34,35] It is likely that cisplatin reaches cells in its neutral form considering high chloride concentration in the extracellular environment. More recently, it was discovered that cisplatin might find its way into cells via active transport mediated by the plasma-membrane copper transporter Ctr1p present in yeast and mammals.[36] Details about this active transport remain to be elucidated. Recent studies with Ctr1p-/- mouse embryonic fibroblasts exposed to 2 µM cisplatin or carboplatin revealed only 35% of platinum accumulation compared to that taken up by Ctr1p wild type cells, which supports such an active transport mechanism. Most likely there are multiple pathways by which the drug is internalized.[32] Details for these process are summarised in figure 4.

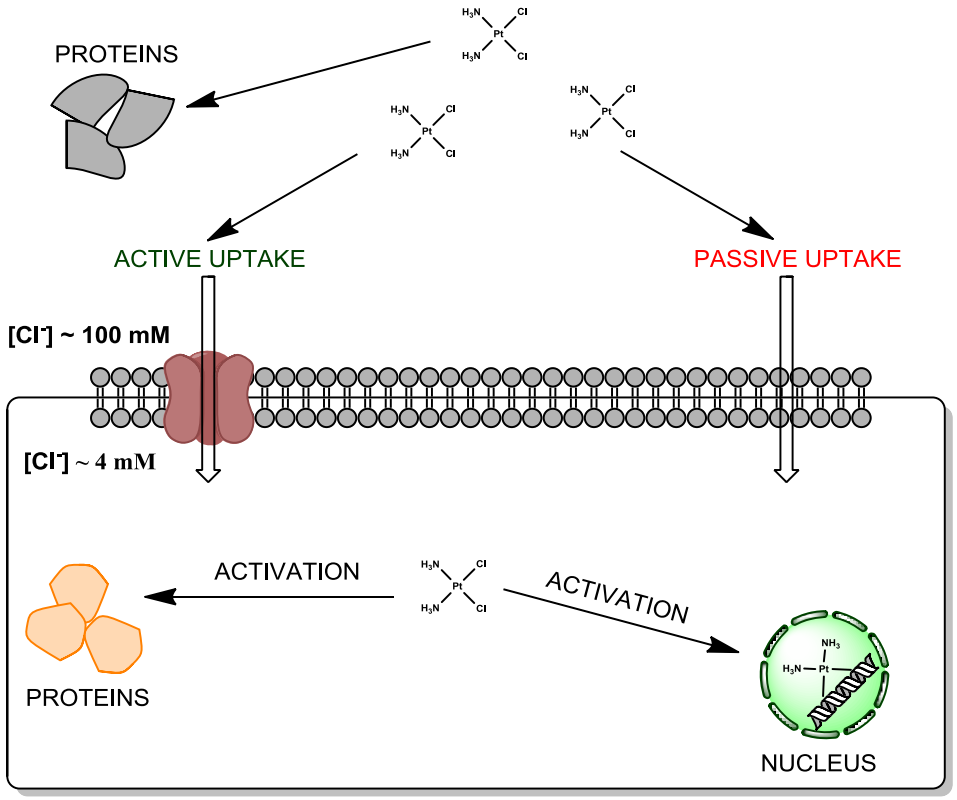

Figure 4 Cellular uptake of Cisplatin. Before internalization the drug may react with proteins (e.g. HSA). Internalisation occurs through active and/or passive transportation. Activation occurs due to the drop of [Cl^-] inside the cells. Despite DNA is believed to be the main target for final pharmacological effect, even interactions with protein lead to cellular processes alteration/response.

1.2.2 Activation and binding to biological targets

As already reported above, activation of cisplatin occurs when the drug is internalised in the cell. Here, the drop of chloride anion concentration triggers a series of reaction leading to the corresponding aquated cationic species of cisplatin (Figure 5). These species are very reactive and able to bind biological targets such as DNA and proteins.[37]

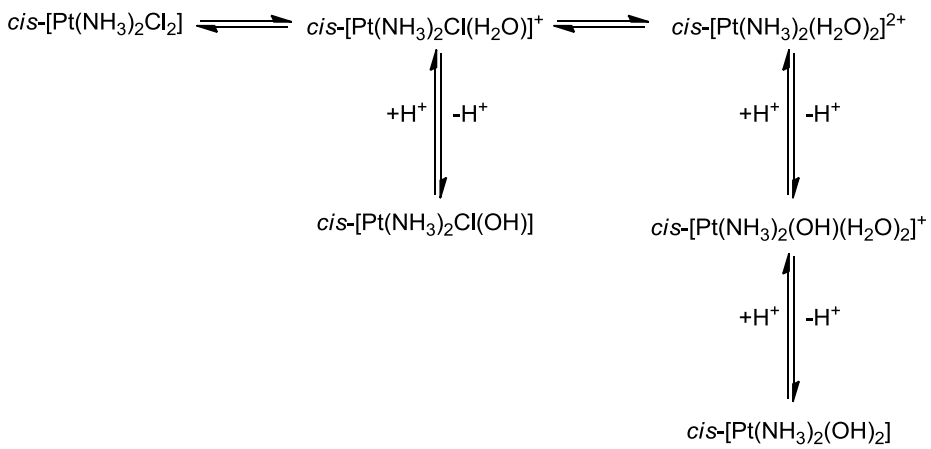

Figure 5 Activation of cisplatin in the cellular environment.

After activation, Pt(II) aqua complexes are capable to react with a number of targets, through release of water molecules. Interaction with nuclear DNA is believed to contribute in a major way to the antitumor activity of cisplatin being the purine bases at the N7 position the primary target for the formation of cisplatin-DNA adducts. The major cisplatin–DNA adduct is the intrastrand 1,2-d(GpG) cross-link, which accounts for 60–65% of the bound platinum. Interactions, which distort and bend the DNA structure, impede transcription and the downstream effects of transcription inhibition ultimately lead to cell death.[11,38]
Overall, formation of different adducts in different positions of double helix DNA is possible, as depicted in figure 6.[38]

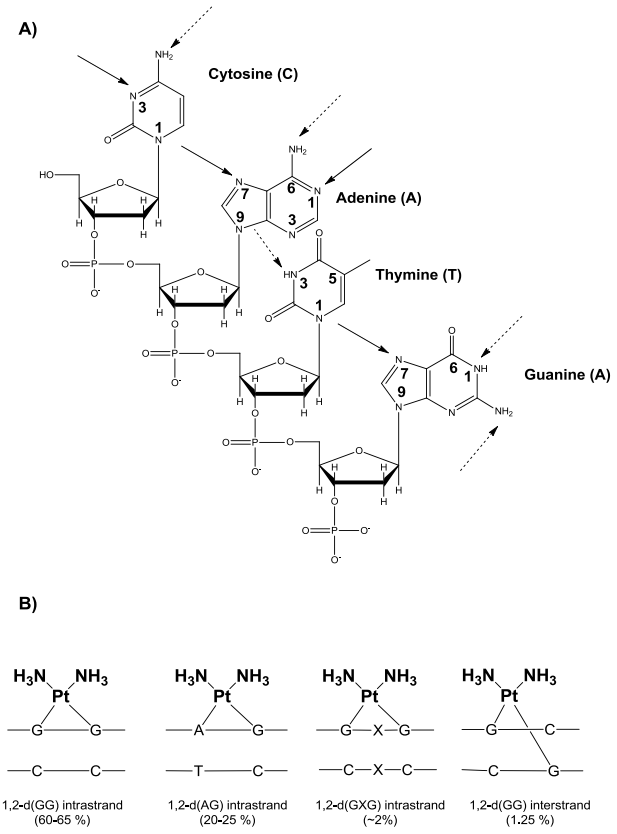

Figure 6 Platinum binding site on DNA bases (**A**) and types of cisplatin-DNA adducts and their frequency (**B**) (arrow: possible platination site; dotted arrow: possible metal binding only after loss of H^+).[38]

Apart from DNA, cisplatin and its analogues are able to bind aminoacidic residues of proteins. Due to the high affinity of thiolate anions for platinum, the complex may bind sulfur atoms. Important examples of this mode of interaction is represented by coordination of metal center to glutathione and metallothionein.[39] This latter aspect is of central importance since these proteins defend the cell against cisplatin itself,[40] and continuous exposure to the drug can build up resistance owing to increased levels of glutathione and metallothioneins.[41]

In addition cisplatin may binds also to blood serum proteins with important consequences in terms of toxicity (i.e. by inhibition of crucial role of proteins) as well as in terms of bioavailability (i.e. drug inactivation or "drug reservoir"). Remarkable, between many protein, serum albumin (HSA) is the most abundant (average blood content of 40-45 g L^{-1} in

healthy humans) and one day after intravenous administration of cisplatin, 65 to 98% of total Pt is bound to plasma proteins, in particular to HSA. Different opinions still exist on the consequences of cisplatin binding to HSA. Some authors report that HSA inactivates cisplatin and its analogues through coordination and binding of metal fragments, some others suggest that HSA is a reservoir of activated species of cisplatin still capable to transport and deliver these species to tissues.[42]
These issues are not trivial to be solved, but nowadays appears clear that interaction with proteins of metal-based drugs, plays a key role in terms of final pharmacological effect and thus, it is of great interest its understanding and characterisation.

1.2.3 Cellular processing, response to DNA damage

The pharmacological effect of cisplatin is determined by its interaction (and adducts formation) with nuclear DNA. Consequently a series of different pathways are activated and these, finally lead to inhibition of DNA transcription and replication. The interstrand and intrastrand crosslinks disrupt the structure of the DNA and this alteration in the structure is recognized by the cellular proteins to repair cisplatin-induced DNA damage.[31,32]
To date several families of proteins are considered to be important from this point of view: 1) nucleotide excision repair (NER) proteins, 2) mismatch repair (MMR) proteins, 3) DNA-dependent protein kinase (DNA-PK), and 4) high-mobility group (HMG) proteins.
Since the intrastrand cross-link is the major lesion caused by cisplatin-induced DNA damage, it is primarily repaired via the nucleotide excision repair (NER) system. The activity and efficacy of this process varies depending upon the nature of the adducts. NER in human cells depends on many factors, which include the XPA and RPA proteins, incision by structure-specific endonucleases, and repair DNA synthesis mediated by DNA polymerase.[43,44] Characterisation of the different repair pathways is of central importance to design more efficient platinum complexes able to overcome the cancer resistance due to these mechanisms of damage recognition. In this frame one potentially important factor is specific binding of HMGB proteins to 1,2-intrastrand cisplatin–DNA crosslinks, which shield these lesions from recognition of NER.[45-47] Furthermore, very important role is played by the p53 gene. When the DNA in a cell undergoes damage by cytotoxic agents (i.e. cisplatin or its analogues), radiation, p53 protein is extremely important in order to determine

whether the DNA will be repaired or the damaged cell will self-destruct (undergoes apoptosis). If the DNA can be repaired, p53 activates other genes to fix the damage. If the DNA cannot be repaired, this protein prevents the cell from dividing and signals it to undergo apoptosis.[47,48]

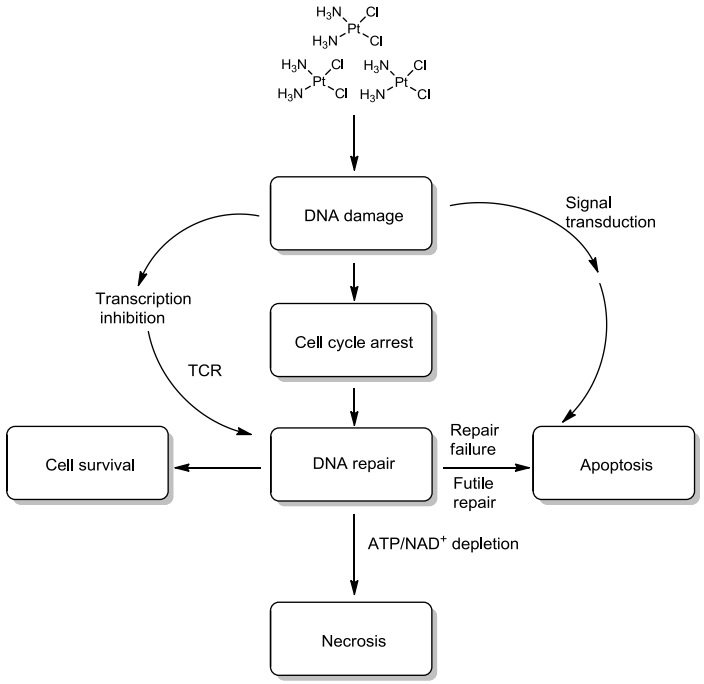

Figure 7 Schematic representation of cell response to cisplatin-induced DNA damage.[48]

Thus, there are many pathways involved in the response to DNA damage, that overall, determine the fate of the cell. Still, efforts of researchers are focused on a complete understanding of all these processes.

References

[1] Nelson N. EMBO J., **1999**, 18, 4361-4371.
[2] Lippard S.J. (**1994**) *Metals in Medicine*. In *Bioinorganic Chemistry*, University Science Books: Mill Valley, CA pp. 505-583.
[3] Farrell N. (**1989**) *Transition metal complexes as drugs and chemotherapeutic agents*, Springer: New York, Vol. 11.
[4] Pricker S.P. Gold Bull., **1996**, 29, 53-60.
[5] Medici S., Peana M., Nurchi V.M., Lachowicz J.I., Crisponi G., Zoroddu M.A. Coordin. Chem. Rev., **2015**, 284, 329-350.
[6] Peyrone M. Ann. Chem. Pharm., **1884**, 51, 1.
[7] Rosenberg B., Van Camp L., Krigas T. Nature, **1965**, 205, 698-699.
[8] Rosenberg B. Interdiscip. Sci. Rev., **1978**, 3, 134-147.
[9] Kauffman G.B., Pentimalli R., Doldi S., Hall M.D. Platinum Metals Rev., **2010**, 54, 250-256.
[10] O'Dwyer P.J., Stevenson J.P., Johnson S.W. (**1999**) *Clinical Status of Cisplatin, Carboplatin, and Other Platinum-Based Antitumor Drugs*. In Cisplatin, Lippert B. Ed., Verlag Helvetica Chimica Acta: Zürich, pp 29-69.
[11] Wilson J.J and Lippard S.J., Chem. Rev., **2014**, 114, 4470-4495.
[12] Macciò A., Madeddu C. Expert Opin Pharmacother., **2014**, 14, 1839-1857.
[13] Weiss R.B., Christian M.C. Drugs, **1993**, 46, 360-377.
[14] Lebwohl D., Canetta R. Eur. J. Cancer, **1998**, 34, 1522-1534.
[15] O'Dwyer P.J., Johnson S.W., Hamilton T.C. (**1997**) *Cisplatin and Its Analogues*. In Cancer Principles and Practice of Oncology 5th ed., DeVita V.T., Hellman S., Rosenberg S.A., Eds., Lippincott-Raven, Philadelphia, Vol. 2, pp 418-431.
[16] Cleare M.J. and Hoeschele J.D. Platinum Metal Review, **1973**, 17, 2-13
[17] Cleare M.J. and Hoeschele J.D. Bioinorganic Chemistry, **1973**, 2, 187-210.
[18] Christian M.C. Semin. Oncol., **1992**, 19, 720-733.
[19] Burcheranal J.H., Kalaher K., Dew K. Biochemie, **1978**, 60, 961-965.
[20] Dabrowiak J.C. (**2009**) *Platinum Anticancer Drugs*. In Metals in Medicine, John Wiley & Sons Ltd, The Atrium, Southern Gate,Chichester, West Sussex, United Kingdom, pp 109-147.
[21] Kelland L. Nat. Rev. Cancer, **2007**, 7, 573-584.
[22] Graham J., Mushin M. and Kirkpatrick P. Nat. Rev. Drug Discov., **2004,** 3, 11-12.

[23] Argyriou A.A., Polychronopoulos P., Iconomou G., Chroni E., Kalofonos H.P. Cancer Treat. Rev., **2008**, 34, 368-377.
[24] Galanski M., Jakupec M.A. and Keppler B.K. Curr. Med. Chem., **2005**, 12, 2075-2094.
[25] Yonezawa A., Masuda S., Yokoo S., Katsura T., Inui K. J Pharmacol Exp Ther., **2006**, 319, 879-886.
[26] Reedijk J. Proc. Natl. Acad. Sci. U S A, **2003,** 100, 3611-3616.
[27] Bhargava A., Vaishampayan U.N. Expert Opin. Investig. Drugs, **2009**, 18, 1787-1797.
[28] Kelland, L. Expert Opin. Investig. Drugs, **2007**, 16, 1009-1021.
[29] Hamilton G. Expert Opin. Drug Metab. Toxicol., **2013,** 9, 1381-1390.
[30] Siddik Z.H. Oncogene, **2003**, 22, 7265-7279.
[31] Basu A., Krishnamurthy S. J. Nucleic Acids, **2010**, No pp. given.
[32] Dhar S. and Lippard S.J. (**2011**) *Current Status and Mechanism of Action of Platinum-Based*. In Bioinorganic Medicinal Chemistry, Wiley-VCH Verlag & Co. KGaA, Boschstr. 12, 69469 Weinheim, Germany edited by Enzo Alessio, pp 79-95.
[33] Gately D.P. and Howell S.B. Br. J. Cancer, **1993**, 67, 1171-1176.
[34] Arnesano F., Scintilla S., Natile G. Angew. Chem., **2007**, *119*, 9220-222.
[35] Sharp S.Y., Rogers P.M., Kelland L.R. Clin Cancer Res., **1995**, 9, 981-989.
[36] Ishida, S., Lee, J., Thiele, D.J., and Herskowitz, I. Proc. Natl. Acad. Sci. USA, **2002**, 99, 14298-14302.
[37] Berners-Price S.J. and Appleton T.G. (**2000**) *The Chemistry of Cisplatin in Aqueous Solution*. In Platinum-Based Drugs in Cancer Therapy, Humana Press, edited by Kelland L.R. and Farrel N.P., pp 3-35.
[38] Robillard M.S., Reedijk J. (**2005**) *Platinum-Based Anticancer Drugs*. In Encyclopedia of Inorganic and Bioinorganic Chemistry, John Wiley & Sons, Ltd., pp 4488-4498.
[39] Ishikawa T. and Ali-Osman F. J. Biol. Chem., **1993**, 268, 20116-20125.
[40] Kraker A., Schmidt J., Krezoski S. and Petering, D.H. Biochem. Biophys. Res. Commun., **1985**, 130, 786-792.
[41] Schilder R.J., Hall L., Monks A., Handel L.M., Fornace A.J. Jr, Ozols R.F., Fojo A.T. and Hamilton, T.C. Int. J. Cancer, **1990**, 45, 416-422.
[42] Ferraro G., Massai L., Messori L., Merlino A. Chem. Commun., **2015**, 51,46, 9436-9439.
[43] Tapias A., Auriol J., Forget D., Enzlin J.H., Scharer O.D., Coin F., Coulombe B. and Egly, J.M. J. Biol. Chem. **2004**, 279, 19074-19083.

[44] Aboussekhra A., Biggerstaff M., Shivji M. K., Vilpo J. A., Moncollin V., Podust V.N., Protic M., Hubscher U., Egly, J.M. and Wood, R. D. Cell, **1995**, 80, 859-868.
[45] Reeves R. and Adair J.E. DNA Repair, **2005**, 4, 926-938.
[46] Gonzalez, V.M., Fuertes M.A., Alonso C., Perez J.M. Molecular Pharmacology, **2001**, 59, 657-663.
[47] Jung Y., Lippard S.J. Chem. Rev. **2007**, *107*, 1387-1407.
[48] Wang D. and Lippard S.J. Nat. Rev. Drug Discov., **2005**, 4, 207-320.

2

AIMS AND OBJECTIVES OF THE RESEARCH

2. AIMS AND OBJECTIVES OF THE RESEARCH

In the last decades the research on inorganic drugs in medicine has registered remarkable progresses with particular emphasis to the field of anticancer drugs.[1] Cisplatin, carboplatin and oxaliplatin are today widely used in the treatment of different type of malignance and often represent, even in combination with other drugs, a first choice therapy.[2] Since the serendipitous discover of cisplatin and despite the efforts, still nowadays, these drug are the most important research products in this field, although resistance to the treatments and heavy side effects, are important limiting factors to their use in clinical protocols.[3-5] Thus, there is urgent need of new and more effective Pt-based anticancer drugs able to circumvent these problems.

The development of new metal-based anticancer molecules is not easy, mostly because it is difficult to predict their effects *in vivo*, starting from the analysis of the cellular effects *in vitro*. Furthermore it should taken into account the extreme complexity of biological systems; even limiting our consideration only to studies at the cellular level, already, there are an outstanding number of factors and variables to be consider.

In this frame we have carried out studies on cell-free systems as well as cellular studies, characterising the reactivity and the cellular effects of cisplatin and a series of its analogues to shed light on analogies and differences between these drugs. Interestingly, it has been extensively characterised their interaction with model proteins. Despite today it is recognised that formation of Pt-protein adducts, is of central importance in relation to overall pharmacological and toxicological impact of cisplatin and its analogues, yet, the structural information concerning platination of protein, and the characterization of the resulting adducts, is limited.[6-8]

Thus the studies summarising in this thesis aimed to:

i) gather information on mechanistic aspects correlated with the mode of action of Pt-based anticancer compounds that, to date, remains in part unclear;

ii) compare, at different level, the behaviour of conventional platinum anticancer drugs with experimental complexes in order to find differences that may be significant in terms of pharmacological effect *in vivo*,

iii) evaluate or re-evaluate comparatively the anticancer properties of selected cisplatin analogues.

All these issues are addressed within this work, where the comparative characterization of protein binding for conventional platinum-based anticancer drugs is reported (chapter 3) as well as the reappraisal of old cisplatin analogues, overlooked so far as anticancer agents, studied in comparison with clinical used Pt compounds (chapter 4 and 5). Preliminary *in vivo* studies are also described (chapter 6).

References

[1] Barry Nicolas P.E. and Sadler P.J. Chem. Commun., **2013**, 49, 5106-5131.
[2] O'Dwyer P.J., Stevenson J.P., Johnson S.W. (**1999**) *Clinical Status of Cisplatin, Carboplatin, and Other Platinum-Based Antitumor Drugs*. In Cisplatin, Lippert B., Ed. Verlag Helvetica Chimica Acta: Zürich, pp 29-69.
[3] Daugaard G., Abildgaard U. Cancer Chemother. Pharmacol., **1989**, 25, 1-9.
[4] Cvitkovic E. Cancer Treat. Rev., **1998**, 24, 265-281.
[5] Screnci D., McKeage M.J. J. Inorg. Biochem., **1999**, 77, 105-110.
[6] Pinato O., Musetti C., Sissi C. Metallomics, **2014,** 6, 380-395.
[7] Arnesano F., Natile G. Pure Appl. Chem., **2008**, 80, 2715-2725.
[8] Casini A., Reedijk, J. Chem. Sci., **2012**, 3, 3135-3144.

3

PROTEIN METALATION BY CONVENTIONAL Pt-BASED ANTICANCER DRUGS

3. PROTEIN METALATION BY CONVENTIONAL Pt-BASED ANTICANCER DRUGS

The results presented in this chapter have been published in the following manuscripts:

*Luigi Messori, Tiziano Marzo and Antonello Merlino "The X-ray structure of the complex formed in the reaction between oxaliplatin and lysozyme", **2014**, Chem. Comm., 50, 8360-8362.*

*Daniela Marasco, Luigi Messori, Tiziano Marzo and Antonello Merlino, "Oxaliplatin vs Cisplatin: competition experiments in the binding to Lysozyme", **2015**, Dalton Trans., 2015,44, 10392-10398.*

*Luigi Messori, Tiziano Marzo and Antonello Merlino "Interactions of Carboplatin and Oxaliplatin with Proteins: insights from X-ray structures and mass spectrometry studies of their Ribonuclease A adducts", **2015**, J. Inorg. Biochem., DOI: 10.1016/j.jinorgbio.2015.07.011.*

3.1 Introduction

In our body we have thousands of proteins involved in many processes that are essential for life. Within these processes, proteins have structural, catalytic and transport roles. When a metal is introduced in the body, (e.g. as metal-based drug) it may bind to the aminoacidic residues.
If an amminoacid is crucial for the biological activity of protein, (e.g. aminoacidic residues in the catalytic site of enzymes), the protein itself may undergo a perturbation that leads to the partial or complete lack of ability to perform its task, which could be enough to kill the cell.[1,2]
Cisplatin and its analogues as well as many other metal-based drugs, are known to behave as pro-drugs. This implies that these complexes exert their interaction with biological targets and their pharmacological effects, after undergoing an activation process. Often (as in the case of cisplatin) this activation involves displacement of one or more weak ligands (leaving groups) and their replacement with water molecules; is this species that may react with protein side chains.[3] Furthermore, activation, may occur through a redox process.[4,5]
Among the 20 common amino acids found in proteins, only seven, aspartic and glutamic acids, histidine, lysine, methionine, cysteine and tyrosine, have donor atoms in their side chains that, from the standpoint of coordination chemistry, are potential targets for metallo-drugs.[2]
The reaction of activated metallodrugs with protein side chains leads to formation of metallodrug-protein complexes, or adducts, in which metallic fragments are coordinatively bound to proteins. These adducts usually manifest a quite good stability.[6-8] Moreover if the bound metal fragment presents additional reactive site or, if the metalated protein is reacted with other biomolecules with higher affinity for the metal, a residual reactivity may be expected. This residual reactivity may represent an important aspect in order to assess whether the formed species will conserve some biological role/activity.[7]
Furthermore, the difficulties in developing new anticancer complexes is due to the limited knowledge of mechanistic aspects that lead to their internalization in tumor tissue and/or inactivation. Since drugs as cisplatin and its analogues, are administered intravenously, a particular attention should be devoted to the interactions occurring between metal complexes and biomolecules such as serum proteins. In fact these proteins may have a transport function for metal-based antineoplastic agents and may "assist" the uptake process. Also, plasma proteins may concur in

inactivation pathways of metal-based anticancer drugs (see chapter 1, section 1.2) and in those processes that are determining for activity, toxicity, bioavailability and for excretion of the drugs themselves.[9-11]

In this sense human serum albumin (HSA) and human serum transferrin play an important role. The former, is the most abundant plasma protein (about 52%) with a 40-45 g L^{-1} content in healthy humans (ca. 0.6 mM; Mw 66-67 kDa). It is a 66 kDa single-chain protein consisting of three domains (called I, II, and III), each comprising two helical subdomains (named A and B).[12-15] Terminal regions of sequentially close domains form the interface helices that link domains to each other. Remarkably, the modular structural organization of HSA provides a variety of ligand binding sites that were extensively explored.[15,16]

At physiological pH, albumin adopts helical conformation (67% R-helix content), and its amino acid sequence contains 17 disulfide groups, one thiol group (cysteine-34), and one tryptophan residue (tryptophan-214) with the mutual binding potential toward many types of compounds. The binding sites are located in hydrophobic cavities in subdomains IIA and IIIA. These binding locations were determined crystallographically for several binding partners.[12] The protein was proven to bind and transport a variety of compounds, for example, fatty acids, bilirubin, metal ions, steroid hormones, vitamins, and pharmaceuticals, including metallodrugs.[17] Serum albumin performs a number of physiologically important functions-control of osmotic blood pressure, transport, metabolism, distribution of various compounds (including drugs), radical deactivation and delivery of amino acids after hydrolysis for the synthesis of other proteins.[12,14]

Human serum transferrin has a molecular mass of about 80 kDa and is found in blood plasma at a concentration of about 2.5 g L^{-1} (35 μM).[18] The members of the transferring group in general possess a high degree of sequence homology, for example, 60% for trans- and lactoferrin. They are single-chain glycoproteins containing ca. 700 amino acids (679 amino acids in the case of transferrin). The chief physiological function of serum transferrin is undoubtedly in iron transport within the circulatory system.

Transferrin is capable of binding two iron ions in oxidation state +3 (Fe^{3+} is bound selectively over Fe^{2+}). The iron(III) binding sites are located both in the N- and in the C-terminal lobe, and the two lobes are highly homologous (ca. 40%). Each lobe contains a distorted octahedral Fe^{3+}-binding site consisting of two tyrosines, one histidine, one asparagine, and a bidentate carbonate ion that acts as a synergistic anion in the binding process.

Diferric transferrin was found to associate with cells at 37°C more strongly than the monoferric or apotransferrin (in this order of affinity). Once transferrin of whichever type is bound to the receptor it is processed by the cells.[19] Inside the endosomes, the diferric transferrin releases the iron ions due to a lower pH (about 5.5) and becomes finally recycled back to the cell surface.[9]

3.1.1 Model Proteins

A very important point in this research area, is represented by the accurate characterization (and modellisation) of the interactions taking place between representative metallodrugs and protein side-chains. To reach this goal it is reasonable to assume that, in spite of the intrinsic structural diversity of the various proteins, some common patterns may hold in metal protein interactions related to the specific nature of the metal center and of protein side-chains. To this scope, studies of simple model proteins have turned out to be valuable.[9,20,21] For our research we have selected two of these model proteins i.e. hen egg white lysozyme (HEWL) and Ribonuclease A (RNase A). These, are small size proteins (MW respectively 14300 and 13680 Da), are well known and characterised, commercially available and have been often used to characterise the interactions occurring between proteins and metallodrugs.[20-22]

HEWL (Figure 1A) is a protein that has potent bactericidal properties, primarily ascribed to its enzymic activity, resulting in hydrolysis of b-linkage between the N-acetylglucosamine and N-acetylmuramic acid of the bacterial peptidoglycan, causing cell lysis. Beyond its biological importance, HEWL is one of the most studied and best characterized globular proteins. It was the first enzyme to have its structure determined by X-ray diffraction,[23] and since then hen lysozyme has been used extensively as a system to understand the underlying principles of proteins structure, function, dynamics, and folding through studies of both an experimental and theoretical nature.[24]

Owing to its small size and to the prevalence of positively charged groups, is a particularly suitable protein for ESI-MS investigations as previously shown. In addition HEWL is very prone to crystallise, thus turning out very appropriate for X-ray diffraction characterisations of its metallodrug adducts.[5,20,21] Potential binding sites for interaction with complexes are the histidine (e.g. His15) and methionine (e.g Met105 and

12) as well as aspartate residues. The 8 cysteine are instead involved in four disulphide bonds.

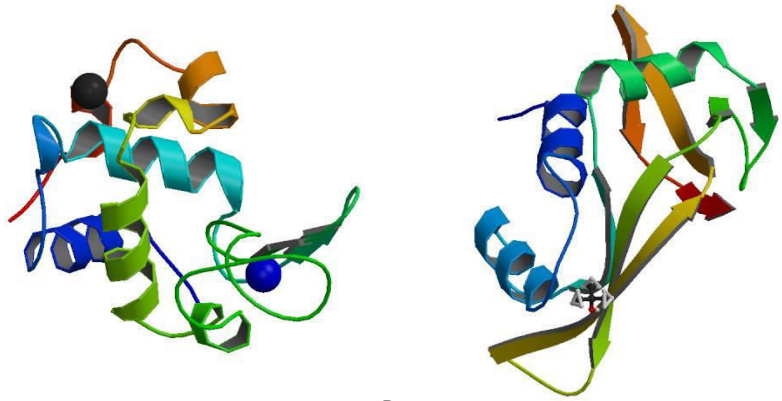

A B

Figure 1 3D structure of HEWL solved at 1.33 Å. RCSB PBD 193L (A) and RNase solved at 1.26 Å RCSB PDB 7RSA (B).

At variance, RNase (Figure 1B) was the first enzyme and third protein (after insulin and haemoglobin) for which a correct amino acid sequence was determined,[25,26] and the third enzyme and fourth protein (after myoglobin, lysozyme, and carboxypeptidase A) whose three-dimensional structure was determined by X-ray diffraction analysis.[27]

It is an endoribonuclease with the important role in catalysing the cleavage of the phosphodiester bond between the 5'-ribose of a nucleotide and the phosphate group attached to the 3'-ribose of an adjacent pyrimidine nucleotide. This cleavage forms a 2',3'-cyclic phosphate, which is then hydrolysed to the corresponding 3'-nucleoside phosphate.

RNase A contains four disulfide bonds, which are critical to the stability of the native enzyme. Two of these disulfide bonds lie between an alpha-helix and a beta-sheet and contribute more to the thermal stability than do the other two. Likely binding sites for interaction with complexes are histidine, methionine and aspartate residues of protein side chains. Since its structure makes it very stable protein and, as in the case of HEWL, well suitable for ESI-MS experiments as well as for crystallography; RNase A has been the object of landmark work on the folding, stability, and chemistry of proteins; in enzymology and in molecular evolution beyond the metal-protein interaction studies.[28]

Overall, studies on metallodrugs and model proteins permit a precise characterisation of their interactions at molecular level. Of course, it is mandatory to remember that we are studying very simplified systems. Indeed, in most cases the various biophysical studies have been mainly conducted on a two component systems containing a single metallodrug and a single protein. Nevertheless, despite these approximations, very interesting and useful informations may be derived from these studies, allowing to formulate mechanistic hypothesis. In addition comparing the different behaviour of complexes under the same conditions, it is possible to highlight those small differences that may have important consequences *in vivo*.

3.1.2 Molecular mechanisms of protein platination, comparative studies of the adducts formed in the reaction of HEWL with oxaliplatin, cisplatin and carboplatin.

3.1.2.1 Introduction

Cisplatin, carboplatin and oxaliplatin (Figure 2) are the three most important platinum-based anticancer drugs in widespread clinical use for the medical treatment of various kinds of cancers.[29] The mechanism of action of these compounds is believed to rely mostly on tight platinum(II) binding to DNA and consequent DNA damage.[30] If not recognised and repaired, such DNA damage ultimately triggers apoptotic death of cancer cells.

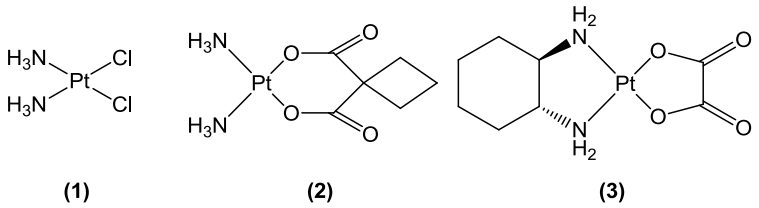

Figure 2 Structure of Cisplatin (1), Carboplatin (2) and Oxaliplatin (3).

In spite of the strict similarities in chemical structures and in DNA binding properties, these three Pt compounds manifest significant differences in their respective pharmacological profiles resulting in different therapeutic uses and indications.[31] In particular, the pharmacological profile of oxaliplatin turns out to be markedly distinct from those of cisplatin and

carboplatin: owing to its peculiar biological behaviour, oxaliplatin has become the election drug for the treatment of colorectal cancer, a very common type of cancer scarcely responsive to cisplatin and carboplatin.[32] Recent investigations pointed out that, in order to better understand the complete pharmacological profiles of Pt-based drugs, their interactions with proteins and consequent adduct formation must be understood in greater detail.[1,33] Platinum drugs are known to behave as prodrugs or "functional metal based drugs" according to Enzo Alessio's categorisation:[3] upon activation and release of a labile ligand, they are able to bind coordinatively to protein side chains. Extensive documentation of protein platination by established Pt drugs has been gathered during the last 15 years with the help of various biophysical methods.[34-39] ESI-MS measurements on small model proteins allowed a direct insight into details of the protein metalation process.[35] Conversely, a number of crystal structures of platinated proteins have been solved. In particular, the cisplatin adducts of hen egg white lysozyme,[36] bovine pancreatic ribonuclease,[37] bovine erythrocyte Cu, Zn superoxide dismutase[38] and copper chaperone Atox-1[39] were structurally characterised. In the case of carboplatin, only the crystal structure of its lysozyme adduct has been determined.[36] These studies showed that platination occurs through coordinative binding of Pt containing fragments to a few protein side chains such as histidines, cysteines or methionines. Also, we realised that no crystal structure was reported for protein adducts of oxaliplatin.

These arguments prompted us to investigate the interactions of oxaliplatin with the model enzyme hen egg white lysozyme (HEWL) from the structural point of view. We chose HEWL for this study since its structure has been often used to characterise the interactions occurring between proteins and metallodrugs[22,40]; in addition, crystal structures of its complexes with both cisplatin and carboplatin are available.[36]

3.1.2.2 Results

Crystals of HEWL in the presence of oxaliplatin (protein to metal drug ratio 1:10, incubation time=24 h) have been grown by hanging drop vapour diffusion method using a reservoir solution of 0.6 M $NaNO_3$, 0.1 M sodium acetate pH 4.4 and 20 % ethylene glycol. X-ray diffraction data have been collected on these crystals at 1.73 Å resolution using a Saturn944 CCD detector equipped with CuKα X-ray radiation from a Rigaku Micromax 007 HF generator (see experimental section for details)

and the crystal structure determined. This represents the first crystallographic study at high resolution for a protein adduct of oxaliplatin. The overall structure of the oxaliplatin-HEWL complex is shown in figure 3. The structure has been refined to a R-factor of 0.180 (R-free=0.235). The general conformation of the protein is not significantly affected by oxaliplatin binding. Inspection of the difference Fourier electron-density map (Fo-Fc) clearly revealed one >15σ peak close to Asp119 (Figure 4). This peak has been easily attributed to the platinum ion. The coordination geometry around the metal center is almost planar. Pt(II) is covalently attached to Asp119 OD2 atom, to a water molecule and to the two N atoms of the cyclohexyldiamine ligand.

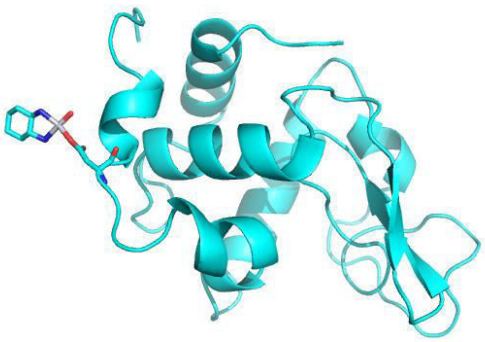

Figure 3 Overall structure of HEWL-oxaliplatin. Coordinates and structure factors were deposited in the Protein Data Bank (PDB code 4PPO).

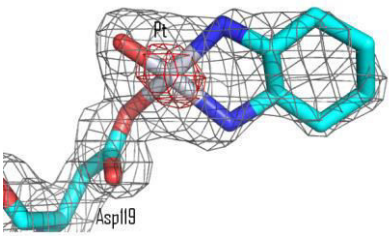

Figure 4 Details of the binding site of oxaliplatin to HEWL. The Pt ion is coordinated to Asp119. The binding of oxaliplatin to HEWL is accompanied by the loss of the oxalate ion. 2Fo-Fc electron density maps are contoured at 5σ (red) and 1σ (grey) level.

Structural refinements suggested an occupancy value for the Pt atom around 0.7, this representing a quite relevant degree of protein metalation. The cyclohexyldiamine ligand well fits into a cavity formed by the side chains of residues Trp62, Trp63, Asp101 and Asn103 of a

symmetry-related molecule (Figure 5). This interchain complementarity allows a clear definition of this region.

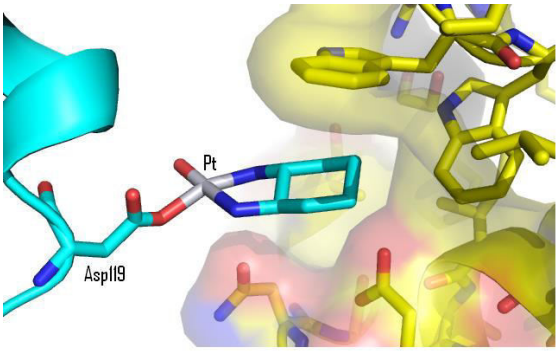

Figure 5 Stick representation of Pt binding site. Pt is bound to Asp119 side chain (cyan). The cyclohexyldiamine ligand is inserted into a cavity formed by Trp62, Trp63, Asp101 and Asn103 residues of a symmetry related molecule (yellow).

It is very instructive to compare the newly determined oxaliplatin-HEWL structure with those previously obtained for the HEWL adducts of cisplatin and carboplatin.[36] Structures of the three adducts are synoptically represented in figure 6.

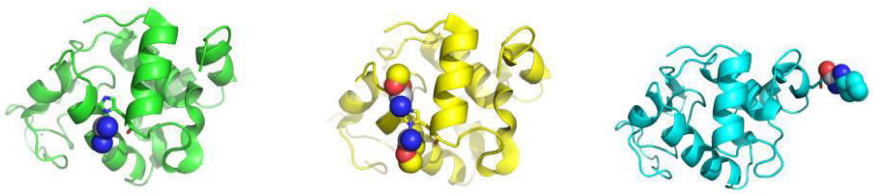

Figure 6 Overall structures of HEWL-cisplatin (green), HEWL-carboplatin (yellow) and HEWL-oxaliplatin (cyan). The metallodrug moieties bound to the protein are shown as spheres.

Comparative analysis offers several clues on the reaction between Pt drugs and the model protein lysozyme and on the associated protein metalation processes. In particular, the following features clearly emerge from inspection of these structures:

i) cisplatin and carboplatin behave very similarly, as they both produce a metalated lysozyme adduct where a $[Pt(NH_3)_2]^{2+}$ fragment is invariantly

coordinated to solvent accessible His15; there is just some variability in the anchoring mode of the platinum fragment to His15. No other Pt binding sites are detected.

ii) Oxaliplatin modifies lysozyme through protein coordination of a $[Ptdach]^{2+}$ fragment; a monometalated protein derivative is formed. At variance with cisplatin and carboplatin, coordination of the $[Ptdach]^{2+}$ cation selectively occurs at the level of the free carboxylate group of Asp119. Again, no secondary Pt binding sites are detected.

To gain independent information on the oxaliplatin/HEWL system the reaction was investigated through ESI-MS according to previously established experimental procedures.[36a] The resulting ESI-MS spectra, collected after increasing time intervals, are shown in figure 7 (see experimental part for full spectrum).

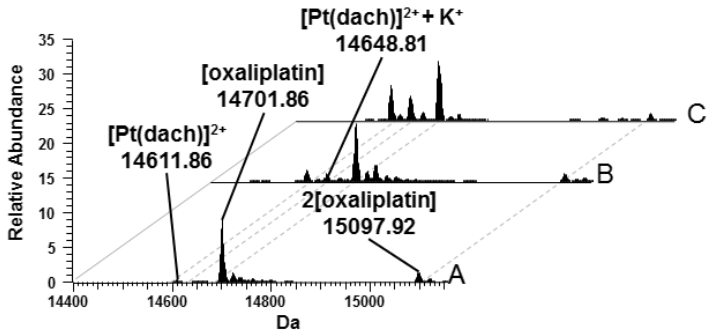

Figure 7 Close up of deconvoluted ESI-MS of HEWL treated with $3*10^{-4}$ mol L^{-1} oxaliplatin (metal:protein ratio = 3:1 in 20 mmol L^{-1} ammonium acetate buffer, pH 6.8) recorded after 24 h (A), 48 h (B), 72 h (C) of incubation at 37°C.

Notably, the ESI-MS spectrum, recorded after 24 hours, manifests a peak at 14701.86 Da, which matches the mass of a non-covalent adduct between oxaliplatin and HEWL in accordance with previous observations;[36a-41] alternatively, this peak might be assigned to a covalent oxaliplatin-HEWL adduct with monodentate oxalate coordination to Pt(II). Remarkably, for longer incubation times, two new peaks centred at 14611.86 and 14648.81 Da show up, which correspond respectively to a HEWL-$[Ptdach]^{2+}$ and the same adduct plus K^+ ion (see also experimental section for experimental and calculated isotope pattern). These results suggest that oxaliplatin could first interact non-covalently with HEWL, then the oxalate ligand is progressively released and the $[Ptdach]^{2+}$ fragment coordinates to the protein. In a final ESI-MS experiment, HEWL

was simultaneously challenged with oxaliplatin and cisplatin. Evidence was gained for the formation of a bis-platinum adduct, though in very small amounts, supporting the view that the two platinum binding sites are independent (see paragraph 3.1.3). Thus, ESI-MS data are roughly consistent with the picture arising from crystallographic studies, though the applied experimental conditions in the two kinds of experiments are obviously different.

3.1.2.3 Discussion and conclusions

On the ground of the structural and solution results reported here for the reaction of oxaliplatin with HEWL, some general trends in the reaction of Pt drugs with proteins may be delineated as summarised below.
With the three major Pt complexes in clinical use, monometalated derivatives of lysozyme are mainly formed. Before protein binding, Pt complex activation is required consisting in the release of one or more labile ligands: two chlorides in the case of cisplatin, the cyclobutandicarboxylate ligand in the case of carboplatin; oxalate in the case of oxaliplatin. The activation process may manifest a large kinetic variability depending on the nature of the leaving group and on the possible "assistance" offered by the protein. Notably, the activation process could be preceded by non-covalent binding of the intact Pt drug to the protein; then, coordinative binding to the protein of the Pt containing fragment occurs: $[Ptdach]^{2+}$ coordinates Asp119 while $[Pt(NH_3)_2]^{2+}$ fragments are selective for His15.
These results well reflect the fact that cisplatin and carboplatin manifest strictly related pharmacological profiles while oxaliplatin shows a rather distinct behaviour. It is possible that differences in reactivity and adduct formation with the model protein HEWL, as those above underscored, may have a more general meaning with respect to Pt drugs/protein interactions, and may account, at least in part, for the conspicuous differences in the respective pharmacological and toxicological profiles.

3.1.2.4 Experimental section

Crystallization, Data collection and refinement

Oxaliplatin and hen egg white lysozyme were obtained from Sigma. Crystals of HEWL in the presence of oxaliplatin were grown by hanging-drop vapor diffusion technique at 298 K mixing a protein solution containing 15 mg mL^{-1} of HEWL incubated for 24 h with an excess of oxaliplatin (protein to metal drug ration 1:10) with equal volumes of reservoir solution. Best crystals grow within 2-4 days from the following conditions: 0.6 M $NaNO_3$, 0.1 M sodium acetate pH 4.4 and 20 % ethylene glycol. X-ray diffraction data were collected from a single crystal at the CNR Institute of Biostructure and Bioimages, Naples, Italy, using a Saturn944 CCD detector equipped with CuKα X-ray radiation from a Rigaku Micromax 007 HF generator. Crystals were slowly dehydrated at air[42] and flash-frozen at 100 K using nitrogen gas produced by an Oxford Cryosystem (and maintained at 100 K during the data collection) without using cryoprotectants,[43] following the procedure used in other works.[44] Data set was processed and scaled using the HKL2000 package.[45] Data collection statistics are reported in table 1.
The structure was solved by molecular replacement method, using the PDB file 4J1A,[22] without water molecules and ligands, as starting model. The refinement was carried out with Refmac5.7,[46] model building and map inspections were performed using Coot.[47] 5% of the data was used for calculation of the R-free value. After several rounds of refinement using the maximum likelihood option in Refmac, manual adjustments of side-chain atoms and addition of water molecules to the coordinates, the structure converged to Rfactor of 0.180 and to Rfree of 0.235. Refinement statistics are reported in table 1. Structure validation has been carried out using Procheck.[48] Coordinates and structure factors were deposited in the Protein Data Bank (PDB code 4PPO).
Distances between Pt and the other ligands are reported in table 2.

PDB code	4PPO
Data-collection Space group	$P4_32_12$
Unit cell parameters a=b,c (Å)	77.05,37.29
Molecules per asymmetric unit	1
Observed reflections	44549
Unique reflections	12001
Resolution (Å)	50-1.73 (1.76-1.73)
Completeness (%)	97.8 (96.8)
Rmerge	0.088 (0.393)
I/σ(I)	11.8 (2.8)
Multiplicity	3.7 (2.3)
Refinement Resolution (Å)	30.8-1.73
number of reflections in working set	11406
number of reflections in test set	570
R factor/Rfree (%)	0.180 (0.235)
Number of non-H atoms used in the refinement	1163
Occupancy of Pt ion	0.70
B-factor of Pt ion	48.3
Ramachandran values (%) Most favoured/ Additional allowed	88.5/11.5
Generously allowed/ Disallowed	0/0
R.m.s.d. bonds (Å)	0.019
R.m.s.d. angles(Å)	1.85

Table 1 Data collection and refinement statistics for the oxaliplatin-HEWL structure.

	In the adduct	In the CSD structure[49]	In the structure of the adduct with 1,2-D(GpG)[50]
PDB code	4PPO	CUHKEV	1IHH
Pt-OD1 Asp119	2.05	-	-
Pt-O	1.98	2.01-2.03	-
Pt-N	1.98-2.10	2.04-2.06	2.03-2.04
Pt-N (DNA)	-	-	1.94-1.98
N-Pt-O angle (°)	94.2	98.4-95.4	-
O-Pt-O angle (°)	94.5	82.5	-
N-Pt-N angle (°)	86.0	83.9	84.0
N-Pt-N(DNA) angle (°)	-	-	79.6-97.7
N (DNA)-Pt-N(DNA) angle (°)	-	-	98.4

Table 2 Selected bond lengths (Å) and angles (°) for the Oxaliplatin binding site in the adduct formed with HEWL, in the crystal structure of the Oxaliplatin (CSD code CUHKEV)[49] and in the structure of the adduct with 1,2-d(GpG) (PDB code 1IHH).[50]

ESI-MS experiments

A solution of oxaliplatin ($3*10^{-4}$ mol L^{-1}) with HEWL (3:1 complex/protein molar ratio) was incubated in ammomium acetate buffer solution 20 mM pH=6.8 at 37°C for 72 h and ESI-MS spectra were recorded after 6, 24, 48, 72 h (Figure 8). After a 20-fold dilution with water, ESI-MS spectra were recorded by direct introduction at 5 µL min^{-1} flow rate in an Orbitrap high-resolution mass spectrometer (Thermo, San Jose, CA, USA), equipped with a conventional ESI source. The working conditions were the following: spray voltage 3.1 kV, capillary voltage 45 V, capillary temperature 220°C, tube lens voltage 230 V. The sheath and the auxiliary gases were set, respectively, at 17 (arbitrary units) and 1 (arbitrary units). For acquisition, Xcalibur 2.0. software (Thermo) was used and monoisotopic and average deconvoluted masses were obtained by using the integrated Xtract tool. For spectrum acquisition a nominal resolution (at m/z 400) of 100,000 was used.

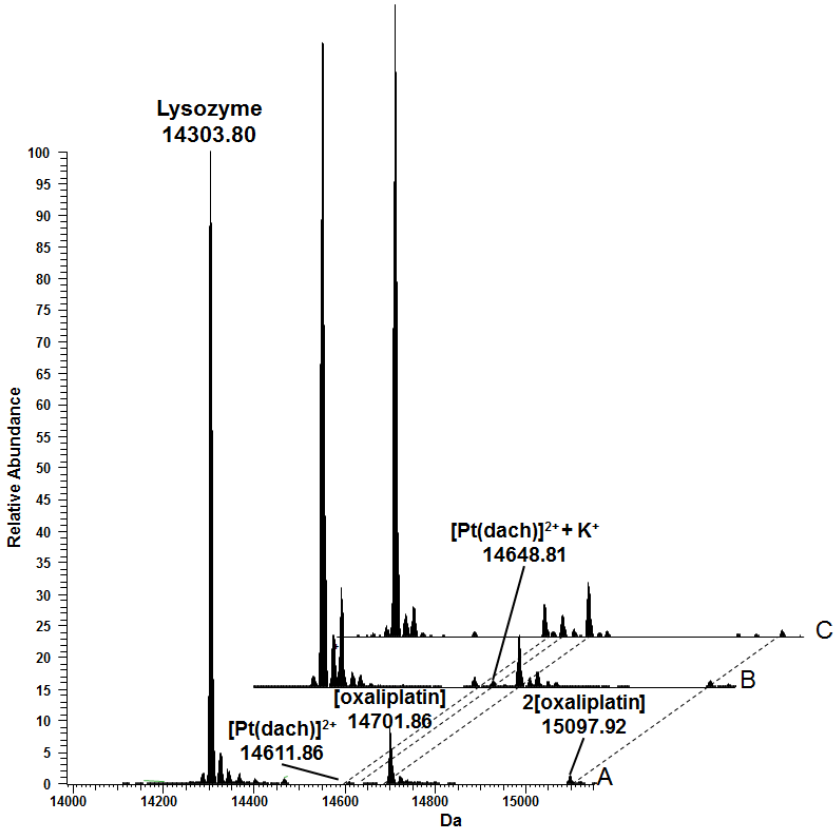

Figure 8 Deconvoluted ESI-MS of HEWL treated with $3*10^{-4}$ mol L^{-1} oxaliplatin (metal:protein ratio = 3:1 in 20 mmol L^{-1} ammonium acetate buffer, pH 6.8) recorded after 24 h (A), 48 h (B), 72 h (C) of incubation at 37°C.

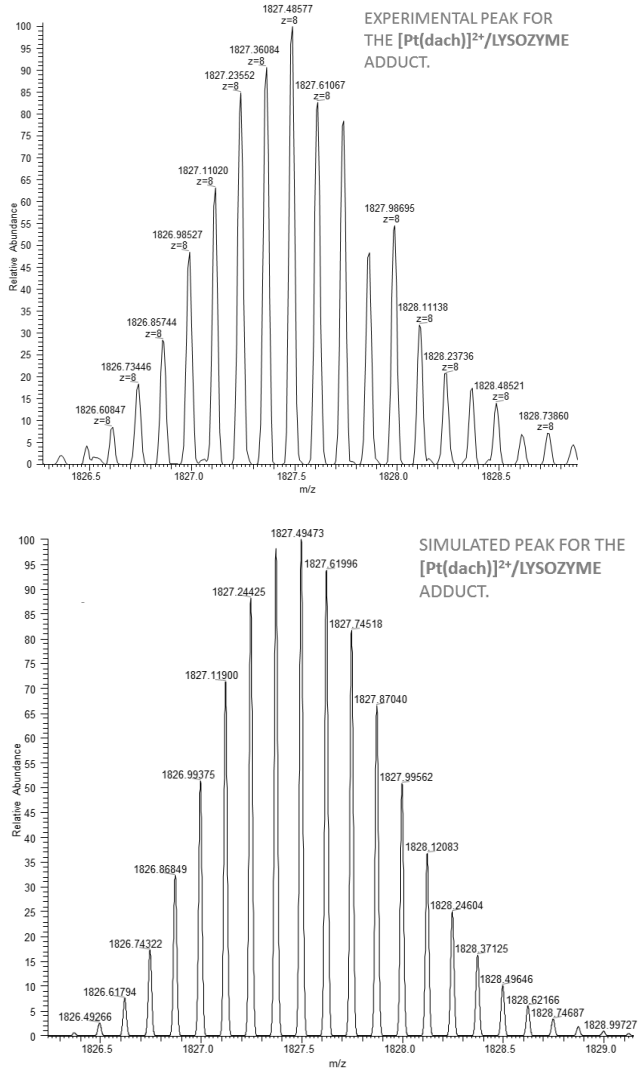

Figure 9 Experimental and simulated peak corresponding to $[Pt(dach)]^{2+}$/lysozyme adduct.

3.1.3 Oxaliplatin vs Cisplatin: competition experiments in the binding to lysozyme

3.1.3.1 Introduction

In the previous section (3.1.2), we have shown that HEWL is able to bind cisplatin and oxaliplatin in two distinct binding sites,[51] whereas cisplatin and carboplatin compete for the same residue side chain.[52] In particular, upon reaction between cisplatin and HEWL, platination occurs at the level of His15, with a *cis*-$Pt(NH_3)_2^{2+}$ fragment bound to the protein surface.[36,52] On the other hand, the reaction between HEWL and oxaliplatin leads to the formation of a complex with $Pt(dach)^{2+}$ moiety bound to Asp119.[51] These data suggest that, at least in principle, it is possible for these two Pt-drugs to bind HEWL simultaneously, although it is unpredictable if the binding of the former drug can alter the affinity of the protein for the latter. In fact, even subtle structural alterations can affect the HEWL dynamics, as already demonstrate in other works,[55] thus altering the drug affinity for the protein.

These arguments prompted us to investigate the formation of the adducts that are obtained when oxaliplatin and cisplatin are incubated with HEWL. These results are of potential interest if one considers that cisplatin and oxaliplatin might be clinically used in combination and that studies of cisplatin/oxaliplatin combination on patients with advanced ovarian cancer already revealed acceptable hematologic toxicity, and reversible cumulative neurosensory toxicity.[56-58] Simultaneous injection of cisplatin and oxaliplatin was reported to produce a synergistic antitumor activity against cisplatin-resistant murine leukemia L1210.[59,60] In addition, the feasibility and efficacy of a cisplatin/oxaliplatin combination was evaluated in patients with testicular tumors and encouraging results were obtained.[61]

Along this line of reasoning, it should be also recalled that phase I clinical studies of a carboplatin/oxaliplatin combination revealed that the combination treatment seems feasible and active, although it does not allow a significant increase in platinum dose-intensity delivery.[62]

3.1.3.2 Results

Electrospray mass spectrometry

First, we registered ESI-MS spectra of HEWL sample in the presence of a mixture of equimolar concentrations of cisplatin and oxaliplatin (Figure 10). A number of HEWL-platinum adducts are clearly visible in this experiment whose assignment is reported in table 3.

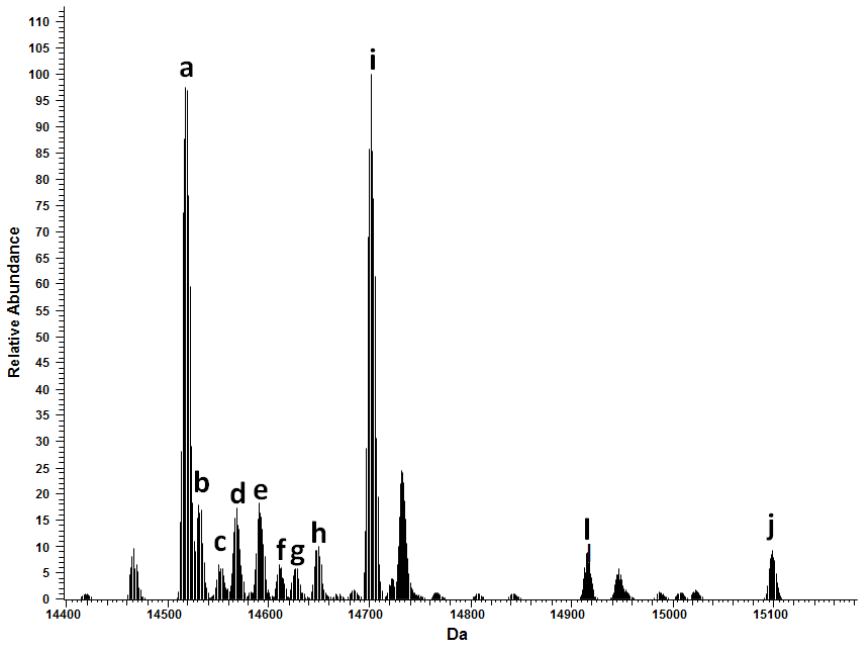

Figure 10 ESI-MS spectrum registered to investigate the possible competition between oxaliplatin and cisplatin for the same binding site. The spectrum has been collected after 24 h incubation of equimolar concentration of the two drugs (cisplatin and oxaliplatin) with HEWL in 20 mM ammonium acetate buffer pH=6.8 at 37°C (see experimental section for further details). For the peak assignment see table 3.

Label	Bound fragment	Mass (Da)
a	$Pt+Na^+$	14517.76
b	$[Pt(NH_3)_2]^{2+}$	14530.77
c	$[Pt(NH_3)Cl]^+$	14550.50
d	$[Pt(NH_3)_2Cl]^+$	14567.76
e	$[Pt(NH_3)_2Cl]^+ + Na^+$	14590.80
f	$[Pt(dach)]^{2+}$	14610.82
g	$[Pt(NH_3)_2Cl_2] + Na^+$	14627.78
h	$[Pt(NH_3)_2Cl_2] + 2Na^+$	14648.82
i	Oxaliplatin	14701.84
l	**Oxaliplatin + $[Pt(NH_3)]^{2+}$**	**14915.82**
j	2 Oxaliplatin	15098.89

Table 3 Assignment of peaks in the ESI-MS spectrum (Figure 10).

Interestingly, a protein-metallodrug complex is detected corresponding to a bis-Pt adduct (bis-adduct) with lysozyme simultaneously bearing an $Pt(NH_3)^{2+}$ fragment and an oxaliplatin molecule (peak l). The observation of this bis-adduct, though in a quite small amount, implies that the two drug binding sites on HEWL surface are independent one another.

Crystallography

Afterward, we tried to grow crystals of the bis-adduct following different strategies (see experimental section for further details). Attempts to obtain crystals of the bis-adduct mixing the protein to a mixture of cisplatin+oxaliplatin or adding first cisplatin and then oxaliplatin to the protein sample failed. In these cases we obtain crystals of the adduct between HEWL and cisplatin alone, i.e. structures of HEWL with Pt centre only bound to His15. On the other hand, tetragonal crystals of the bis-adduct were successfully grown using a protein sample that was first incubated for 24 h with an excess of oxaliplatin and then incubated for 24 h with an excess of cisplatin (final protein to metal ratio 1:10) and a reservoir solution containing 0.6 M $NaNO_3$, 0.1 M sodium acetate pH 4.4 and 20 % ethylene glycol. In the same experimental conditions, we also grew tetragonal crystals of a protein solution obtained when a HEWL sample with excess of cisplatin (1:10 protein to metal ratio) is mixed with equal amounts of protein with excess of oxaliplatin (1:10 protein to metal ratio). The results of the structural analyses carried out on crystals grown using these last two strategies show that the bis-adduct is formed (Figure

11). The structures were refined to R-factor of 0.155 and 0.159 and R-free of 0.218 and 0.230 for the datasets collecting using the former and the latter procedure, respectively. The results obtained using the two datasets are almost identical, for this reason only one structure will be described. Both structures were deposited in the Protein Data Bank (accession code 4Z46 and 4ZEE). The overall structure of HEWL in the bis-adduct is not significantly affected by the binding of the two drugs.

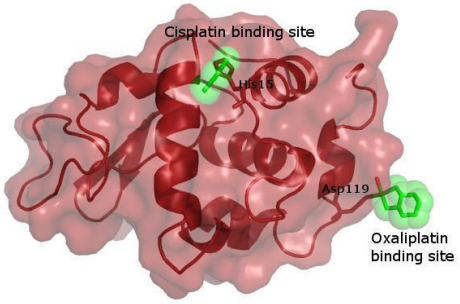

Figure 11 Overall structure of the bis-Pt HEWL adduct. Coordinates and structure factors were deposited in the Protein Data Bank (PDB code 4Z46).

The CA root mean square deviation (rmsd) from the structure of ligand-free HEWL (PDB code 193L) is as low as 0.26 Å. When the structure of the bis-adduct is compared with that of HEWL solved at ultrahigh resolution (PDB code 2VB1) and crystallized under similar experimental conditions, but in the triclinic space group, rmsd is in the range 0.79-0.81 Å. The most significant differences between the atomic resolution structure of HEWL and the bis-adduct (Figure S1 in the supplementary material) are located in loop regions, close to residues 44-51 and 69-73 (Figure S2A in the supplementary material), at the end of helix constituted by residues 88-101 and in the region connecting this helix to that encompassing residues 108-115 (Figure S2B in the supplementary material). These structural differences seem to be due to an altered disposition of nitrate ions on the molecular surface rather than to the binding of the drugs (Figure S2A and B).

The inspection of the electron density maps of both bis-adduct structures suggest that there are two Pt binding sites on HEWL surface (Figure 12A and B and figures S3 and S4 in the supplementary material). As expected on the basis of the comparison between the structure of HEWL-cisplatin[52] and that of HEWL-oxaliplatin,[51] the former binding site, i.e. presumably that of an oxaliplatin moiety, is close to Asp119 (Figure 12A). The latter, i.e. that presumably due to the binding of a cisplatin moiety, is found close

to His15 (Figure 12B). No other bindings sites are found, although multiple sites of cisplatin on HEWL had been found by ESI-MS combined with trypsin digestion.[63]

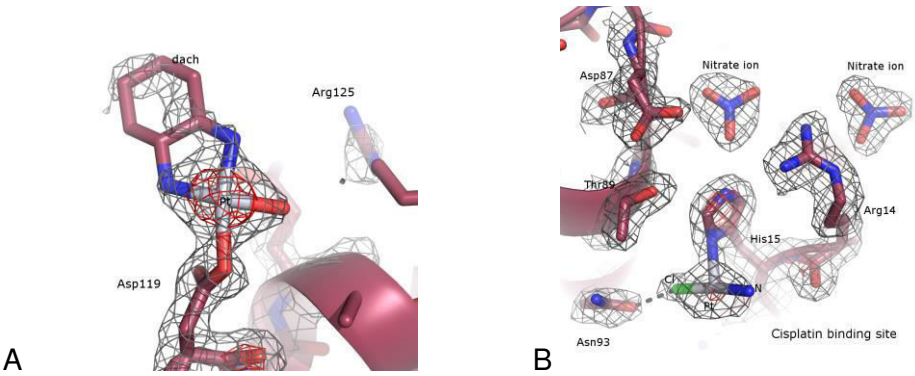

Figure 12 Binding sites of Oxaliplatin (A) and Cisplatin (B).2Fo-Fc electron density maps are contoured at 3σ (red) and 1σ (grey) level.

In both the Pt binding sites observed in the bis-adduct, the Pt center has a low occupancy (Pt occupancy factor=0.40, B-factor=52.5-55.8 Å^2 for the Asp119 binding site and Pt occupancy factor=0.35, B-factor=63.6-67.0 Å^2 for the His15 binding site, respectively). The location of the Pt centres is confirmed by the inspection of anomalous difference maps, which clearly identify the positions of the Pt atoms and of sulphur atoms of Cys6, Met12, Cys30, Cys64, Cys76, Cys80, Cys94, Met105, Cys115, Cys127 (Figure 13 and Figure S5 in the supplementary material).

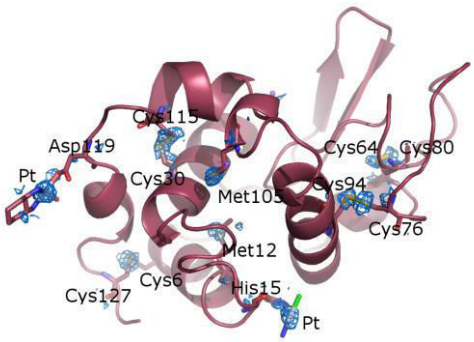

Figure 13 Anomalous difference map calculated from anomalous data collected for the bis-adduct crystal. The anomalous map is rendered in blue and contoured at 2.0 σ. The map clearly identifies the positions of Pt and sulphur atoms of Cys6, Met12, Cys30, Cys64, Cys76, Cys80, Cys94, Met105, Cys115, Cys127.

Due to the low occupancies, details on the Pt coordination sphere cannot be easily resolved. However, a $Pt(dach)^{2+}$ fragment close to Asp119 and a $[Pt(NH_3)Cl]^+$ fragment close to His15 have been identified and included in the final model. An independent confirmation of these assignments derives from the finding that the electron density maps of the Pt binding sites are almost identical in the two structures of the bis-adduct obtained using the two different preparations (Figure S3 and S4 in in the supplementary material). In the previous crystallographic study on the HEWL/carboplatin+cisplatin structures, both Pt drugs bind to His15, but cisplatin seems to have an overall higher binding affinity for the His15 side-chain compared with carboplatin.[64]
However, our structures cannot be directly compared with that obtained for HEWL/carboplatin+cisplatin,[64] since the bis-adduct has not been obtained using the same procedure by Helliwell and Tanley.

Surface plasmon resonance and circular dichroism analyses

To further investigate the nature of HEWL/cisplatin+oxaliplatin interaction, surface plasmon resonance (SPR) and circular dichroism studies were also performed. First, the affinities of cisplatin and oxaliplatin toward HEWL were measured separately by SPR. This technique has been already used to evaluate the affinity of Pt complexes for G-quadruplexes.[65] HEWL was efficiently immobilized on a CM5-chip and Pt complexes were employed as analytes (concentration range 0.1-2.0 mM). Dose-response sensorgrams (Figure S6A and B in the supplementary material) revealed that, in 20 mM sodium citrate buffer at pH 4.4, the two molecules bind HEWL with similar affinities, in the low millimolar range (K_D =1.83 ± 0.03 mM and 1.51 ± 0.02 mM, for cisplatin and oxaliplatin, respectively). Kinetic and thermodynamic parameters obtained by the SPR analysis are reported in table 4. For comparative purposes, the same experiments were then carried out in HBS (HEPES buffered saline) at pH 7.4 (Figure S6C). Cisplatin binding assays provided a similar value of K_D (1.69 ± 0.05 mM), while oxaliplatin binding could not be evaluated due to the instability of the complex in the presence of NaCl.[66] In fact, EXAFS spectra of oxaliplatin in NaCl solution concentrated between 0.08 M and 3 M show that a slight enlargement of the band appears after a few hours, indicating that Pt chloration occurs.[65]
Then, an experiment performed by injecting first oxaliplatin and then cisplatin (after reaching the saturation curve associated with the binding of the first ligand) was carried out (Figure 14).

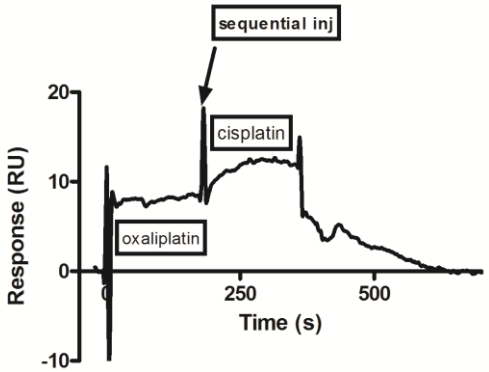

Figure 14 SPR Sensorgram for the sequential injection of oxaliplatin and (then) cisplatin, both at 1 mM, to immobilized HEWL in the presence of 20 mM sodium citrate buffer at pH 4.4 (see experimental section for further details).

Ligand	k_{on} *($M^{-1}s^{-1}$)*	k_{off} *(s^{-1})*	K_D *(mM)*
Cisplatin	9.4	0.0173	1.83 ± 0.03
Oxaliplatin	16.9	0.0256	1.51 ± 0.02

Table 4 Equilibrium dissociation constants (K_D) and kinetic parameters for the interaction of HEWL with cisplatin and oxaliplatin obtained using SPR method.

This experiment, performed using a Pt complex concentration of 1 mM and 20 mM sodium citrate buffer at pH 4.4 as running buffer, shows an increase of Resonance unit (RU) signal after the injection of the second Pt complex. This finding clearly indicates that the two metallodrugs bind different sites on the HEWL surface. To further corroborate these results, thermal shift assays were carried out. In particular, we employed circular dichroism to determine the melting temperature of HEWL alone and in the presence of the two Pt complexes. In figure 15, the overlay of denaturation profiles of the wild type protein, of its adducts with cisplatin and oxaliplatin and of the bis-adduct formed using different strategies is reported. In particular, for the formation of the bis-adduct the two drugs are concomitantly added to HEWL (HEWL/cisplatin+oxaliplatin), or added to the protein at different times, i.e. first adding cisplatin and then oxaliplatin (HEWL/cisplatin then oxaliplatin) or *vice-versa* (HEWL/oxaliplatin then cisplatin). The comparison of Tm values points out that the cisplatin binding does not significantly alter the HEWL thermal stability, whereas oxaliplatin binding slightly decreases the protein melting

temperature. The formation of the bis-adduct, which seems to be afforded following different strategies, can be well evidenced by comparing melting temperatures of the different protein complexes examined (Table 5).

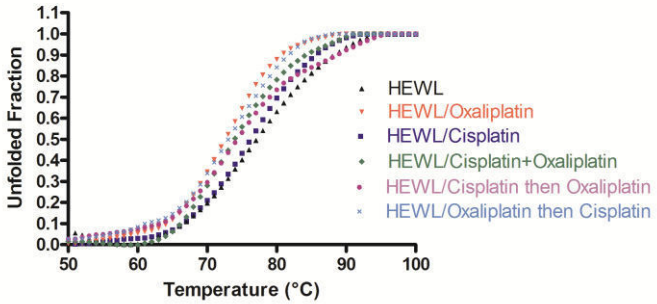

Figure 15 Unfolding curves of HEWL and HEWL/Pt complexes as followed by monitoring the variation of molar ellipticity at 222 nm as function of temperature. Experiments have been performed using 20 μM protein or protein adduct in 10 mM sodium acetate buffer at pH 4.4.

Complex	Tm (°C)
HEWL	77.2±0.1
HEWL/cisplatin	76.5±0.5
HEWL/oxaliplatin	73.0±0.1
bis-adducts:	
HEWL/cisplatin+oxaliplatin	74.3±0.3
HEWL/cisplatin then oxaliplatin	74.0±0.1
HEWL/oxaliplatin then cisplatin	73.8±0.5

Table 5 Denaturation temperatures determined by Circular Dichroism spectroscopy for the protein-Pt complex adducts formed upon the interaction of HEWL with cisplatin and oxaliplatin in 10 mM sodium acetate buffer at pH 4.4.

3.1.3.3 Discussion and conclusions

In conclusion, unambiguous evidence is provided here that cisplatin and oxaliplatin can be used in combination to produce a bis-metalated HEWL adduct where a $[Pt(NH_3)]^{2+}$ fragment is bound to His15 and an oxaliplatin/$[Ptdach]^{2+}$ fragment is bound to Asp119. The results of our experiments suggest that the two drugs manifest similar affinities for the protein, at least under the investigated experimental conditions, and that thermal shift analysis can be used to reveal the formation of the protein-Pt complex adducts. Obviously, the conditions required for the crystallization and the model protein used do not allow to obtain conclusions that are relevant for clinical cancer treatments. However, although the combination of drugs acting synergistically can offer a means of overcoming drug resistance,[67-68] the results of our analysis suggest that in principle combination treatment of Pt drugs can possibly lead to a greater array of side effects than previously imagined as different protein sites may be damaged. Also it can be highlighted and confirmed, as the two drug with similar pharmacological effects (i.e. cisplatin and carboplatin), form the same adduct with protein; instead oxaliplatin well known to possess pharmacological effect rather different from cisplatin and carboplatin, forms a different adduct that has been here described.

3.1.3.4 Experimental section

ESI-MS experiments

cisplatin and oxaliplatin (3.0×10^{-4} M) were incubated for 24 h with lysozyme (10^{-4} M) in ammonium acetate buffer pH=6.8 at 37 °C. After a 20-fold dilution with water, ESI-MS spectra were recorded by direct introduction at 5 µl min^{-1} flow rate in an Orbitrap high-resolution mass spectrometer (Thermo, San Jose, CA, USA), equipped with a conventional ESI source. The working conditions were the following: spray voltage 3.1 kV, capillary voltage 45 V, capillary temperature 220°C, tube lens voltage 230 V. The sheath and the auxiliary gases were set, respectively, at 17 (arbitrary units) and 1 (arbitrary units). For acquisition, Xcalibur 2.0. software (Thermo) was used and monoisotopic and average deconvoluted masses were obtained by using the integrated Xtract tool. For spectrum acquisition, a nominal resolution (at m/z 400) of 100,000 was used.

Crystallization, Data collection and refinement

cisplatin, oxaliplatin and hen egg white lysozyme (HEWL) were purchased from Sigma chemicals and used without further purification. Stock solution of HEWL was obtained dissolving the protein at a concentration of about 40 mg x mL^{-1} in 5 mM sodium acetate buffer at pH 5 and stored at 4 °C. cisplatin and oxaliplatin solutions were freshly prepared for each experiment.

Crystals of the bis-adduct have been obtained following two different protocols. Firstly, a protein sample has been first incubated for 24 h in the presence of an excess of oxaliplatin (protein to metal drug ratio 1:10) and then for 24 h in the presence of an excess of cisplatin (protein to metal drug ratio 1:10). Secondly, a protein sample incubated for 24 h in the presence of an excess of oxaliplatin (protein to metal drug ratio 1:10) has been mixed to a protein sample incubated for the same time in the presence of an excess of cisplatin (protein to metal drug ratio 1:10). Crystals of the bis-adduct were grown by hanging-drop vapor diffusion technique at 298 K mixing this sample containing 15 mg x mL^{-1} of HEWL incubated for a total of 48 h with the two metallodrugs with equal volumes of reservoir solution. Best crystals grow within 2-10 days from the following conditions: 0.6 M $NaNO_3$, 0.1 M sodium acetate pH 4.4 and 20 % ethylene glycol. Attempts to obtain crystals of the bis-adduct mixing the protein to a mixture of cisplatin+ oxaliplatin or adding first cisplatin and then oxaliplatin to the protein sample failed. In these cases we obtain crystals of the adduct between HEWL and cisplatin alone, i.e. structures of HEWL with Pt centre only bound to His15.

X-ray diffraction data were collected from single crystals at the CNR Institute of Biostructure and Bioimages, Naples, Italy, using a Saturn944 CCD detector equipped with CuKα X-ray radiation from a Rigaku Micromax 007 HF generator. Crystals were slowly dehydrated at air[42] and flash-frozen at 100 K using nitrogen gas produced by an Oxford Cryosystem (and maintained at 100 K during the data collection) without using cryoprotectants, following the procedure used in other works.[69-70] Data set was processed and scaled using the HKL2000 package.[45] Data collection statistics are reported in Table 6.

	Bis-adduct1	Bis-adduct2
PDBcode	4ZEE	4Z46
DataCollection		
Spacegroup	$P4_32_12$	$P4_32_12$
Unit-cellparameters		
a,b,c(Å)	77.377,77.377,37.600	77.318,77.318,37.325
Moleculespera.u.	1	1
Resolution(Å)	54.71-1.95(1.98-1.95)	54.67-1.85(1.88-1.85)
Observed reflections	47779	58591
Uniquereflections	8452	10100
Completeness(%)	95.8(83.2)	99.4(92.2)
R merge	0.113(0.611)	0.095(0.471)
I/σ(I)	11.7(2.3)	13.8(2.2)
Multiplicity	5.7(4.3)	5.8(3.1)
Refinement		
Resolution(Å)	54.71-1.95(1.98-1.95)	54.67-1.85(1.88-1.85)
Number of reflections in working set	8023	9585
Number of reflections in test set	403	482
Rfactor/Rfree(%)	15.8/23.0	15.5/21.8
Number of non-H atoms used in the	1209	1210
Occupancy of Pt ions	0.40,0.35	0.40,0.35
B-factor of Pt ions ($Å^2$)	55.8,63.6	52.5,67.0
OverallB-factor	27.6	26.8
R.m.s.d.bonds (Å)	0.019	0.019
R.m.s.d.angles (Å)	1.94	1.94
Estimated overall coordinate errors(Å)	0.148	0.196

Table 6 Data collection and refinement statistics.

The structures were solved by molecular replacement method, using the PDB file 4J1A,[22] without water molecules and ligands, as starting model. The refinement was carried out with Refmac5.7,[71] model building and map inspections were performed using Wincoot.[47] 5% of the data was used for calculation of the R-free value. After several rounds of refinement using the maximum likelihood option in Refmac, manual adjustments of side-chain atoms and addition of water molecules to the coordinates, the structures converged to Rfactor of 0.155/0.159 and to Rfree of 0.218/0.230. Refinement statistics are reported in Table S1. Structure validations have been carried out using Procheck.[48]

Coordinates and structure factors of the two structures were deposited in the Protein Data Bank (PDB codes 4Z46 and 4ZEE).

For further details on surface plasmon resonance (SPR) and circular dichroism thermal denaturation experiments, see supplementary material.

3.1.4 Cisplatin, carboplatin and oxaliplatin bind to RNase: studies of interaction and mechanistic hypothesis

3.1.4.1 Introduction

To gather further details in the reactivity of clinically used Pt drugs with proteins we have studied their interactions with RNase.
In a recent paper, the structure formed in the reaction of RNase with cisplatin has been reported.[37] This structure, shows as platinum(II) binding takes place exclusively at the level of Met29. These data have been compared with those obtained for carboplatin and oxaliplatin. ESI-MS measurements are nicely supported by crystallographic structures and obtained results are an independent confirmation of the results presented in the previous sections; furthermore, on the basis of the available data, a likely mechanism for oxaliplatin hydrolysis and binding to the protein is proposed.

3.1.4.2 Results

Crystallography

The structures of RNase A-carboplatin and RNase A-oxaliplatin have been solved at 2.09 and 2.27 Å resolution, respectively. The overall structures of the two adducts are reported in figure 16B and 16C. The structures have been refined to Rfactor=20.5 and 22.4 (Rfree=26.2 and 30.1), for the RNase A complexes with carboplatin and oxaliplatin, respectively. In both structures, the electron density maps of protein regions are rather well defined, with exceptions consisting of a few portions in both the molecules present in the asymmetric unit (molecule A and B, hereafter) of the two complexes. Similarly to what found for the RNase A-cisplatin complex (Figure 16A),[37] in both RNase A-carboplatin and RNase A-oxaliplatin adducts platination does not affect the overall conformation of the protein, which remains very similar to the wild-type (CA root mean square deviations in the range 0.36-0.60 Å).

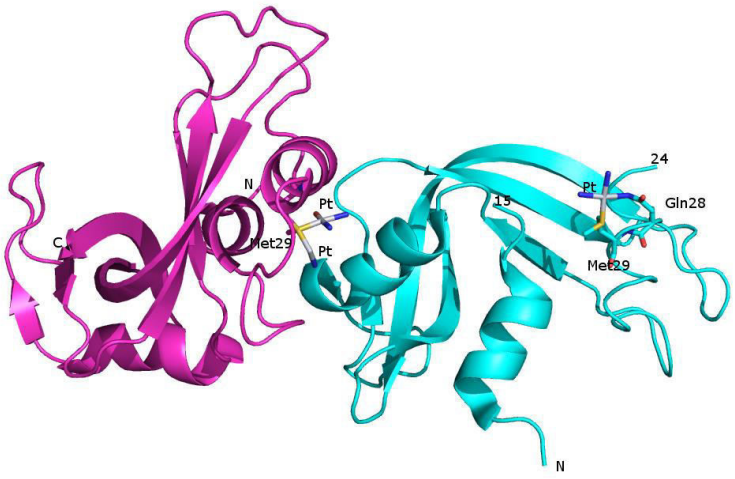
N
Pt
Met29
Pt
C
24
Pt
15
Gln28
Met29
N

A

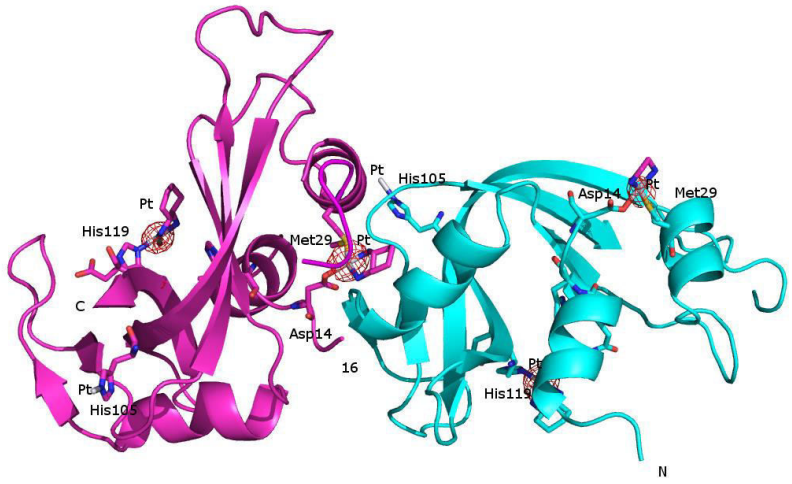
Pt
His105
Pt
Asp14
Pt
Met29
Pt
His119
Met29
Pt
C
Asp14
16
Pt
His105
Pt
His119
N

B

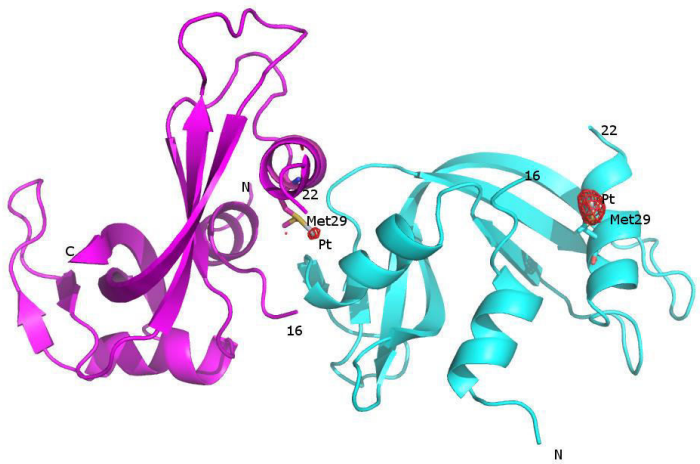

C

Figure 16 Ribbon representation of the asymmetric unit of the RNase A-cisplatin (panel A), RNase A-oxaliplatin (panel B) and RNase A-carboplatin (panel B) structures. The molecules A and B are coloured in cyan and purple, respectively. Side chains of residues involved in the Pt drugs recognition are shown along with Pt centres. In panel B and C, 2Fo-Fc electron density maps are coloured in red and contoured at 4σ. The structures of RNase A-oxaliplatin and RNase A-carboplatin have been deposited in the Protein Data Bank with entry codes 4S18 and 4S0Q. The structure of RNase A-cisplatin was already solved and deposited in the PDB with entry code 4OT4.

As previously found for cisplatin[37] and chloroplatinite ($PtCl_4^{2-}$),[73] the RNase A-carboplatin interaction in both A and B molecules mainly occurs at the SD atom of the side chain of Met29. However, due to unclear electron density maps likely associated with low occupancy and to the possible conformational disorder of this site, the local environment of the bound Pt(II) center, in the RNase A-carboplatin adduct, could not be unambiguously determined (Figure 17A and B). The refinement of B-factors of Pt ligands and the inspection of residual Fo-Fc electron density maps suggests that the Pt ions have occupancy= 0.50 and 0.35 for molecule A and B, respectively. In both these chains, platination of Met29 induces a disordering of residue 16-22 and of Tyr25 side chain.

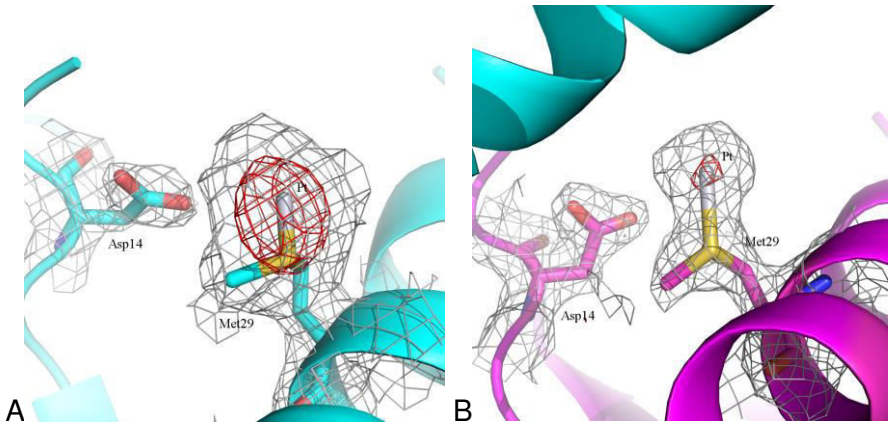

Figure 17 Details of the binding sites of Pt(II) in the RNase A-carboplatin adduct. Pt ion is bound to Met29 in the molecule A (panel A) and B (panel B). Asp14 side chain is included in the figure, since it is involved in the recognition of oxaliplatin (see below). 2Fo-Fc electron density maps are contoured at 0.8σ level (grey) and 4.0σ level (red).

Although crystals of RNase A-oxaliplatin diffract to a resolution slightly lower than that obtained for RNase A-carboplatin and RNase A-cisplatin[37] complexes, the electron density maps clearly reveal details of the binding. In the RNase A-oxaliplatin structure, six Pt binding sites have been identified, i.e. three binding sites for each molecule of the asymmetric unit.

In the main oxaliplatin binding site, the Pt(II) ion is bound to ND1 atom of His119 (Figure 18A and B). In this site, the electron density map is well defined and clearly shows that oxaliplatin retains the dach ligand upon binding to the protein. A water molecule complete the coordination sphere of the Pt centre. Retention of the dach ligand of oxaliplatin is observed during binding to model peptides in other studies.[79] These results are also in line with the experimental observation by Shoeib and coworkers that β-alanyl-L-histidine dipeptide (carnosine) is able to bind oxaliplatin inhibiting its cytotoxic action.[79] Notably, the occupancy factor for the oxaliplatin fragment is = 0.8 in both A and B chains, but its orientation is different in the two molecules: indeed, the dach moiety is exposed to the solvent in molecule A, whereas it orients toward the active site in molecule B. In both cases, an extensive network of hydrogen bonds stabilizes the binding.

In the second binding site (Figure 18C and D), the Pt(II) ion is coordinated to SD atom of Met29, as for RNase A-cisplatin[37] and RNase A-carboplatin adducts. Furthermore, in both molecules A and B, beyond the SD atom of Met29, Pt also coordinates to OD2 atom of Asp14. Residual Fo-Fc electron density map in this site indicates a possible variability in the anchoring mode of oxaliplatin also close to Met29 and Asp14 side chains. Platination induces a disordering of residues 16-23 in molecule A and 18-21 in molecule B. The occupancy factor for the oxaliplatin fragment (Figure 18C and D) in this site is = 0.4 in molecule A and = 0.6 in molecule B. The relatively low occupancy of the oxaliplatin fragment in molecule A does not allow the modelling of the dach moiety (Figure 18C). Finally, a minor binding site has been observed close to His105 (Figure 18 E and F). In this site only the Pt atom with occupancy = 0.20 has been modelled.

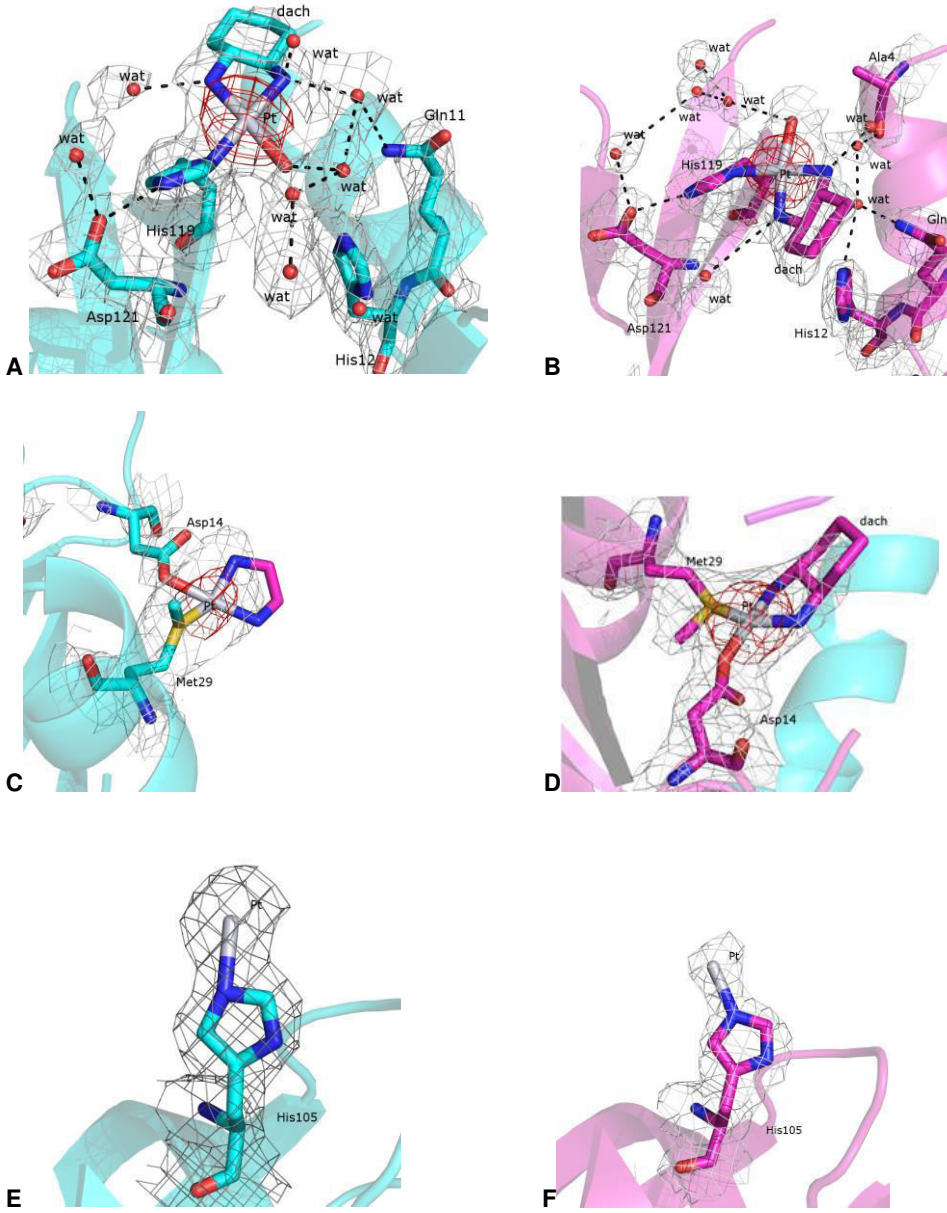

Figure18 Details of the binding sites of Pt(II) in the RNase A-oxaliplatin structure. The drug is bound to protein through a coordinative interaction with side chain of His119 (panel A and B for molecules A and B, respectively). The $[Ptdach]^{2+}$ fragment is involved in a number of hydrogen bonding interactions with water molecules that form an intricate network stabilizing the structure. Furthermore, Pt ion is bound to Met29 and Asp14 side

chains (panel C and D for molecules A and B, respectively). Oxaliplatin binding to sulfur atoms of physiologically important molecules like glutathione has been already observed in other studies.[79] Finally, a minor Pt binding site has been identified close to side chain of His105 (panel E and F for molecules A and B, respectively). 2Fo-Fc electron density maps are contoured at 0.8σ level (grey) and 4.0σ level (red). Molecule A is coloured in cyan and molecule B in purple. In panels C, E and F only the atoms included in the final models are reported, for this reason in panel C some atoms of dach fragment are omitted, whereas in panels E and F only the Pt atoms are reported.

Electrospray mass spectrometry

A further validation of the proposed RNase A-Pt ligation patterns and of the above interpretation of the electron density maps was achieved by performing independent ESI-MS measurements on Pt drug-protein adducts according to the established experimental procedure developed in our laboratory (see experimental section and Figure 19). ESI-MS spectra were recorded for RNase A-oxaliplatin (Figure 19A), RNase A-carboplatin (Figure 19B), and also for RNase A-cisplatin adducts (Figure 19C).

Inspection of mass spectrometry results provides evidence for the formation of a variety of Pt adducts of different nature, in considerable amounts.

In all cases, monometalated adducts are preferentially formed, though appreciable amounts of bis metalated derivatives are seen, especially in the case of oxaliplatin.

Oxaliplatin forms, at first, two kinds of derivatives, of mass 13988.3 and 14078.3 Da, in comparable amounts, assignable respectively to bidentate and monodentate species (Figure 19A); with time, the relative abundance of the bidentate adduct become higher and predominant on monodentate adduct, with associated release of oxalate ligand. In analogy with oxaliplatin, carboplatin (Figure 19B), first, forms a predominant monodentate derivative; for longer incubation times the cyclobutane-1,1-dicarboxylate ligand (CBD) is progressively released and a peak assignable to the bidentate adduct increases in intensity. Though of low intensity, a peak falling at 14423.4 Da, is representative for bis-adduct formation.

Comparative analysis of peak intensities for the metal-protein adducts suggests that oxaliplatin and cisplatin (Figure 19C) are far more reactive than carboplatin, although differing ionization efficiencies may also be a contributing factor.

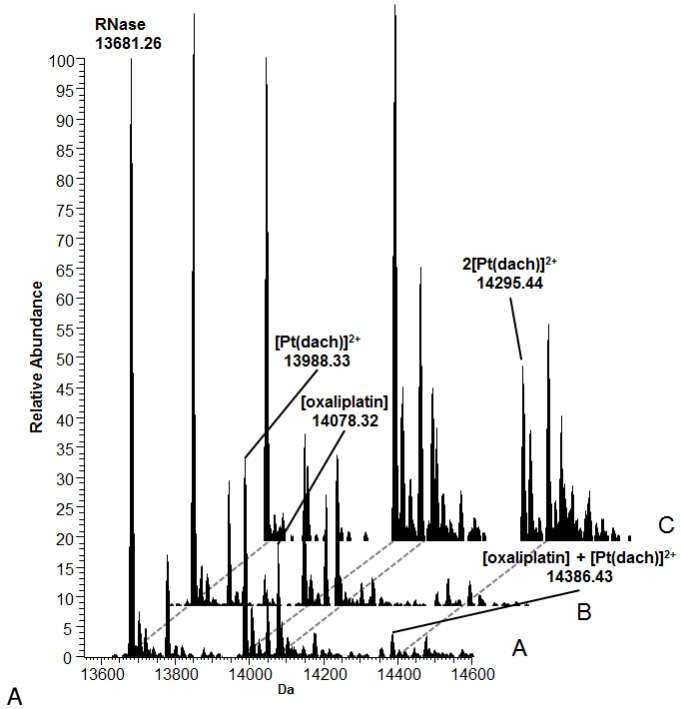
RNase
13681.26
2[Pt(dach)]2+
14295.44
[Pt(dach)]2+
13988.33
[oxaliplatin]
14078.32
[oxaliplatin] + [Pt(dach)]2+
14386.43
C
B
A
Relative Abundance
Da

A

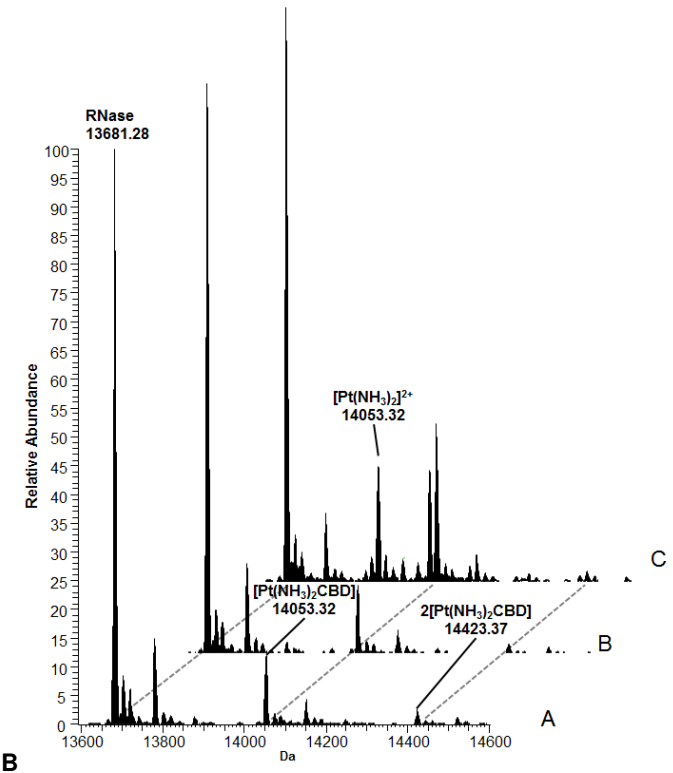
RNase
13681.28
[Pt(NH3)2]2+
14053.32
[Pt(NH3)2CBD]
14053.32
2[Pt(NH3)2CBD]
14423.37
C
B
A
Relative Abundance
Da

B

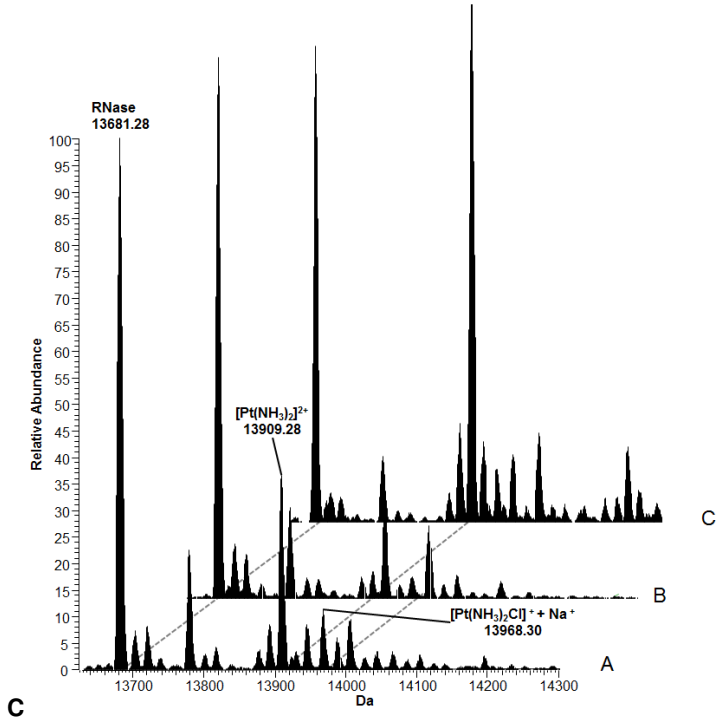

Figure19 Deconvoluted ESI-MS spectra of RNase A treated respectively with $3*10^{-4}$ M of oxaliplatin (panel A), carboplatin (panel B) and cisplatin, (panel C) recorded after 24h (A), 72h (B), 168h (C) of incubation at 37 °C. Experimental conditions: Metal:protein ratio = 3:1; buffer: 20 mM ammonium acetate pH 6.8.

3.1.4.3 Discussion and conclusions

We have reported here the X-ray structures of the RNase A-carboplatin and RNase A-oxaliplatin adducts. As the crystal structure of the RNase A-cisplatin had been previously solved,[37] we are in the fortunate position that structures are now available for RNase A adducts with the three main Pt drugs; this allows making instructive structural comparisons. Notably, such an analysis is carried out using structures obtained by soaking metallodrugs into pre-existing isomorphous RNase A crystals grown under very similar conditions. The finding that the RNase A crystals contain two molecules in the asymmetric unit adds an internal validation to our results. Moreover, the crystallographic investigation has been nicely complemented by ESI-MS data on the same adducts which support the correct identification of the Pt species bound to the protein. The importance of using two independent biophysical methods such as X-ray crystallography and ESI-MS on the same system is thus further documented[40b,40e] and underscored. In particular, ESI-MS data turn very

valuable in elucidating the nature of protein bound platinum fragments for the RNase A-carboplatin adduct where crystallographic data are ambiguous, whereas X-ray diffraction data add molecular details on the binding of oxaliplatin to the protein. The results of this comparative structural analysis are summarized in table 7. On the basis of the reported data, the following considerations can be done:

- cisplatin and carboplatin behave in a similar way, as they both produce, under the applied experimental conditions, a monometalated protein derivative where the Pt ion of the drug fragment mainly coordinates to SD atom of Met29. The platinum fragment coordinated to Met29 is distinct for the two drugs: it is $[Pt(NH_3)_2]^{2+}$ for cisplatin and $[Pt(NH_3)_2CBD]$ for carboplatin. Analyzing the metal binding site of carboplatin and cisplatin in detail, minor differences are observed that are probably due to the different steric hindrance of the Pt ligands. In the molecule B of the RNase A-cisplatin adduct,[37] Pt can coordinate both SD atom of Met29 and NE atom of Gln28 (bidentate interaction),[37] whereas only a monodentate interaction with Met29 seems to occur for carboplatin. Notably, ESI-MS results performed after a long incubation time point out that the CBD ligand may be released, so that a type of Pt fragment identical to that arising from cisplatin is eventually associated with the protein, and that a dimetalated adduct can also be formed. In addition, it must be stressed that cisplatin shows a greater reactivity than carboplatin in terms of amounts of formed derivatives as well witnessed by ESI-MS results.

- Oxaliplatin also binds Met29, but it coordinates RNase A through interaction of a $[Ptdach]^{2+}$ fragment. Furthermore, a bidentate coordination is observed that involves the OD1 atom of Asp14. The result confirms previous observations obtained with HEWL in which coordination of the $[Ptdach]^{2+}$ cation selectively occurs at the level of the free carboxylate group of Asp residues.[51] ESI-MS data suggest that the binding of oxaliplatin to the protein could occur according to a two-step process. Combining our data with the mechanism proposed for the acid hydrolysis of oxaliplatin,[81,82] a picture of the RNase A-oxaliplatin recognition can be drawn: the

oxalate ligand of Pt is detached in two consecutive steps, which involve the formation of oxalate monodentate complex. The ring-opening step allows the replacement of oxalate with the carboxylate from the Asp residue (Figure 20). Ring-opened Met adducts of carboplatin have been studied previously.[83] Since the formation of hydrolysis product species has been observed *in vivo*, this mechanism could be operative also under physiological conditions.[81,82]

Pt drug	RNase A binding sites as revealed by X-ray structural analysis of the adducts obtained by soaking procedure*	N° of binding sites	Binding mode suggested by X-ray structural analysis	Drug Fragment suggested by X-ray structural analysis	Drug Fragment as revealed by ESI MS
cisplatin**	Mol A: Met29	1	monodentate	$[Pt(NH_3)H_2O]^{2+}$	$[Pt(NH_3)Cl]^{+}$
	Mol B: Met29, Gln28		bidentate	$[Pt(NH_3)_2]^{2+}$	$[Pt(NH_3)_2]^{2+}$
carboplatin	Mol A: Met29	1	monodentate	undefined	$[Pt(NH_3)_2]^{2+}$
	Mol B: Met29		monodentate	undefined	$[Pt(NH_3)_2CBD]$
					$2[Pt(NH_3)_2CBD]$
oxaliplatin	Mol A: His119 Met29, Asp14 His105	3	monodentate	$[Pt(dach)(H_2O)]^{2+}$	
			bidentate	$[Pt(dach)]^{2+}$	Oxaliplatin
			monodentate	undefined	$[Pt(dach)]^{2+}$
	Mol B: His119 Met29, Asp14 His105		monodentate	$[Pt(dach)(H_2O)]^{2+}$	Oxaliplatin
			bidentate	$[Pt(dach)]^{2+}$	$+[Pt(dach)]^{2+}$
			monodentate	undefined	$2[Pt(dach)]^{2+}$

Table 7 Structural features of Pt-drug binding sites from the X-ray structures of the adducts obtained by soaking procedure on C2 crystals of RNase A and by ESI-MS data. *from ref. 37

** It is interesting to note that all RNase A residues involved in the three platinated adducts (Asp14, Gln28, Met29, His105 and His119) are conserved in the human pancreatic enzyme (HP-RNase).

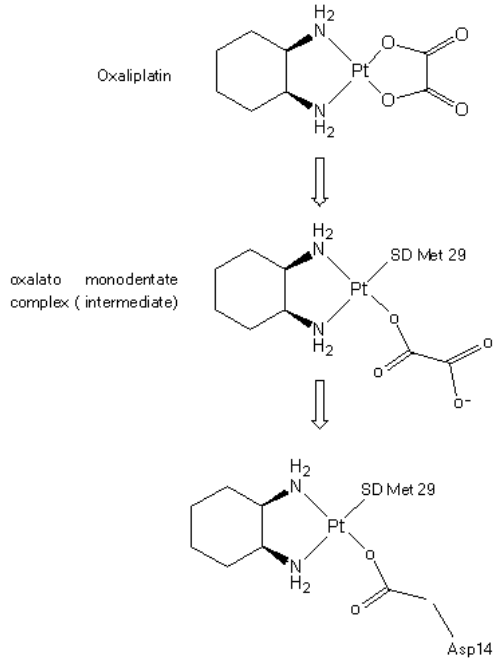

Figure 20 Proposed mechanism for oxaliplatin hydrolysis and binding to Met29 and Asp14 residues of RNase A. The bidentate adduct formation proceeds through ring opening and initial formation of a monodentate intermediate.

Notably, in the RNase A-oxaliplatin adduct, other Pt binding sites are also detected. In the main binding site, Pt coordinates the ND1 atom of His119. Furthermore, oxaliplatin can also bind, with low occupancy, the NE2 atom of His105. These results are interesting since it has been previously shown, by studying its interaction with HEWL, that oxaliplatin preferentially binds Asp side chains,[51] while both carboplatin and cisplatin show a preference for His side chains.[36a,84] This is even more surprising if one takes into account that the oxaliplatin fragment bound to RNase A is larger than those of carboplatin and cisplatin. These results could be explained by considering the kinetics of the protein-metallodrug recognition. In fact, it has been shown that, contrary to its DNA binding capacity, the rate of protein binding of oxaliplatin may be significantly higher than that of cisplatin and carboplatin.[31,85] On the other hand, these data also agree with previous crystallographic findings on the adduct formed in the reaction between trans-Pt derivatives and RNase A.[53] It

should be also noted that cisplatin has been found to bind both His105 and His119 in RNase A-cisplatin crystals of a different space group and obtained under different crystallization conditions.[75] In this respect, we cannot exclude that carboplatin could be able to bind His105 and His119, using the approach described in reference 75 or after longer soaking time.

The results of this comparative structural analysis suggest that cisplatin and carboplatin behave similarly when they react with proteins, while oxaliplatin shows a significantly different behavior. We suggest that differences in reactivity and adduct formation with proteins, which could be related to a different kinetics of metallodrug-protein binding, may have a more general significance and may be at the basis of the different pharmacological and toxicological profile of the three drugs. Altogether these data support previous hypotheses that metal ligands play a key role in the protein-metallodrug interactions, driving the drug-biological target recognition and stabilizing the structure of the final adduct.[86] The binding of cisplatin, carboplatin and oxaliplatin to Met appears also interesting if one considers that Pt binding to S-donor ligands, including methionine and glutathione, occur in physiological conditions and that it plays a relevant role in the Pt-drugs metabolism. S-donor binding of Pt-drugs was suggested to be involved as an intermediate in transport to the DNA in nucleus.[86,89] Finally, our data point out that the three Pt drugs mainly bind proteins through formation of monodentate (like carboplatin or cisplatin in molecule A)[37] or bidentate (like oxaliplatin, or cisplatin in molecule B)[37] derivatives.

Before binding, the Pt complex needs to be activated. Activation consists of the release of labile ligands: two chlorides in the case cisplatin, the cyclobutandicarboxylate ligand in the case of carboplatin; oxalate in the case of oxaliplatin. The activation process and the consequent protein metalation may manifest a large kinetic variability depending on the nature of the leaving group and on the possible “assistance” offered by the protein.

3.1.4.4 Experimental section

Crystallization, Data collection and refinement

Oxaliplatin, carboplatin and RNase A (type XII-A), sodium citrate and PEG4K were obtained from Sigma. Crystals of the RNase A adducts were obtained by soaking experiments where pre-grown monoclinic

protein crystals were incubated with an excess of the platinum drug (at a protein to platinum ratio 1:10). This procedure has been already used to obtain crystals of productive complexes of RNase A including that with cisplatin[37] and other metallodrugs.[53,76,77] Briefly, the crystals of RNase A were grown as previously described[37,53,76,77] by hanging-drop vapor mixing 1 µL of RNase A at 20 mg mL^{-1} with equal volumes of reservoir solution containing 20% PEG4000 and 20 mM sodium citrate buffer pH 5.0 at 298 K. Two weeks after their appearance, crystals have been soaked for four days in a solution of carboplatin or oxaliplatin dissolved in 10 µL of reservoir. Final Pt drugs:protein concentration ratios were 10:1.

X-ray diffraction data have been collected from single crystals at the CNR Institute of Biostructure and Bioimages, Naples, Italy, using a Saturn944 CCD detector equipped with CuKα X-ray radiation from a Rigaku Micromax 007 HF generator. Crystals have been flash-frozen at 100 K using nitrogen gas produced by an Oxford Cryosystem (and maintained at 100 K during the data collection) without using cryoprotectants, following the dehydration procedure[42] already used in many other works.[40c,69,70] Data sets were processed and scaled using the HKL2000 package.[45] Although the soaking significantly affects the quality and the diffraction power of RNase A crystals, X-ray diffraction data have been collected at 2.09 Å and 2.27 Å resolution for carboplatin and oxaliplatin, respectively. Attempts to improve the resolution collecting datasets on crystals soaked with Pt drug with a reduced time of soaking (up to 5 hours) leads to acquisition of data corresponding to ligand-free RNase A. Data collection statistics are reported in table 8. The structures have been solved by molecular replacement method, using the PDB file 1JVT,[78] without water molecules and ligands, as starting model. The refinement was carried out with Refmac5,[46] model building and map inspections were performed using Coot.[47] 5% of the data was used for calculation of the R-free value. The initial 2Fo-Fc and Fo-Fc electron density maps clearly indicated the position of Pt ions. The binding of carboplatin induces the disordering of residues 16-22 and of the Tyr25 side chains, which are not included in the final model. The binding of oxaliplatin induces disordering of residues 16-23 in molecule A, 18-21 in molecule B and of Gln28 side chain. In this last structure residues 16-23 in molecule A and residues 18-19 in molecule B have been omitted from the final model, the other disordered residues (residues 16-17 and 20-21 of molecule B) are fitted in a poor electron density Refinement statistics are reported in table 8. Structure validation has been carried out using Procheck.[48] Coordinates

and structure factors for the adducts have been deposited in the Protein Data Bank (PDB codes 4S0Q and 4S18).

	RNase A-Carboplatin	RNase A-Oxaliplatin
PDB code	4S0Q	4S18
Data-collection		
Space group	C2*	C2*
Unit cell parameters		
a,b,c (Å)	100.52, 32.50, 72.71	100.72, 32.74, 73.23
β (°)	89.59	90.36
Molecules per asymmetric unit	2	2
Observed reflections	78969	70667
Unique reflections	14095	10764
Resolution (Å)	50-2.09 (2.14-2.09)	50-2.27 (2.29-2.27)
Completeness (%)	99.7 (100.0)	95.4 (93.8)
Rmerge†	0.124 (0.672)	0.161 (0.718)
I/σ(I)	12.0 (3.0)	10.5 (2.6)
Multiplicity	5.6 (5.6)	6.6 (5.1)
Refinement		
Resolution (Å)	30.9-2.09	50.0-2.27
number of reflections in working set	13380	10237
number of reflections in test set	709	520
R factor/Rfree (%)	0.205 (0.262)	0.224(0.301)
Number of non-H atoms used in the refinement	1948	1935
Occupancy of Pt ions	0.50/0.35	0.40/0.60 0.80/0.80 0.20/0.2*
B-factor of Pt ions	65.5/66.7	55.4/52.9/51.6/55.3/55.6/60.9
Overall B-factor	37.8	46.4
Deviations from ideality values		
R.m.s.d. bonds(Å)	0.016	0.012
R.m.s.d. angles(Å)	1.76	1.96

* for Met29/Asp14,His119 and His105 binding sites in the A and B chains

Table 8 Data collection and refinement statistics for the RNase A-carboplatin and RNase A-oxaliplatin structures.

ESI-MS experiments

A solution of cisplatin, carboplatin or oxaliplatin with RNase A (10^{-4} M) (3:1 metal/protein ratio) in 20 mmol L^{-1} ammonium acetate pH 6.8 was incubated at 37°C for one week and ESI-MS spectra were recorded after 24, 72 h and one week. After a 20-fold dilution with water, ESI MS spectra have been recorded by direct introduction at 5 µl min^{-1} flow rate in an Orbitrap high-resolution mass spectrometer (Thermo, San Jose, CA, USA), equipped with a conventional ESI source. The working conditions were the following: spray voltage 3.1 kV, capillary voltage 45 V, capillary temperature 220°C, tube lens voltage 230 V. The sheath and the auxiliary gases were set, respectively, at 17 (arbitrary units) and 1 (arbitrary units). For acquisition, Xcalibur 2.0. software (Thermo) was used and monoisotopic and average deconvoluted masses were obtained by using the integrated-Xtract tool. For spectrum acquisition, a nominal resolution (at m/z 400) of 100,000 was used.

References

[1] Casini A., Reedijk, J. Chem. Sci., **2012**, 3, 3135-3144.
[2] Dabrowiak J.C. (**2009**) *Metallo-Drugs and their interactions*. In Metals in Medicine, John Wiley & Sons Ltd, The Atrium, Southern Gate,Chichester, West Sussex, United Kingdom, pp 109-147.
[3] Gianferrara T., Bratsos I. and Alessio E. Dalton Trans., **2009**, 7588-7598.
[4] Shi Y., Liu Shu-an, Kerwood D.J.,Goodisman J., Dabrowiak J.C. J. Inorg. Biochem., **2012**, 107, 6-14.
[5] Ghote Y., Messori L., Marzo T., Metzler-Nolte N. Chem. Comm., **2015**, 51, 3151-3153.
[6] Mügge C., Marzo T., Massai L., Hildebrandt J., Ferraro G., Merlino A., Metzler-Nolte N., Messori L., Weigand W. Inorg. Chem., **2015**, 54, 8560-8570.
[7] Ferraro G., Massai L., Messori L., Merlino A. Chem. Commun., **2015**, 51,46, 9436-9439.
[8] Rudnev A.V., Aleksenko S.S., Semenova O., Hartinger C.G., Timerbaev A.R. and Keppler B. J. Sep. Sci., **2005**, 28, 121-127.
[9] Gabbiani C. (**2009**) *Proteins as possible targets for antitumor metal complexes: biophysical studies of their interactions*, Firenze University Press, Premio FUP. Tesi di dottorato 9.
[10] Timerbaev A.R., Hartinger C.G., Aleksenko S.S., Keppler B.K. Chem.Rev., **2006**, 106, 2224-2248.
[11] M. J. McKeage, *Drug Safety* **1995**, *13,* 228-244.
[12] Carter D.C. and Ho J.X. Adv. Protein Chem., **1994**, 45, 153-203.
[13] Peters T. Jr. Adv. Protein Chem., **1985**, 37, 161-245.
[14] He X.M. and Carter D.C. Nature, **1992**, 358, 209-215.
[15] Fasano M., Curry S., Terreno E., Galliano M., Fanali G., Narciso P., Notari S. and Ascenzi P. IUBMB Life, **2005**, 57, 787-796.
[16] Liu M., Lim Z.J., Gwee Y.Y., Levina A. and Lay P.A. Angew. Chem. Int. Ed., **2010**, 49, 1661-1664.
[17] Esposito B.P., Najjar R. Coord. Chem. Rev., **2002**, 232, 137-149
[18] Sun H., Li H., Sadler P.J. Chem. Rev., **1999**, 99, 2817-2842.
[19] Young S.P., Bomford A., Williams R. Biochem. J., **1984**, 219, 505-510.
[20] Messori L., Marzo T., Sanches R.N., Rehman H.-U., de Oliveira Silva D. and Merlino A. Angew. Chem., Int. Ed., **2014**, 53, 6172-6175.
[21] Messori L., Scaletti F., Massai L., Cinellu M.A., Gabbiani C., Vergara A. and Merlino A. Chem. Commun., **2013**, 49, 10100-10102.

[22] A. Vergara, D' Errico G., Montesarchio D., Mangiapia G., Paduano L. and Merlino A. Inorg. Chem., **2013**, 52, 4157-4159.
[23] Blake C.C.F., Koenig D.F., Mair G.A., North A.C.T., Phillips D.C., Sarma V.R. Nature, **1965**, 206, 757-761.
[24] Schwalbe H., Grimshaw S.B., Spencer A., Buck M., Boyd J., Dobson C.M., Redfield C. and Smith L. Protein Sci., **2001**, 10, 677-688.
[25] Hirs C.H.W., Moore S., Stein W.H.J. Biol. Chem., **1960**, 235, 633-647
[26] Smyth D.G., Stein W.H., Moore S.J. Biol. Chem., **1963**, 238, 227-234.
[27] Kartha G., Bello J., Harker D. Nature, **1967**, 213, 862-865.
[28] Raines R.T. Chem. Rev., **1998**, 98, 1045-1065.
[29] (a) Siddik Z.H. Oncogene, **2003**, 22, 7265-79. (b) Kelland L. Nature Reviews Cancer, **2007**, 7, 573-84. (c) Green M.H. J. Nat Cancer Inst., **1992**, 84, 306–312. (d) Sanderson B.J.S., Ferguson L.R., Denny W.A. Mutat. Res-Fundam. Mol. Mech. Mut., **1996**, 355, 59-70. (e) Rixe O., Ortuzar W., Alvarez M., Parker R., Reed E., Paull K., Fojo T. Biochem. Pharmacol. **1996**, 52, 1855-1865.
[30] (a) Todd R.C., Lippard S.J. Metallomics. **2009**, 1, 280-91; (b) Wang D., Lippard S.J. Nat. Rev. Drug Discov., **2005**, 4, 307-20; (c) Zhai X., Beckmann H., Jantzen H.M., Essigmann J.M. Biochemistry **1998**, 37, 16307-16315; (d) Eastman A. Pharmacol. Ther. **1987**, 34, 155-166; (e) Ohndorf M., Rould M.A., He Q., Pabo C.O., Lippard S. J. Nature **1999**, 399, 708-712; (f) Casini A., Gabbiani C., Mastrobuoni G., Messori L., Moneti G., Pieraccini G. Chem. Med. Chem. **2006**, 1, 413-417.
[31] Raymond E., Faivre S., Chaney S., Woynarowski J., Cvitkovic E. Mol. Cancer Ther. **2002**, 1, 227-235.
[32] (a) André T., Boni C., Mounedji-Boudiaf L., Navarro M., Tabernero J., Hickish T., Topham C., Zaninelli M., Clingan P., Bridgewater J., Tabah-Fisch I., de Gramont A. N. Engl. J. Med, **2004**, 350, 2343-2351; (b) Raymond E., Chaney S.G., Taamma A., Cvitkovic E. Ann. Oncol., **1998**, 9, 1053-1071; (c) Seetharam R., Sood A., Goel S. Ecancermedicalscience, **2009**, 3, 153; (d) M.A. Jakupec, M.Galanski, V. B. Arion, C.G. Hartinger, B.K. Keppler. Dalton Trans., **2008**, 2, 183-94; (e) O.M. Alian, A.S. Azmi, R. M. Mohammad. Clin. Transl. Med., **2012**,1,26; (f) Y. Kidani. Drugs Future, **1989**, 14, 529-532.
[33] (a) C.A. Rabik, M.E. Dolan, Canc. Treat. Rev., **2007**, 33, 9-23; (b) O. Pinato, C. Musetti, C. Sissi. Metallomics, **2014**, 6, 380-395.
[34] Panzner M.J., Bilinovich S.M., Youngs W.J. and Leeper T.C. Chem. Commun., **2011**, 47, 12479-12481.

[35] (a) Mandal R., Kalke R., Xing-Fang L. Rapid Commun. Mass Spectrom., **2002**, 17, 2748-2935. (b) Zhao T., King. F.L. J. Am. Soc. Mass Spectrom., **2009**, 20, 1141-1147; (c) Gibson D., Costello C.E. Eur. J. Mass Spectrom., **1999**, 5, 501-510; (d) Hartinger C.G., Ang W.H., Casini A., Messori L., Keppler B.K., Dyson P.J. J. Anal. At. Spectrom., **2007**, 22, 960-967.
[36] (a) Casini A., G. Mastrobuoni, C. Temperini, C. Gabbiani, S. Francese, G. Moneti, C.T. Supuran, A. T. Scozzafava, L. Messori. Chem. Commun. **2007**, 2, 156-158; (b) Tanley S.W.M., A.M.M. Schreurs A.M.M., Kroon-Batenburg L.M.J., Meredith J., Prendergast R., Walsh D., Bryant P., Levy C., Helliwell J.R. Acta Cryst., **2012**, D68, 601-612; (c) Helliwell J.R., Tanley S.W.M. Acta Cryst., **2013**, D69, 121-125; (d) Tanley S.W.M., Schreurs A.M.M., Kroon-Batenburg L.M.J., Helliwell J.R. Acta Cryst., **2012**, F68, 1300-1306.
[37] Messori L., Merlino A. Inorg. Chem., **2014**, 53, 3929-3931.
[38] (a) Calderone V., Casini A., Mangani S., Messori L., Orioli P.L. Angew. Chem., **2006**, 45,1267-1269; (b) Banci L., Bertini I., Blazevits O., Calderone V., Cantini F., Mao J., Trapananti A., Vieru M., Amori I., Cozzolino M., Carrì M.T. J. Am. Chem. Soc., **2012**, 134, 7009-7014.
[39] (a) Palm M.E., Weise C.F., Lundin C., Wingsle G., Nygren Y., Björn E., Naredi P., Wolf-Watz M., Wittung-Stafshede P. Proc. Natl. Acad. Sci. USA, **2011**, 108, 6951-6956; (b) Boal A.K., Rosenzweig A.C. J. Am. Chem. Soc., **2009**, 131, 14196-14197; (c) Arnesano F., Banci L., Bertini I., Felli I.C., Losacco M., Natile G. J. Am. Chem. Soc., **2011**, 133, 18361-18369.
[40] (a) Messori L., Scaletti F., Massai L., Cinellu M.A., Gabbiani C., Vergara A. and Merlino A. Chem. Commun., **2013**, 49, 10100-10102; (b) Messori L., Marzo T., Gabbiani C., Valdes A.A., Quiroga A.G., Merlino A. Inorg. Chem. **2013**, 52, 13827-13829; (c) Messori L., Merlino A. Dalton Trans. **2014**, 43, 6128-6131. (d) Santos-Silva T., Mukhopadhyay A., Seixas J.D., Bernardes G.J., Romao C.C., Romao M.J. J. Am. Chem. Soc., **2011**, 133, 1192-1195; (e) Messori L., Marzo T., Sanches R.N., Rehman H.-U., de Oliveira Silva D. and Merlino A. Angew. Chem., Int. Ed., **2014**, 53, 6172-6175.
[41] Allardyce C.S., Dyson P.J., Coffey J., Johnson N. Rapid Commun. Mass Spectrom., **2002**, 16, 933-935.
[42] Russo Krauss I., Sica F., Mattia C.A., Merlino A. Int. J. Mol. Sci., **2012**, 13, 3782-3800.
[43] Pellegrini E., Piano D., Bowler M.W., Acta Cryst.D, **2011**, 67, 902-906.

[44] Messori L., Merlino A. Dalton Trans., **2014**, 43, 6128-6131.
[45] Otwinowski Z., Minor W. Methods Enzymol., **1997**, 276, 307-326.
[46] Murshudov N., Skubak P., Lebedev A.A., Pannu N.S., Steiner R.A., Nicholls R.A., Winn M.D., Long F., Vagin A.A. Acta Cryst.D, **2011**, 67, 355-367.
[47] Emsley P., Cowtan K. Acta Cryst.D, **2004**, 60, 2126-2132.
[48] Laskowski R.A., Macarthur M.W., Moss D.S., Thornton. J.M. J Appl Cryst, **1993**, 26, 283-291.
[49] Bruck M.A., Bau R., Noji M., Inagaki K., Kidani Y. Inorg. Chimica Acta, **1984**, 92, 279-284.
[50] Spingler B., Whittington D.A., Lippard S.J. Inorg. Chem., **2001**, 40**,** 5596-5602.
[51] Messori L., Marzo T., Merlino A. Chem. Commun., **2014**, 50 , 8360-8362.
[52] Tanley S.W.M., Diederichs K., Kroon-Batenburg L. M., Levy C., Schreurs A.M., Helliwell J.R. *Acta Cryst.* F, **2014**, 70, 1135-1142.
[53] Messori L., Marzo T., Michelucci E., Russo Krauss I., Navarro-Ranninger C., Quiroga A.G., Merlino A. Inorg Chem*,* **2014**, 53, 7806-7808.
[54] Ferraro G., Messori L., Merlino A. Chem Commun*,* **2015**, 51, 2559-2561.
[55] Verma D., Jacobs D.J., Livesay D.R. *PLOS* Computational Biology, **2012**, 8:e1002409.
[56] Delaloge S., Laadem A., Taamma A., Chouaki M., Cvitkovic E. , Pautier P., Misset J.L., Lhommé C., Am. J. Clin. Onc., **2000**, 23, 569-74.
[57] Soulie P., Bensmaine A., Garrino C., Chollet P., Brain E., Fereres M., Jasmin C., Musset M., Misset J.L., Cvitkovic E. Eur. J. Cancer*,* **1997**, 33, 1400-1406.
[58] Soulie P., Garrino C., Bensmaine M.A., Bekradda M., Brain E., Di Palma M., Goupil A., Misset J.L., Cvitkovic E. J. Cancer Res. Clin. Oncol*.,* **1999**, 125, 707-711.
[59] Mathe G., Chenu E., Bourut C., Florentin I. Proc. Am. Assoc. Cancer. Res*.,* **1989**, 30, 471.
[60] Mathe G., Kidani Y., Segiguchi M., Eriguchi M., Fredj G., Peytavin G., Misset J.L., Brienza S., de Vassals F., Chenu E. Biomed. Pharmacother., **1989**, 43, 237-50.
[61] Rixe O., Ortuzar W., Alvarez M., Parker R., Reed E., Paull K., Fojo T. Proc. Am. Soc. Clin. Oncol, **1998**, **17**, 302a.
[62] Mita C., Chatelut E., Bekradda M., Soulié P., Canal P., Misset J.L., Cvitkovic E., Buga R. Annals of Oncology, **2003**, 14, 1776-1782.

[63] Zhang N., Du Y., Cui M., Liu Z., Liu S. Anal. Bioanal Chem., **2014**, 406, 3537-3537.
[64] Helliwell J.R., Tanley S.W.M. Acta Cryst. D, **2013**, 69, 121-125.
[65] Zheng X.H., Zhong Y.F., Tan C.P., Ji N.N., Mao Z.W. Dalton Trans., **2012**, 41, 11807-11812.
[66] Curis E., Provost K., Bouvet D., Nicolis I., Crauste-Manciet S., Brossard D., Benazeth S. J. Synchrotron. Rad., **2001**, 8, 716-718.
[67] Nessa M.U., Beale P., Chan C., Yu J.Q., Hug F. Anticancer Res., **2011**, 31, 3789-3797.
[68] Nessa M.U., Beale P., Chan C., Yu J.Q., Hug F. Anticancer Res. **2012**, 32, 4843-4850.
[69] Messori L., Cinellu M.A., Merlino A. ACS Med. Chem. Letters, **2014**, 5, 1110-1113.
[70] Russo Krauss I., Messori L., Cinellu M.A., Marasco D., Sirignano R., Merlino A., Dalton Trans., **2014**, 43, 17483-17488.
[71] McCoy A.J., Grosse-Kunstleve R.W., Adams P.D., Winn M.D., Storoni L.C., Read R.J. J. Appl. Cryst., **2007**, 40, 658-674.
[72] Huliciak M., Reinhard L., Laursen M., Fedosova N., Nissen P., Kubala M. Biochem. Pharmacol., **2014**, 92, 494-498.
[73] Sadler P.J., Benz F.W., Roberts G.C.K. Biochim. Biophys. Acta **1974**, 359, 13-21.
[74] Helliwel J.R., Tanley S.W.M. Acta Cryst.F, **2014**, 70, 1127-1131.
[75] Picone, D., Donnarumma F., Ferraro G., Russo Krauss I., Fagagnini A.; Gotte G., Merlino A. J. Inorg. Biochem., **2015**, 146, 37-43.
[76] Vergara A., Montesarchio D., Russo Krauss I., Paduano L., Merlino A. Inorg. Chem., **2013**, 52, 10714-10716.
[77] Messori L., Scaletti F., Massai L., Cinellu M.A., Russo Krauss I., di Martino G., Vergara A., Paduano L., Merlino A. Metallomics, **2014**, 6 233-236.
[78] Vitagliano L., Merlino A., Zagari A., Mazzarella L. Proteins, **2002**, 46, 97-104.
[79] Moustafa E.M., Camp C.L., Youssef A.S., Amleh A., Reid H.J., Sharp B.L., Shoeib T. Metallomics, **2013**, 5, 1537-1546.
[80] Shoeib T., Sharp B. L. Metallomics, **2012**, 4, 1308-1320.
[81] Lucas M.F.A., Pavelka M., Alberto M.E., Russo N.J. Phys. Chem. B, **2009**, 113, 831-838.
[82] Luo F.R., Wyrick S.D., Chaney S.G. Cancer Chemother. Pharmacol., **1999**, 44, 29-38.
[83] Barnham K.J., Frey U., Murdoch P.S., Ranford J.D., Sadler P.J., Newell D.R. J. Am. Chem. Soc., **1994**,116, 11175-11176.

[84] Marasco D., Messori L., Marzo T.; Merlino A. Dalton Trans., **2015**, 10392-10398.
[85] Pendyala L., Creaven P.J. Cancer Research, **1993**, 53, 5970-5976.
[86] Lempers E.L.M., Inagaki K., Reedijk J. Inorg. Chim. Acta, **1988**, 3, 201-207.
[87] Li C., Li Z., Sletten E., Arnesano F., Iosacco M., Natile G., Liu Y. Angew. Chem. Int. Ed. Engl., **2009**, 48, 8497-8500.
[88] van Boom S.S.G.E., Reedijk J. J. Chem. Soc., Chem. Commun. **1993** 1397-1398.
[89] Lempers E.L.M., Reedijk J. Inorg. Chem., **1990**, 29, 217-222.

4

cis-$PtI_2(NH_3)_2$: A REAPPRAISAL

4. *cis*-$PtI_2(NH_3)_2$: A REAPPRAISAL

The results presented in this chapter have been published in the following manuscripts:

*Luigi Messori, Tiziano Marzo, Chiara Gabbiani, Amparo A. Valdes, Adoracion G. Quiroga, and Antonello Merlino "Peculiar Features in the Crystal Structure of the Adduct Formed between cis-$PtI_2(NH_3)_2$ and Hen Egg White Lysozyme", **2013**,52, 13827-13829.*

*Tiziano Marzo, Serena Pillozzi, Ondrej Hrabina, Jana Kasparkova, Viktor Brabec, Annarosa Arcangeli, Gianluca Bartoli, Mirko Severi, Alessandro Lunghi,Federico Totti, Chiara Gabbiani, Adóracion G. Quiroga and Luigi Messori "cis-$PtI_2(NH_3)_2$: a reappraisal", **2015**, Dalton Trans., 44, 14896-14905.*

4.1 Introduction

It was long believed that iodido analogues of classical anticancer platinum(II) compounds should be poor pharmacological agents, their inactivity being ascribed to the greater stability and lower reactivity of Pt-I bonds as compared to Pt-Cl bonds in aqueous solution.[1-3] Moreover, early studies on *cis*-$PtI_2(NH_3)_2$ reported it to be inactive as an anticancer agent in an animal model.[4] These considerations greatly hampered the further development of iodidoplatinum complexes as experimental anticancer agents. However, a few subsequent studies highlighted a considerable and unexpected reactivity for iodido Pt(II) and Pt(IV) complexes[5] toward important biomolecular targets (e.g. serum albumin and glutathione).[6,7] For the reasons reported above it is important to reconsider in more depth iodidoplatinum complexes as a source of new anticancer agents, for which there is still a wide margin for the development of new molecules with different chemical properties that could present innovative characteristics, and hopefully ability to overcome the limits of the conventional anticancer drugs.

4.1.1 Peculiar features in the interaction between lysozyme and *cis*-$PtI_2(NH_3)_2$

4.1.1.1 Introduction

In chapter 3, we have shown as, through a comparative study of cisplatin, carboplatin and oxaliplatin, it is possible to find interesting differences in their interaction with model proteins. Remarkably, a tentative correlation between the differences in their protein metalation and their well known pharmacological effects, has been highlighted. Overall, cisplatin and carboplatin that have similar pharmacological effect, behave very similarly, while oxaliplatin, that possesses a quite different pharmacological characteristics, exerts its interaction with protein in a different manner. These considerations, lead us to investigate the reaction of iodido analogues of cisplatin, a family of potential anticancer drugs, overlooked so far, toward the model protein lysozyme. Although cisplatin remains one of the most effective chemotherapeutic agents for cancer treatment, recently, a number of *cis* and *trans* diaminediiodoplatinum compounds (such as *cis*-$PtI_2(ammine)_2$, *trans*-$PtI_2(ammine)_2$) showing unconventional reactivity have been synthetized

and their cytotoxicity evaluated towards a number of human tumor cell lines.[8,9]
As a model for the interaction of iodido analogues of platinum(II) drugs with proteins, and to compare directly results with cisplatin, the cisplatin analogue *cis*-$PtI_2(NH_3)_2$, has been chosen to perform a detailed investigation of its reactions with HEWL by X-ray crystallography and ESI-MS spectrometry.

4.1.1.2 Results

Crystals of the adduct between HEWL and *cis*-$PtI_2(NH_3)_2$ have been obtained by soaking experiments where pre-grown HEWL crystals were incubated for two months with an excess of the platinum drug.
These crystals were subject to X-ray diffraction data collection and the structure of the adduct could be solved at 1.99 Å resolution. Details of crystallization, data collection and structure refinement are given in the experimental section. The overall structure of the adduct between HEWL and *cis*-$PtI_2(NH_3)_2$ (HEWL-*cis*-$PtI_2(NH_3)$ adduct) (Figure 1), which refines to Rfactor=18.4 (Rfree=23.4), is very similar to that of the native protein (PDB code 193L): the root mean square deviation in positions of CA atoms is 0.3 Å**.**

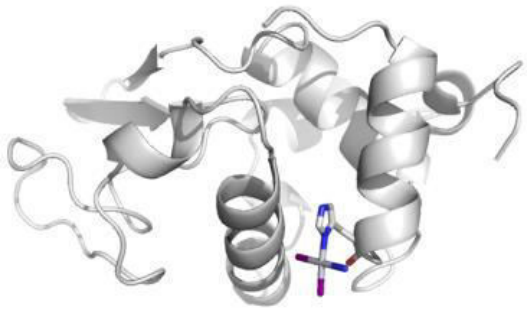

Figure 1 Ribbon representation of the structure of the adduct between HEWL and *cis*-$PtI_2(NH_3)_2$. The side chain of His15, which is solvent accessible, being situated on the protein surface, is shown along with Pt, ammonium and I ligands. For sake of clarity just one of the two different modes of binding of *cis*-$PtI_2(NH_3)_2$ to HEWL is shown. The structure has been deposited in the Protein Data Bank under the accession code 4MR1.

In agreement with what found in the case of cisplatin by Casini *et al.*,[10] platination occurs at the ND1 atom of the imidazole ring of His15, i.e. at the right-handed site. The local environment of the protein bound Pt(II) center was identified by observation of a very clear electron density map (Figure 2). Notably, the Pt(II) ion is coordinated to ND1 atom of His15, to two I atoms and a N, in a classical square planar geometry. The refinement of temperature factors of Pt ligands and the inspection of residual Fo-Fc electron density maps indicate that two equivalent modes of Pt binding are present in the crystal structure, which differ only in the location of I atoms with respect to ND1 of His15 (Figure 3). The existence of two alternative modes of binding was further supported by inspection of the anomalous scattering map which confirmed the presence of anomalous signals of I and Pt atoms in the binding moieties (Figure S9 in the supplementary material).

In the former mode of binding, the NH_3 group is close to N and OD1 atoms of Asn93 (distances 3.8 and 4.5 Å, respectively); in the latter, the NH_3 group is solvent exposed and interacts with two water molecules, which, in turn are in contact with Arg14, whereas I atom occupies the position close to Asn93 (Figure 3A and 3B). Within these assumptions, His(N)-Pt distance is of 2.1 Å, whereas the Pt-I and Pt-N(NH_3) distances are, on average, both close to 2.4 Å

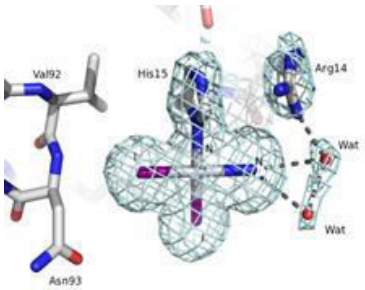

Figure 2 Details of the binding site of Pt(II) in HEWL-*cis*-$PtI_2(NH_3)$ showing the Pt ion bound to His15. 2Fo-Fc electron density maps are contoured at 1σ level. For sake of clarity just one of the two different modes of binding of *cis*-$PtI_2(NH_3)_2$ to HEWL is shown.

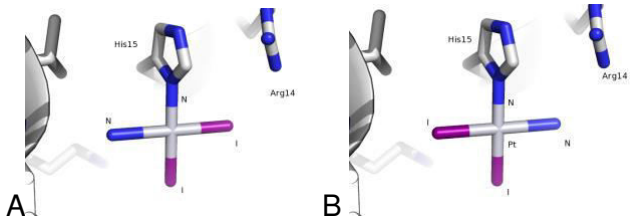

Figure 3 The two modes of binding of *cis*-$PtI_2(NH_3)_2$ to HEWL. I atoms are coloured in purple, N atoms are coloured in blue.

Remarkably, the present structure shows that the platinum(II) ion binds the protein with an occupancy value close to 1.0. To the best of our knowledge, this is the highest occupancy ever observed for Pt in adducts between proteins and cisplatin-like drugs. No other significant modifications of the electron density map were observed ruling out the presence of additional (secondary) binding sites. This finding supports the view that the interaction of cisplatin-like drug with HEWL is highly selective for His15.

Independent valuable information on the same system was subsequently gained through application of ESI-MS (see experimental section). Electrospray ionization mass spectrometry is indeed a powerful and informative tool to characterise the interactions of metal based drugs with small model proteins. Precise information may be derived on the stoichiometry and kinetics of binding as well as on the exact nature of the protein bound metal fragments.[9,11,12] HEWL dissolved in a suitable buffer (20 mM ammonium acetate buffer, pH 6.8) was treated with a 3:1 excess of a fresh solution of the study compounds and ESI-MS spectra measured after increasing time intervals. Deconvoluted ESI-MS spectra recorded at the indicated time intervals (6, 24, 48 and 72 h) are shown in figure 4. Progressive formation of adducts is well witnessed by the appearance of a number of peaks of higher molecular mass than the native protein. Interestingly, the dominant peak within those attributed to platinum adducts shows a value of 14769.63 Da, that perfectly matching the mass of an adduct where a single $[PtI_2NH_3]$ fragment is bound to the protein. This observation offers further and independent support to the above reported crystallographic results.

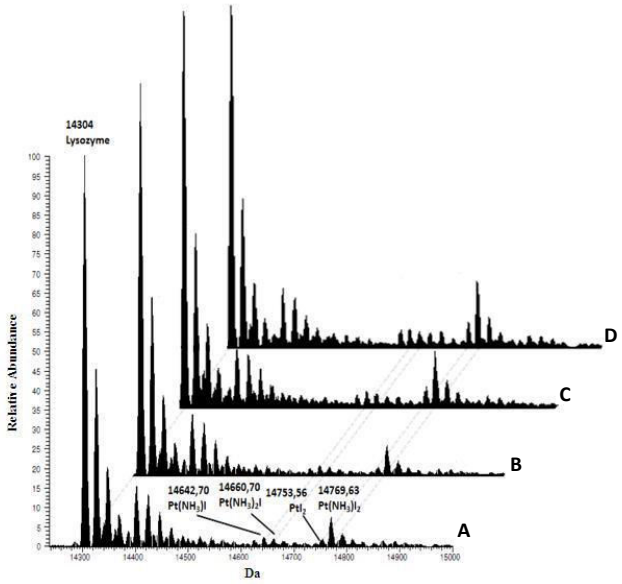

Figure 4 . Deconvoluted ESI MS of HEWL treated with 10^{-4} M *cis*-$PtI_2(NH_3)_2$ (metal:protein ratio = 3:1) in 20 mM ammonium acetate (pH 6.8) buffer recorded after 6h (A), 24h (B), 48h (C), 72 h (D) of incubation at RT.

4.1.1.3 Discussion and conclusions

In conclusion we have provided here unambiguous structural evidence that the diiodido analogue of cisplatin forms stable protein adducts containing a different type of protein bound metal fragment. While cisplatin typically affords protein platination through coordination of a $[Pt(NH_3)_2]^{2+}$ fragment to selected protein side-chains,[10] *cis*-$PtI_2(NH_3)_2$ preferentially gives rise to a protein bound $[PtI_2NH_3]$ fragment with full retention of the two halide ligands. This finding is of great interest implying that the diiodido analogue produces a type of biomolecular metalation remarkably distinct from that inferred by cisplatin. It would be interesting to verify if this kind of metalation is operative even toward double helix DNA. This might result in different patterns of DNA and proteins platination and, accordingly, in a different pharmacological profile. Thus, the present results highlight that the simple chloride to iodide replacement in cisplatin may have spectacular consequences on the reactivity and the biological actions of platinum(II) compounds and may lead to classes of innovative platinum compounds not obeying classical Hoeschele's rules.[4]

4.1.1.4 Experimental section

Synthesis of *cis*-$PtI_2(NH_3)_2$

cis-$PtI_2(NH_3)_2$ was synthesized according to published procedures, using (1:4) Pt:KI in order to avoid further purifications.[8,13] The purity of the product was checked by elemental analysis of C, N and H [Calculated C: 0%, H: 1,26%, N: 5,84%, Experimental: C: 0%, H: 1,12%, N: 5,71%.], and as described in ref. 14. The correct *cis* geometry was assessed by comparison with its *trans* analogue as describe in the literature.[14,15]

Crystallization, Data collection and refinement

HEWL crystals were grown at 293 K using the hanging drop vapour diffusion method. The reservoir (600 µL) contained 20 mM sodium acetate buffer at pH 4.2 and 1.0 M NaCl; the drop (0.5+0.5 µL) contained hen egg white lysozyme (10 mg mL^{-1}) in the same acetate buffer (5mM) and reservoir solution. Crystals grow in 1 day. After 5 days, HEWL crystals were soaked for two months in a DMSO solution of *cis*-$PtI_2(NH_3)_2$. Final concentration of the metal complex in solution was >10 times higher than HEWL. X-ray diffraction data were collected at the Institute of Biostructures and Bioimages using a Saturn944 CCD detector equipped with CuKα wavelength X-ray radiation from a Rigaku Micromax 007 HF generator at 100 K. Data were collected without cryoprotectant, using a procedure recently developed.[16] This procedure partly dehydrates the crystals, enhancing in some cases the resolution of X-ray diffraction data.[17] Data were processed using the program HKL2000.[18] The structure was solved using the Fourier difference method and the structure of HEWL without ligands deposited in the Protein Data Bank with code 4JS3[19] as starting model. The refinement has been performed using CNS.[20] Model building and map inspections were performed using O.[21]
The coordinates have been deposited in the Protein Data Bank (PDB) under the accession code 4MR1. Data statistics: space group, $P4_32_12$; unit cell, 77.02 Å, 77.02 Å, 36.83 Å; Resolution range: 50–1.99Å; observed reflections (unique) = 14571 (743); I/σ(I) = 47.6 (1.9); completeness = 99.9 % (100%); Rmerge: 10.9% (71.0%). Values in parenthesis relate to the highest resolution shell (2.02–1.99 Å). Refinement: R-factor: 18.4%, R-free: 23.4%; rms bonds = 0.018Å, rms angles (°) = 3.82.

ESI-MS experiments

A solution of *cis*-$PtI_2(NH_3)_2$ (10^{-4} M) with HEWL (3:1 metal/protein ratio) was incubated at RT for 72 h and ESI MS spectra were recorded after 6, 24, 48, 72 h. After a 20-fold dilution with water, ESI-MS spectra were recorded by direct introduction at 5 µl/min flow rate in an Orbitrap high-resolution mass spectrometer (Thermo, San Jose, CA, USA), equipped with a conventional ESI source. The working conditions were the following: spray voltage 3.1 kV, capillary voltage 45 V, capillary temperature 220°C, tube lens voltage 230 V. The sheath and the auxiliary gases were set, respectively, at 17 (arbitrary units) and 1 (arbitrary units). For acquisition, Xcalibur 2.0. software (Thermo) was used and monoisotopic and average deconvoluted masses were obtained by using the integrated Xtract tool. For spectrum acquisition a nominal resolution (at m/z 400) of 100,000 was used.

4.1.2 Further insight into antineoplastic properties of *cis*-$PtI_2(NH_3)_2$

4.1.2.1 introduction

As reported in paragraph 4.1, iodide analogues of cisplatin possess peculiar characteristic concerning their reactivity toward model protein with respect to cisplatin. It is also quite surprising that, despite the huge research efforts made on platinum analogues over the last three decades, only rare studies were carried out on *cis*-$PtI_2(NH_3)_2$ (*cisPtI*$_2$), the strict iodo analogue of cisplatin. Accordingly, even the cytotoxicity profile of *cisPtI*$_2$ against the 60 cancer cell lines panel of NCI has never been reported.
Altogether, these arguments led us to reconsider, in a more systematic way, some key chemical and biological aspects of *cisPtI*$_2$ with respect to cisplatin.
Specifically, we have focused our attention on the four following issues : *i*) the activation process of *cisPtI*$_2$ in aqueous solutions both at physiological and slightly acidic pH; *ii*) a computational rationalization of the spectral results; *iii*) the investigation of the direct reaction of *cisPtI*$_2$ with DNA; *iv*) the cellular effects of *cisPtI*$_2$ in a small panel of cancer cell lines. Some notable results have emerged from these studies that are comprehensively analysed and discussed here in direct comparison to cisplatin, with relevant mechanistic and medical implications.

4.1.2.2 Results

Solution Chemistry of *cis*-$PtI_2(NH_3)_2$: logP determination and activation profile in aqueous buffers

We first investigated some unexplored chemical features of *cisPtI*$_2$; in particular we determined its logP value and analysed its solution behaviour under various conditions and the inherent metal complex activation processes.
The logP of *cisPtI*$_2$ was measured according to the method reported in the experimental section; a value of -0.13 was determined versus a value of -2.4 previously determined for cisplatin and here again confirmed. This result implies that *cisPtI*$_2$, in its intact form, is far more lipophylic than cisplatin: this might have some appreciable impact on its cellular uptake (see later).
Then, the solution behaviour of *cisPtI*$_2$ was studied spectrophotometrically under physiological-like or slightly acidic pH conditions. Remarkably,

freshly prepared aqueous solutions of *cisPtI*$_2$, at pH=7.4, manifest two intense bands in the UV-visible region, located at 290 and 350 nm, respectively, that allow the direct and continuous monitoring of the solution behaviour of this platinum complex (Figure 5).

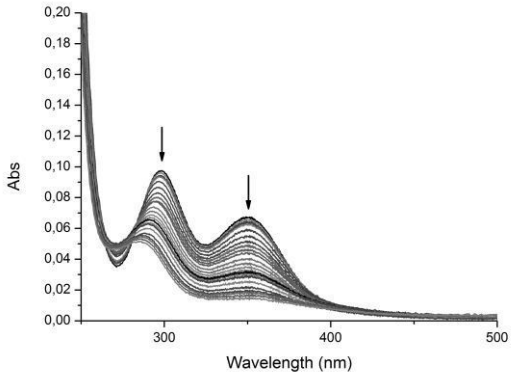

Figure 5 time dependent UV-Vis analysis of complex *cis*-$PtI_2(NH_3)_2$ 10^{-4} M in 50 mM phosphate buffer (pH=7.4) followed for 72 h.

Some important spectral changes are slowly detected consisting in the progressive and regular decrease of the two main bands and in the appearance of a new band, of lower intensity, around 280 nm. The observed spectral changes are tentatively traceable to the progressive release of the two iodido ligands and to their replacement by water molecules. This would mean that the aquation process of *cisPtI*$_2$ reproduces quite closely that of cisplatin, involving the progressive detachment of the two halide ligands while both ammonia ligands are kept as confirmed by some further experiments. In particular, addition of KI at increasing concentrations completely abolished and even reverted the above described spectral changes (see supplementary material) strongly supporting the proposed interpretation. In any case, the rate of the aquation process for *cisPtI*$_2$ is appreciably slower than for cisplatin (by at least a factor 2) possibly because of the greater strength of the *Pt-I* bond and/or greater inertness related to the increased "soft" character of iodide over chloride (more details for hydrolysis process and UV-Vis analysis are given in the supplementary material).

To gain further insight into the activation processes of *cisPtI*$_2$, we also analysed its spectral behaviour under slightly acidic conditions. Indeed, a

mildly acidic environment is thought to destabilise the ammonia ligands and thus favour ammonia release over iodide release. Accordingly, *cisPtI$_2$* was dissolved in an acetate buffer, at pH 4.5, and its spectral changes monitored over 72 hours. The resulting spectral profile is shown in figure 6: it is apparent that the overall spectral profile is profoundly different from that recorded at physiological pH. In particular, a new and quite intense visible band is clearly detected around 410 nm, at 72 hours, whose assignment is discussed later.

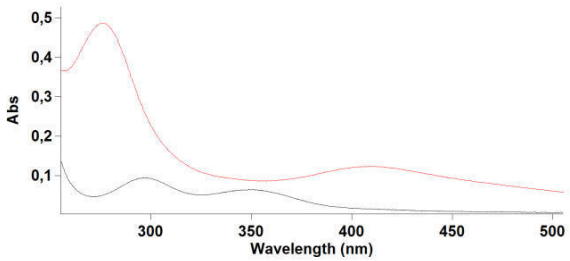

Figure 6 UV-Vis spectral changes of complex *cis*-Pt $I_2(NH_3)_2$ 10^{-4} M in 50 mM, acetate buffer (pH=4.5) followed for 72h. Gray line t=0 h, red line t=72 h.

Computational studies, simulation of UV-Vis spectra

To interpret the reported spectral profiles at two distinct pH values, we performed UV-Vis spectra simulations of 5 species: the native *cisPtI$_2$*, two products of the Iodido aquation mechanism i.e. [*cis*-PtI$(H_2O)(NH_3)_2]^+$ (**1**), [*cis*-Pt$(H_2O)_2(NH_3)_2]^{2+}$ (**2**) and two products related to ammonia aquation mechanism i.e. [*cis*-PtI$_2(NH_3)(H_2O)$] (**3**), [*cis*-PtI$_2(H_2O)_2$] (**4**).
The computed spectrum of *cisPtI$_2$* (cfr. *red line* in Figure 7**a**) is in very good agreement with the experimental one reported in figure 5. The calculated spectra for the mono- and di-Iodido hydrolysis species, i.e. (**1**) and (**2**), reproduce closely the experimental spectral evolution shown in figure 5, offering strong support to the iodide release mechanism.
Simulated bands assignments were done through transition density plots reported in figure 7**b**. It is possible to observe that, for *cisPtI$_2$*, band A is a LMCT transition, I,O($p_{x,y}$) →Pt(d_{x2-y2}), while band B is a platinum *d-d* transition, Pt(d_{xy}) → Pt($d_{x^2-y^2}$). Notably, band A changes from a LMCT to a platinum *d-d* character passing from *cisPtI$_2$* to species (**1**) and (**2**). For (**1**), both bands have a Pt(d_{xy}) → Pt($d_{x^2-y^2}$) character. For (**2**) we observed that (B) band observed for the *cisPtI$_2$* undergoes a blue shift until it turns into band (A).

Band B conserved the Pt(d_{xy}) → Pt($d_{x^2-y^2}$) character observed for (**2**). Such behavior is in agreement with expected *d* orbitals shifts due to substitution of a strong basic π donor as iodide with one water molecule.

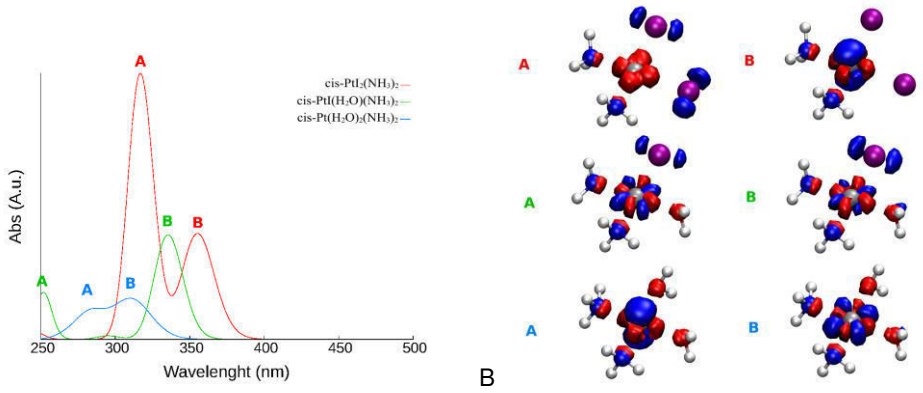

Figure 7 (**a**) Evolution of UV-Vis spectral features for the Iodide hydrolysis mechanism. (**b**) Evolution of the electronic transition's nature of A and B bands during the iodido aquation mechanism (*cis*-$PtI_2(NH_3)_2$ *top*, [*cis*-$PtI(H_2O)(NH_3)_2]^+$ *middle* and [*cis*-$Pt(H_2O)_2(NH_3)_2]^{2+}$ *bottom*): for each transition red densities correspond to arrival orbitals and blue densities correspond to starting molecular orbitals. Platinum ions are coloured in silver, nitrogen in blue, oxygen in red, iodide in violet and hydrogen in white.

To verify the correctness of the supposed iodide hydrolysis mechanism for physiological-like pH conditions, we have calculated the UV-Vis spectra (see Figure 8**a**) also for the species involved in the concurrent amino hydrolysis mechanism, i.e. (**3**) and (**4**). In this case, the two *cisPtI*$_2$ bands undergo a significant red shift keeping their shape and relative intensities practically unchanged. Interestingly, the same behavior is experimentally observed for acidic conditions (cfr. Figure 6), where, indeed, the release of the ammonia ligands is expected. Furthermore, since dimeric species of the type $[Pt(amine)I_2]_2$, that are active on selected cancer cell lines, were reported to be synthesised in acidic conditions,[34] additional ESI-MS experiments were carried out at pH=4.5. Formation of dimers in solution under the latter conditions is confirmed by the presence of few weak peaks assignable to these species (see supplementary material).

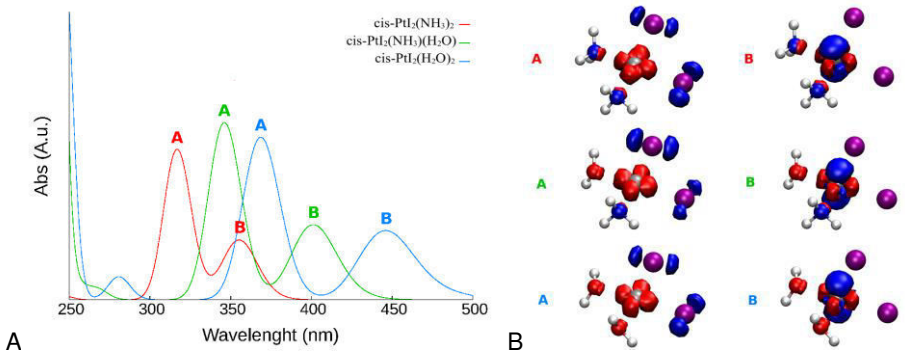

Figure 8 (**a**) Evolution of UV-Vis spectral features for the ammonia hydrolysis mechanism. (**b**) Evolution of the electronic transition's nature of A and B bands during the ammonia aquation mechanism (*cis*-$PtI_2(NH_3)_2$ *top*, [*cis*-$PtI_2(NH_3)(H_2O)$] *middle* and [*cis*-$PtI_2(H_2O)_2$] *bottom*): for each transition red densities correspond to arrival orbitals and blue densities correspond to starting molecular orbitals. Colour code as in Figure 7.

The difference transitions MOs analysis performed for this second group of molecules is shown in Figure 8**b**; it is observed that the nature of the main spectral transitions is retained for all species involved. In this case, only the shift of valence molecular orbitals has been observed due to the similar orbital contributions of ammonia and water molecules. Therefore bands (A) and (B) can be described as I,O($p_{x,y}$) → Pt(d_{x2-y2}), Pt(d_{xy}) → Pt($d_{x^2-y^2}$) transitions, respectively.

DNA binding properties of *cis*-$PtI_2(NH_3)_2$

To determine the nature of the DNA interactions of *cisPtI*$_2$, the DNA binding properties of this complex were examined through a variety of methods and compared with those of cisplatin. First, we aimed at quantifying the binding of *cisPtI*$_2$ to mammalian (CT) double-helical DNA in a cell free medium.
The amount of platinum bound to DNA increased with time and the times at which the binding reached 50% ($t_{50\%}$) are summarized in table 1.

Compound	$t_{50\%}$ (min)[a]
cis-$PtI_2(NH_3)_2$ aged in H_2O	105 ± 11
cisplatin aged in H_2O	64 ± 5
cis-$PtI_2(NH_3)_2$ aged in 10 mM KI	390 ± 24
cisplatin aged in 10 mM KCl	136 ± 19

[a] The time at which the binding reached 50%. Values shown in the table are the means ± SEM of three separate experiments.

Table 1 Binding of *cis*-$PtI_2(NH_3)_2$ and cisplatin to calf thymus DNA.

Importantly, after 24 h, *cisPtI*$_2$ and cisplatin aged in water or in 10 mM KI/KCl were quantitatively bound. As expected, the Pt^{II} complexes preincubated in water reacted with DNA significantly more rapidly than those preincubated in KI/KCl (10 mM), but the rate of the reaction of cisplatin was considerably higher than that of *cisPtI*$_2$.

The lower rate of the reaction of *cisPtI*$_2$ with double-helical DNA in comparison with that of cisplatin can be interpreted to mean[22] that the rate of the aquation of the leaving ligands in *cisPtI*$_2$ is significantly lower than that in cisplatin. Since interstrand and intrastrand cross-links formation are believed to be responsible for anticancer activity of bifunctional platinum compounds, we have quantitated the interstrand cross-linking efficiency of *cisPtI*$_2$ in the linear pUC19 DNA (linearized with EcoRI restriction enzyme). Results point out that interstrand cross-linking efficiency of *cisPtI*$_2$ (5 ± 2%) was similar to that of cisplatin (6 %) (see supplementary material for further details).[23]

Afterward, to gain more information about the adducts formed in the reaction of *cisPtI*$_2$ with DNA, in comparison with those produced by cisplatin, experiments with the fluorescent probe ethidium bromide have been carried out. Double helical DNA was first modified by the Pt^{II} complex (*cisPtI*$_2$ or cisplatin) for 24 h. The levels of the modification corresponded to the values of r_b in the range between 0 and 0.1. Modification of DNA by both platinum complexes resulted in a decrease of EtBr fluorescence (Figure 9).

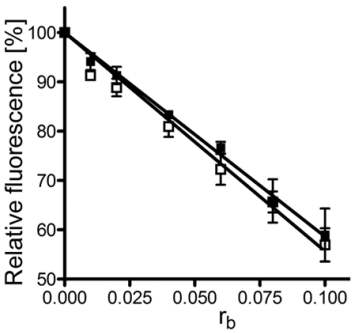

Figure 9 Ethidium bromide fluorescence. Dependences of the EtBr fluorescence on r_b for CT DNA modified by platinum complexes in 10 mM $NaClO_4$ at 37 °C for 24 h. Open symbols, *cis*-$PtI_2(NH_3)_2$; closed symbols, cisplatin.

The formation of adducts of *cisPtI*$_2$ resulted in a progressive decrease of EtBr fluorescence intensity, which was similar to that of cisplatin. This result suggests that the conformational distortion induced in DNA by the adducts of *cisPtI*$_2$ is delocalized and extends over the same number of base pairs around the platination sites as in the case of the adducts of cisplatin.

Even DNA unwinding experiment suggests the same mode of metalation between cisplatin and its iodide analogue (see supplementary material for further experimental details). Using this approach, we determined the DNA unwinding angles to be in the range 11 ± 2° for *cisPtI*$_2$, which is very similar to that found for cisplatin (13°).[24] Finally thermal stability experiment of DNA has been carried out.

CT DNA was modified by *cisPtI*$_2$ to the value of r_b = 0.03–0.09. After the modification, the salt concentration was further adjusted by addition of NaCl to 0.1 M, and the samples were further supplemented by Tris-HCl (1 mM) and EDTA (0.1 mM). Thus, the melting curves for DNA modified by the platinum compounds were measured at a relatively high salt concentration (Table 2). We found that the effect of DNA platination by *cisPtI*$_2$ on the melting temperature of DNA (t_m) is similar to that observed for the modifications by cisplatin.

Three major factors have been invoked to account for the thermal stability of DNA modified by Pt^{II} complexes capable of DNA cross-linking and the observed change in melting temperature of DNA as a consequence of its platination reflects the relative proportion and contribution of these three factors.[25]

These three factors are (i) a destabilizing effect of conformational distortions due to the formation of cross-links induced in DNA by platinum

coordination; (ii) stabilizing effects of DNA interstrand cross-links which prevent dissociation of DNA strands; (iii) the positive charge on the Pt^{II} centers (introduction of a positive charge into the DNA molecule, e.g. by binding of positively charged ligands such as Pt^{II} moieties of platinum compounds, results in a stabilization of the DNA duplex by decreasing electrostatic repulsion of negative charges of phosphate groups located at the complementary strands).

	r_b = 0.03	r_b = 0.06	r_b = 0.09
cis-$PtI_2(NH_3)_2$	-1.9 ± 0.1	-5.0 ± 0.1	-7.9 ± 0.3
cisplatin	-2.1 ± 0.3	-5.2 ± 0.3	-8.3 ± 0.3

[a] Δt_m is defined as the difference between the t_m values of platinated and unmodified DNAs.
[b] The t_m values were measured in the medium containing $NaClO_4$ (0.1 M), Tris–HCl (1 mM, pH 7.4) and EDTA (0.1 mM).
[c] Values shown in this table are the means ± SEM of three separate experiments.

Table 2 Δt_m (°C) values[a] of CT DNA modified by *cis*-$PtI_2(NH_3)_2$ or cisplatin. [b,c]

Thus, it is reasonable to conclude that the decreases in t_m are caused by destabilizing conformational distortions and that these destabilizing factors dominate over the interstrand cross-links formed by both cis-platinum compounds and by positive charges on platinum moieties.
Owing to the fact that both *cisPtI₂* and cisplatin carry the same 2+ charge on platinum moiety and form approximately identical amount of interstrand cross-links (5 or 6%, respectively, *vide supra*), the values of t_m yielded by the adducts of both complexes reflect mainly destabilizing effects of conformational distortions induced by the platinum-DNA adducts. Hence, the results of DNA melting experiments are consistent with the thesis that DNA adducts of *cisPtI₂* distort and destabilize double helix of DNA approximately in the same extent as DNA adducts of cisplatin.
From an overall inspection of the obtained results it is evident that *cisPtI₂* interacts with DNA through a mode of interaction that is very similar to that well documented for cisplatin. Apparently, the major difference consists of a somewhat slower kinetics of platinum association to DNA while the formed adducts are apparently the same.

Cellular actions of *cis*-Pt $I_2(NH_3)_2$

Afterward, the antiproliferative effects of *cisPtI*$_2$ were evaluated in a representative panel of cancer cell lines according to the method described in the experimental section.
The cancer cell panel included the following lines: PANC-1 (human pancreatic cancer), IGROV-1 (human ovarian cancer), A549 (human lung cancer), HT29 (human colon cancer), HCT116-S and HCT116-R (human colon cancer). These cells were exposed to increasing concentrations of the drugs in the range 0-200 μM; after 24 hours viable cells (determined by Trypan blue exclusion) were counted and the IC_{50} values determined. The measured IC_{50} values are reported in table 3.

cell line	cisplatin	*cis*-$PtI_2(NH_3)_2$
PANC-1	2.48±0.11	0.91±0.10
IGROV-1	25.30±0.40	7.36±0.31
A549	5.77±0.60	3.54±0.49
HT29	16.39±1.10	11.69±1.40
HCT116-S	7.65±0.63	13.42±0.49
HCT116-R	21.96±1.11	4.15±0.23

Table 3 IC_{50} values (μM) of cisplatin and its iodo analogue in a panel of cancer cell lines.

From data inspection it is evident that *cisPtI*$_2$, in the four cisplatin sensitive cell lines, produces on the whole cytotoxic effects comparable and often greater than cisplatin. Extremely meaningful is the case of IGROV-1 where the cytotoxicity of *cisPtI*$_2$ is far higher than cisplatin (IC_{50} =7.36 μM versus 25.30 μM). Moreover, very remarkably, *cisPtI*$_2$ is found to overcome completely resistance to cisplatin in the cisplatin-resistant HCT116-R line. These results are very relevant and unexpected if one considers that *cisPtI*$_2$ is commonly reputed as inactive.
The effects of *cisPtI*$_2$ on the cell cycle were also analysed in HCT116-R cells in comparison to cisplatin; an arrest in G2/M phase is clearly detected in both cases as well as a decrease of the S phase (Figure 10).

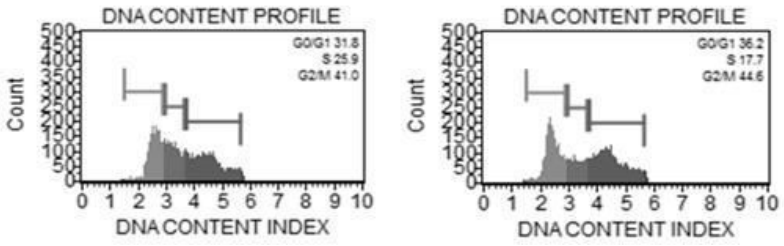

A B

Figure 10 Cell cycle analysis in HCT116 treated with cisplatin (A) or *cis*PtI_2 (B).

Analytical determinations were then carried out to measure intracellular Pt content in HCT116-S and HCT116-R cells after exposure to equimolar concentrations of either cisplatin or *cis*PtI_2. More precisely, cells were exposed to a 20 µM concentration of the Pt complexes for 3 h. Results expressed as Pt content per cell in the various cases and as percentage of internalised Pt are reported in Table 4.

Cell line	Drug	Platinum level	Internalised Pt %
HCT116-S	cisplatin	$2.53x10^{-8}$ µg	0,98
HCT116-S	*cis*-$PtI_2(NH_3)_2$	$5.37x10^{-8}$ µg	1,91
HCT116-R	cisplatin	$1.46x10^{-8}$ µg	0,50
HCT116-R	*cis*-$PtI_2(NH_3)_2$	$6.66x10^{-8}$ µg	2,41

Table 4 Platinum level (per cell) measured after exposure (3 hours) of cell lines to 20 µM of cisplatin and *cis*PtI_2.

From inspection of table 4 it is evident that *cis*PtI_2 manifests a greater ability to enter both types of cells than cisplatin; such difference is more evident in the Pt resistant cell line compared to the Pt sensitive one (5 folds vs 2 folds). This is possibly linked to its greater lipophilic character and larger inertness.

Furthermore, in the resistant cell line (HCT116-R), we can pinpoint the correlation occurring between the above IC_{50} values and Pt uptake in the sense that a greater cytotoxicity is associated to a greater Pt uptake -in terms of a five fold difference- proving the capability of *cis*PtI_2 to overcome chemo-resistance.

4.1.2.3 Discussion and conclusions

The substantial lack of information concerning *cisPtI_2* despite its striking similarity to cisplatin has inspired the present study; notably, some crucial aspects of its chemical and biological profile have been eventually elucidated.

First, we have shown that *cisPtI_2* manifests a solution behaviour very similar to cisplatin when dissolved in an aqueous medium, at physiological pH; indeed, as seen for cisplatin, *cisPtI_2* undergoes activation through sequential slow release of its two iodido ligands that are replaced by water molecules. However, the process is appreciably slower than in the case of cisplatin. These statements are clearly supported both by experimental data (see supplementary material) and computational analysis. The alternative hydrolysis path, where preferential release of NH_3 ligands is observed, could also be induced by changing the pH conditions. Even in this latter case the reaction route has been characterized by spectrophotometric analysis and spectral simulations. The large differences observed between the spectral patterns associated to the two possible mechanisms are very consistent with our interpretation.

Then, the reactions of *cisPtI_2* with DNA were investigated in detail in direct comparison to cisplatin through a robust experimental approach involving a variety of independent biophysical methods. Remarkably, we found that the pattern of DNA platination produced by *cisPtI_2* is highly reminiscent and nearly superimposable to that of cisplatin though the kinetics of the DNA metalation process is again appreciably slower.

Afterward, the cellular effects induced by *cisPtI_2* were explored in a small but representative panel of solid tumor cell lines; the panel included PANC-1 (human pancreatic cancer), IGROV-1 (ovarian cancer), A549 (lung cancer), HT29 (colon cancer), HCT116-S (colon cancer) and HCT116-R cells. Very remarkably, we observed that *cisPtI_2*, in contrast to expectations and to the current opinion, is on the whole more cytotoxic than cisplatin in three out of four cisplatin sensitive cancer cells; on the other hand, *cisPtI_2* was found to overcome completely resistance to cisplatin in the cisplatin resistant HCT116-R cell line. This latter result implies that *cisPtI_2* is able to circumvent the molecular mechanisms that reduce sensitivity to cisplatin in the resistant line. On the other hand, it is unlikely that dimeric Pt species (see supplementary material) play a major role in the observed cytotoxicity as the latter species are detected only at acidic pH and in very low amounts.

Analytical determinations were carried out to measure Pt uptake in the various cases: we found that cisplatin manifested a far lower ability to enter cells than *cis*PtI_2. In addition, a pronounced reduction of Pt uptake was detected in HCT116 resistant cells in comparison to their sensitive counterpart upon cisplatin treatment implying that this is most likely the main mechanism of resistance. In contrast, *cis*PtI_2 is internalised in far greater amounts by both cell types with resistant cells even showing a slightly greater Pt uptake.
However, the correlation between the cytotoxic potency and the intracellular Pt content is not straightforward for both HCT116 cellular lines. For instance, the Pt content measured upon exposure of HCT116-S cells to *cis*PtI_2 is more than two times greater compared to exposure to cisplatin. Yet, cisplatin produces a greater cytotoxic effect than *cis*PtI_2 (by a factor 2). Pairwise, roughly comparable amounts of intracellular Pt are found in HCT116-R and HCT116-S cells upon exposure to *cis*PtI_2; but *cis*PtI_2 is far more cytotoxic in the resistant cells compared to the sensitive ones (by a factor 3). This implies that the nature of the cells and the nature of the Pt complex are still important in determining the overall antiproliferative effect.
We believe that the here reported results are very meaningful and innovative with respect to current mechanistic knowledge on cisplatin and on its analogues for the following reasons:

1. In contrast to expectations and to early claims of inactivity *cis*PtI_2 is found to produce cytotoxic effects comparable and often greater than those caused by cisplatin, at least in four representative cancer cell lines;
2. *cis*PtI_2 overcomes to a large extent resistance to cisplatin in a cancer cell line showing acquired resistance to cisplatin, being taken up in a far greater amount. This implies that the recognition processes for the two Pt complexes are distinct.
3. However, the large differences measured in Pt uptake between *cis*PtI_2 and cisplatin do not correlate with the large differences observed in their respective biological effects. The nature of the Pt complex and the type of cell still play major roles.
4. The aquation process of *cis*PtI_2 at physiological pH reproduces closely that of cisplatin- though being slower- involving the progressive release of the two halide ligands; however, at slightly acidic pH, *cis*PtI_2 is found to release preferentially its ammonia ligands at variance with cisplatin. These processes are

reproduced very satisfactorily through computational analysis of the respective spectral profiles. t is very likely that these differences in reactivity between *cisPtI*$_2$ and cisplatin may lead to different interaction modes with specific biomolecules, in particular with proteins, thus generating distinct pharmacological profiles.

5. Remarkably, *cisPtI*$_2$ produces a kind of DNA damage very similar to cisplatin. Yet, the kinetics of Pt binding to DNA is slower and the final level of DNA platination appreciably lower. As the process of DNA platination is apparently less efficient than in the case of cisplatin it is unlikely that DNA is the only or primary target for *cisPtI*$_2$. when one considers that *cisPtI*$_2$ is even more cytotoxic than cisplatin.

Altogether, the reported results delineate an extremely favourable biological profile for *cisPtI*$_2$ and strongly warrant its further assessment in appropriate preclinical models. Moreover, at least in our opinion, these findings contain relevant implications with respect to the postulated mode of action of cisplatin and of its analogues. As DNA damage produced by *cisPtI*$_2$ is, on the whole, less extensive and less important than that induced by cisplatin and the type of DNA lesion is basically the same, the view that the cytotoxic effects of *cisPtI*$_2$ may arise from mechanisms other than DNA damage is supported. However, more studies are definitely needed to further substantiate this hypothesis.

4.1.2.4 Experimental section

Chemistry of *cis*-$PtI_2(NH_3)_2$

Synthesis of *cis*-$PtI_2(NH_3)_2$ and UV-Vis analysis: *cisPtI*$_2$ was synthesized according to procedure described in section 4.1.1.4. Solution behaviour of *cisPtI*$_2$ was assessed through spectrophotometric studies performed with a Varian Cary 50 Bio UV-Vis spectrophotometer in buffered solutions without use of DMSO and in absence of NaCl. A solution of complex (10^{-4} M) was prepared in 50 mM phosphate buffer (with or without presence of KI) at pH=7.4 or in 20 mM ammonium acetate buffer at pH=4.5 and absorbance monitored in the range between 200 and 800 nm of wave length for 72 h at 25° C.

Density Functional Theory simulations: ORCA package has been used throughout the calculations.[21] Hybrid PBE0 functional[22] and Aldrich TZVP

gaussian basis sets with scalar relativistic (ZORA) corrections[26] were used for both geometry optimizations and spectra simulations. Excited states have been computed within the TDDFT approach[27] and only the first twenty transitions have been computed using 200 expansion vectors in the iterative solution of the CI equations. D3 Grimme's dispersion corrections[25] have also been included. Solvent effects have been take into account within the COSMO model[28,29]with an ε value of 80.4. Highly accurate integration
grids (Grid 5 in the ORCA notation) without pruning of the inner angular part of the wave function and "TightSCF" convergence criteria has been used throughout all the calculations

LogP determination: the octanol-water partition coefficients for cisplatin and *cisPtI$_2$* were determined by modification of reported shake-flask method.[28] Water (50 mL, distilled after milli-Q purification) and n-octanol (50 mL) were shaken together for 72 h to allow saturation of both phases. Solution of the complexes were prepared in the water phase (3 x 10^{-3} M) and an equal volume of octanol was added. Biphasic solutions were mixed for ten minutes and then centrifuged for five minutes at 6000 rpm to allow separation. Concentration in both phases was determined by UV-VIS. Reported logP is defined as log $[complex]_{oct}/[complex]_{wat}$. Final values were reported as mean of three determinations.

Uptake experiment: comparison between cisplatin and *cis*-PtI$_2$(NH$_3$)$_2$ HCT116 cell line: the determination of platinum concentration in the cellular pellets as well as in the corresponding supernatant samples was performed in triplicate by a Varian 720-ES Inductively Coupled Plasma Atomic Emission Spectrometer (ICP-AES) equipped with a CETAC U5000 AT+ ultrasonic nebulizer, in order to increase the method sensitivity. Before the analysis, samples were weighted in PE vials and digested in a thermo-reactor at 80 °C for 24 h with 2 mL of aqua regia (HCl suprapure grade and HNO_3 suprapure grade in 3:1 ratio) and 0.2 mL of H_2O_2 suprapure grade. After digestion, the samples were diluted to about 5 mL with ultrapure water (≤18 MΩ) and accurately weighed; 5.0 mL of each sample were spiked with 1 ppm of Ge used as an internal standard, and analysed. Calibration standards were prepared by gravimetric serial dilution from a commercial standard solution of Pt at 1000 mg L^{-1}. The wavelength used for Pt determination was 214.424 nm whereas for Ge was used the line at 209.426 nm. The operating

conditions were optimized to obtain maximum signal intensity, and between each sample, a rinse solution constituted by HCl suprapure grade and HNO_3 suprapure grade in 3:1 ratio was used in order to avoid any “memory effect”.

Cellular studies

Cell cultures: PANC-1, HCT116-S, HCT116-R, IGROV-1, A549 and HT29 cell lines were cultured in RPMI 1640 (Euroclone; Milan, Italy) with 10% Fetal Bovine Serum (FBS) (Euroclone Defined; Euroclone; Milan, Italy). HCT116 cells were kindly provided by Dr. R. Falcioni (Regina Elena Cancer Insitute, Roma). We cultured at 37 °C in a humidified atmosphere in 5% CO_2 in air.

Pharmacology experiments: cells were seeded in a 96-well flat-bottomed plate (Corning-Costar, Corning, NY, USA) at a cell density of 1×10^4 cells per well in RPMI complete medium. Drugs were used, after solubilisation in water, without use of DMSO, at the final concentrations indicated in the figures and in the legends to the figures. After 24 h, viable cells (determined by Trypan blue exclusion) were counted in triplicate using a haemocytometer. Each experimental point represents the mean of four samples carried out in three separate experiments.

Trypan blue assay: cells viability was assessed by the Trypan blue exclusion assay. In brief, 10 µL of 0.4% trypan blue solution was added to 10 µL cell suspensions in culture medium.
The suspension was gently mixed and transferred to a haemocytometer. Viable and dead cells were identified and counted under a light microscope. Blue cells failing to exclude dyes were considered nonviable, and transparent cells were considered viable. The percentage of viable cells was calculated on the basis of the total number of cells (viable plus non viable). The IC_{50} value (i.e., the dose that caused apoptosis of 50% of cells) was calculated by fitting the data points (after 24 h of incubation) with a sigmoidal curve using Calcusyn software.

Cell cycle analysis: the effect of cisplatin and *cisPtI_2* on cell cycle distribution was assessed by flow cytometry after staining cells with propidium iodide (PI). Briefly, the cells (5×10^5 cells mL^{-1}) were analyzed prior and after treatment with IC_{50s} of both drugs (20.98 µM and 7.3 µM) for 24 h. The cells were harvested, washed with PBS and resuspended in

300 µL 1X Propidium Iodide staining solution and incubate at 4 °C in the dark for 20 minutes. DNA content of the cells was measured by BD FACSCanto Flow Cytometer and the population of each phase was determined using ModFit LT 3.0 analysis software (Verity Software House, Topsham, ME USA).

DNA binding studies

Reaction of *cisPtI*$_2$ with DNA, its putative main target, was analysed in direct comparison with cisplatin through a robust experimental approach including quantification of Pt binding to DNA, DNA interstrand cross-linking analysis, DNA adducts characterization by ethidium bromide fluorescence, DNA unwinding and thermal stability analyses.

Quantitative evaluation of binding of *cis*-$PtI_2(NH_3)_2$ and cisplatin to mammalian DNA in a cell-free medium: solutions of double-helical calf thymus (CT) DNA (42% G + C, mean molecular mass approximately 2 x 10^7) at a concentration of 0.032 mg mL^{-1} (1 x 10^{-4} M related to the phosphorus content) were incubated with *cisPtI*$_2$ (8 µM) or cisplatin (8 µM) at a value of r_f = 0.08 in 0.1 mM KI or KCl, respectively, at 37 °C (r_f is defined as the molar ratio of free platinum complex to nucleotide phosphates at the onset of incubation with DNA). Two different stock solutions of *cisPtI*$_2$ (0.1 mM) or cisplatin (0.1 mM) were prepared. One contained the Pt^{II} complex incubated for 7 days in unbuffered KI or KCl, respectively (0.01 M, pH 6) at 37 °C in the dark, whereas the other contained Pt^{II} complexes incubated for 7 days in double distilled water at 37 °C in the dark. Fifty microliters of the Pt^{II} complex aged in KI/KCl (0.01 M) or in water were quickly mixed with 4950 µL of DNA dissolved in $NaClO_4$ (10 mM), and the reaction mixture was kept at 37 °C. In the experiments in which the Pt^{II} complex aged in water was used, the final reaction mixture was still supplemented at the onset of the reaction with KI or KCl so that the resulting concentration of KI or KCl in the reaction mixtures was always 0.1 mM. At various time intervals, an aliquot of the reaction mixture was withdrawn and assayed by differential pulse polarography (DPP) for platinum not bound to DNA.[30]

Platination reactions: if not stated otherwise, CT or plasmid DNAs were incubated with the platinum complex in 10 mM NaClO4 at 37 °C in the dark. After 24 h, the samples were exhaustively dialyzed against the medium required for subsequent biochemical or biophysical analysis. An

aliquot of these samples was used to determine the value of rb (rb is defined as the number of molecules of the platinum complex bound per nucleotide residue) by flameless atomic absorption spectrophotometry (FAAS) or by differential pulse polarography (DPP).[29]

Unwinding of negatively supercoiled DNA: unwinding of closed circular supercoiled pSP73KB plasmid DNA (2455 bp) was assayed by an agarose gel mobility shift assay.[30] The unwinding angle Φ, induced per platinum–DNA adduct was calculated upon the determination of the r_b value at which the complete transformation of the supercoiled to the relaxed form of the plasmid was attained. Samples of pSP73KB plasmid were incubated with platinum compounds at 37 °C in the dark for 24 h. The samples were subsequently subjected to electrophoresis on 1% agarose gels running at 25°C with tris(hydroxymethyl) aminomethane (Tris)–acetate–EDTA buffer. The gels were then stained with EtBr, followed by photography with a transilluminator.

DNA melting: the melting curves of CT DNAs were recorded by measuring the absorbance at 260 nm. The melting curves were recorded in a medium containing 10 mM or 0.1 M Na^+ with 1 mM Tris–HCl/0.1 mM Na_2H_2EDTA, pH 7.4. The value of the melting temperature (t_m) was determined as the temperature corresponding to a maximum on the first derivative profile of the melting curves.

Interstrand DNA cross-linking in a cell-free medium: *cis*PtI_2 or cisplatin were incubated for 24 h with 0.5 μg of a linear 2686-bp fragment of pUC19 plasmid linearized by EcoRI. The linear fragment was first 3´-end-labeled by means of the Klenow fragment of DNA polymerase I in the presence of [α-^{32}P]dATP. The platinated samples were analyzed for DNA interstrand crosslinks by previously published procedures.[31,23] The number of interstrand cross-links was analyzed by electrophoresis under denaturing conditions on alkaline agarose gel (1%). After the electrophoresis had been completed, the intensities of the bands corresponding to single strands of DNA and interstrand cross-linked duplex were quantified. The frequency of interstrand cross-links was calculated as ICL/Pt (%) = XL/5372r_b (the DNA fragment contained 5372 nucleotide residues), where ICL/Pt (%) is the number of interstrand cross-links per adduct multiplied by 100, and XL is the number of interstrand cross-links per molecule of the linearized DNA duplex, which was calculated assuming a Poisson distribution of the interstrand crosslinks as

XL = -ln A, where A is the fraction of molecules running as a band corresponding to the non-cross-linked DNA.

Characterization of DNA adducts by EtBr fluorescence: these measurements were performed on a Varian Cary fluorescence spectrophotometer using a 1 cm quartz cell.
Fluorescence measurements were performed at an excitation wavelength of 546 nm, and the emitted fluorescence was analyzed at 590 nm. The fluorescence intensity was measured at 25 °C in NaCl (0.4 M) to avoid secondary binding of EtBr to DNA.[28] The concentrations were 0.01 mg mL^{-1} for DNA and 0.04 mg mL^{-1} for EtBr, which corresponded to the saturation of all intercalation sites of EtBr in DNA.[32]

Other physical methods: Absorption spectra were measured with a Beckman 7400 DU spectrophotometer equipped with a thermoelectrically controlled cell holder. The FAAS measurements were conducted with a Varian AA240Z Zeeman atomic absorption spectrometer equipped with a GTA 120 graphite tube atomizer. The gels were visualized with a FUJIFILM BAS 2500 bioimaging analyzer, and the radioactivity associated with the bands was quantified with AIDA Image Analyzer. DPP measurements were performed using an EG&G PARC Electrochemical Analyzer, model 384B.

References

[1] Basolo F., Gray H.B., Pearson R.G. J. Am. Chem. Soc., **1960**, 82, 4200-4203.
[2] Berger I., Nazarov A.A., Hartinger C.G., Groessl M., Valiahdi S.M., Jakupec M.A., Keppler B.K. Chem. Med. Chem., **2007**, 2, 505-514.
[3] Talman E.G., Bruning W., Reedijk J., Spek A.L., Veldman N. Inorg. Chem. **1997**, 36, 854-861.
[4] Cleare M.J., Hoeschele J.D. Bioinorg. Chem., **1973**, 2, 187-210.
[5] Timerbaev A.R., Hartinger C.G., Aleksenko S.S.; Keppler B.K. Chem. Rev., **2006**, 106, 2224-2248.
[6] Kratochwil N.A., Bednarski P.J. Arch. Pharm., **1999**, 332, 279-285.
[7] Kratochwil N.A., Ivanov A.I., Patriarca M., Parkinson J.A., Gouldsworthy A.M., Murdoch P.D., Sadler P.J. J. Am. Chem. Soc., **1999**, 121, 8193-8203.
[8] Messori L., Casini A., Gabbiani C., Michelucci E., Cubo L., Ríos-Luci C., Padrón J.M., Navarro-Ranninger C., Quiroga A.G. ACS Med. Chem. Lett., **2010,** 381-385.
[9] Messori L., Cubo L., Gabbiani C., Alvarez-Valdés A., Michelucci E., Pieraccini G., Ríos-Luci C., León L.G., Padrón J.M., Navarro-Ranninger, C., Casini A., Quiroga, A.G. Inorg. Chem**., 2012**, 51, 1717-1726.
[10] Casini A., Mastrobuoni G., Temperini C., Gabbiani C., Francese S., Moneti G., Supuran C.T., Scozzafava A., Messori L. Chem. Commun., **2007,** 2, 156-158.
[11] Casini A., Guerri A., Gabbiani C., Messori L. J. Inorg. Biochem., **2008**, 102,995-1006.
[12] Timerbaev A.R., Pawlak K., Gabbiani C., Messori L. Trends in Anal. Chem., **2011**, 30, 1120-1138.
[13] Dhara S.C. Indian J. Chem., **1970**,8, 193-194.
[14] Nakamoto K. (**1997**) Infrared and Raman Spectra of Inorganic and Coordination Compounds, Part B. Application in Coordination, Organometallic and Bioinorganic Chemistry. 5th Edition. Wiley Interscience, John Wiley and Sons, Inc. New York.
[15] Rochon F.D., Buculei V. Inorg. Chim. Acta, **2004**, 357, 2218-2230.
[16] Pellegrini E., Piano D., Bowler M.W., Acta Cryst.D, **2011**, 67, 902-906.
[17] Russo Krauss I., Sica F., Mattia C.A., Merlino A. Int. J. Mol. Sci., **2012**, 13, 3782-3800.
[18] Otwinowski Z., Minor W. Methods Enzymol., **1997**, 276, 307-326.
[19] A. Vergara, D' Errico G., Montesarchio D., Mangiapia G.,

Paduano L. and Merlino A. Inorg. Chem., **2013**, 52, 4157-4159.
[20] Brunger A.T., Adams P.D., Clore G.M., Gros P., Grosse-Kunstleve R.W., Jiang J.S., Kuszewski J., Nilges N., Pannu N.S., Read R.J., Rice L.M., Simonson T., Warren G.L. Acta Cryst. D., **1998**, 54, 905-921.
[21] Jones T.A., Zou J.Y., Cowan S.W., Kjedgaard M. Acta Cryst. D., **1991**, 56, 714-721.
[22] Kostrhunova H., Vrana O., Suchankova T., Gibson D., Kasparkova J., Brabec V. Chem. Res. Toxicol., **2010**, 23, 1833-1842.
[23] Brabec V., Leng M., Proc. Natl. Acad. Sci USA, **1993**, 90, 5345-5349.
[24] Keck M.V., Lippard S.J. JACS, **1992**, 114, 3386-3390.
[25] Zaludova R., Kleinwächter V., Brabec V. *Biophys. Chem.*, 1996, **60**, 135-142.
[26] Pantazis D. A., Chen X.Y., Landis C.R. and Neese F. J Chem. Theory. Comput., **2008**,4 ,908-919.
[27] Runge E., Gross E.K. Phys. Rev. Lett., **1984**, 52 , 997-1000.
[28] Klamt A., Schiiiirmann G. J. Chem. Soc., Perkin Trans., **1993**, 2 ,799-805.
[29] Sinnecker S., Rajendran A., Klamt A., Diedenhofen M. and Neese F. J. Phys. Chem. A ,**2006**, 110, 2235-2245.
[30] Kim S.D, Vrana O., Kleinwächter V., Niki K., Brabec V. Anal. Lett., **1990**, 23, 1505-1518.
[31] Farrel N., Qu Y., Feng L., Van Houten B. Biochemistry, **1990**, 29, 9522-9531.
[32] Butour J.L., Alvinerie P., Souchard J.P., Colson P., Houssier C., Johnson N.P. Eur. J. Biochem., **1991**, 202, 975-980.

5

STUDIES ON THE DIBROMIDO ANALOGUE OF CISPLATIN AS POTENTIAL ANTICANCER AGENT: PRELIMINARY RESULTS

5. STUDIES ON THE DIBROMIDO ANALOGUE OF CISPLATIN AS POTENTIAL ANTICANCER AGENT: PRELIMINARY RESULTS.

The results presented in this chapter have been submitted for publication in the following manuscript:

Tiziano Marzo, Gianluca Bartoli, Chiara Gabbiani, Gennaro Pescitelli, Serena Pillozzi, Elena Michelucci, Benedetta Fiorini, Annarosa Arcangeli, Adóracion G. Quiroga and Luigi Messori "Cisplatin and its dibromido analogue: a comparison of chemical and biological profiles", 2015, submitted to J.Inorg. Biochem., Special Issue COST action CM1105.

5.1 Introduction

Re-evaluation of selected compounds that, for different reasons, have been overlooked in the past, may be considered a real strategy for the discovery of new anticancer drugs. Along this line of reasoning, in this chapter we report our preliminary studies on *cis*-$PtBr_2(NH_3)_2$, the dibromide analogue of cisplatin.

5.1.1 Cisplatin and its dibromido analogue: a comparison of chemical and biological profiles

5.1.1.1 Introduction

In chapter 4 we demonstrated that the diiodido analogue of cisplatin manifests truly interesting biological properties and warrants a more extensive pharmacological evaluation.[1] This encouraging result prompted us to prepare and evaluate even the dibromido analogue of cisplatin (Figure1). Accordingly, we report here on the synthesis and the chemical characterisation of *cis*-$PtBr_2(NH_3)_2$ as well as on the initial assessment of its biological and pharmacological profile.

Figure 1 Structure of cisplatin and its dibromido analogue.

5.1.1.2 Results

Solution behaviour of *cis*-$PtBr_2(NH_3)_2$ and its activation profile

cis-$PtBr_2(NH_3)_2$ shows an acceptable solubility in the reference phosphate buffer, at physiological pH, allowing to carry out experiments in the absence of DMSO or other organic solvents, thus avoiding potential interferences. Freshly prepared solutions of *cis*-$PtBr_2(NH_3)_2$ manifest typical absorption bands in the UV-visible, with a main band at 330 nm and a pronounced shoulder at 300 nm (Figure 2). These bands are tentatively assignable to a d-d and LMCT transitions respectively in analogy with other cisplatin derivatives.[1] After dissolution of the study

compound in the reference buffer, progressive spectral changes are observed that are assigned to the progressive release of the two bromide ligands. The process is similar to what observed in the case of cisplatin with a comparable kinetics.[1]

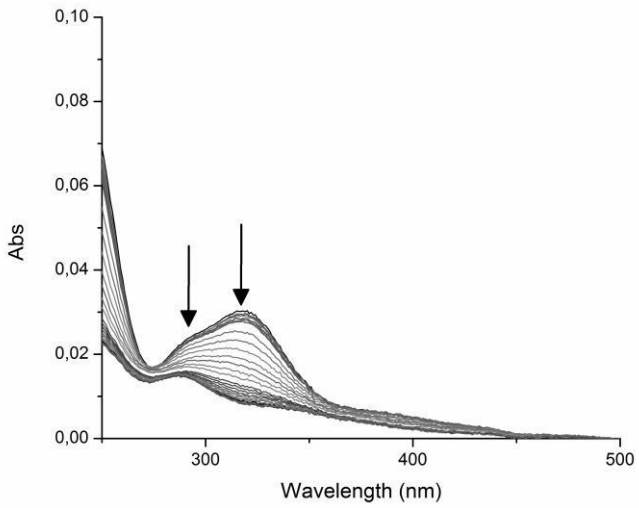

Figure 2 Time course spectra of *cis*-$PtBr_2(NH_3)_2$ 10^{-4} M in 50 mM phosphate buffer over 24 h, RT.

Mechanistic studies: biomolecular interactions

To investigate the possible interactions occurring between *cis*-$PtBr_2(NH_3)_2$ and its likely biomolecular targets we first performed a few ESI-MS experiments for samples where the study complex was incubated with the model protein lysozyme for a certain time period (Figure 3). First attempts to characterise the protein metalation process through ESI-MS detection were carried out by analysing samples after 24 h of incubation, but no clear evidence of adduct formation was obtained. However, upon increasing the incubation time up to 72 h, under identical solution conditions, a number of peaks of higher molecular weight than the native protein, were instead observed that are straightforwardly assigned to metallodrug-lysozyme adducts. From careful inspection of the spectrum, it is evident that Pt coordination occurs through a mechanism that involves preferential detachment of halide ligands and full retention of ammonia ligands; assignments were validated by theoretical calculation (see supplementary material). This kind of protein metalation strictly resembles

that produced by cisplatin resulting in an adduct characterised by selective Pt coordination to His15 after release of the two chloride ligands.[2] Remarkably, this behaviour being in accord with cisplatin is in contrast with that of *cis*-$PtI_2(NH_3)_2$, where metalation of lysozyme occurs through metal fragments resulting from preferential release of the ammonia ligands (see chapter 4, paragraph 4.1.1).[3]

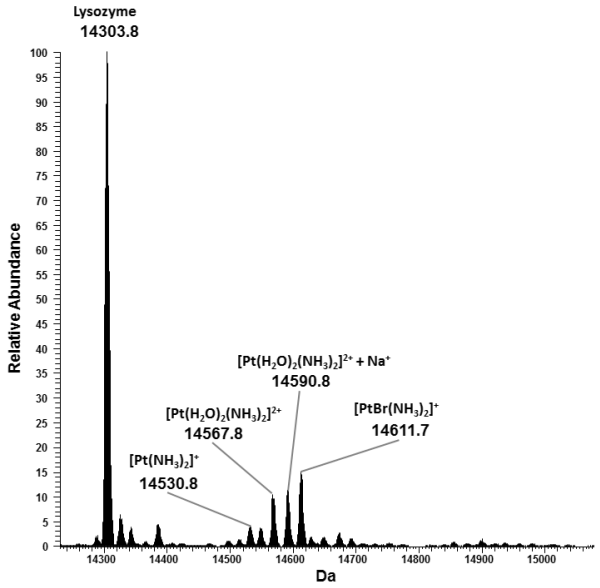

Figure 3 Deconvoluted ESI-MS spectra of lysozyme treated with $3*10^{-4}$ mol L^{-1} of *cis*-$PtBr_2$ recorded after 72 h of incubation at 37 °C, metal : protein ratio = 3:1; ammonium acetate buffer 20 mmol L^{-1} at pH=6.8.

CD experiments, interaction with CT DNA

Since nuclear DNA is believed to be the primary target for the pharmacological effect of cisplatin,[4] we have characterized the interaction of *cis*-$PtBr_2(NH_3)_2$ with calf thymus DNA through CD experiments.
The CD spectrum of CT DNA, before addition of the drugs is in keeping with literature (Figure 4).[5]

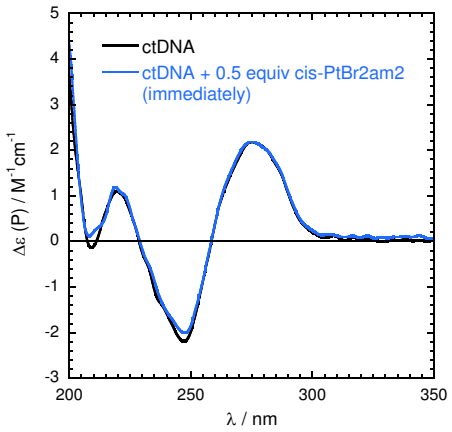

Figure 4 CD spectra of CT DNA without and with *cis*-$PtBr_2(NH_3)_2$ (cis-$PtBr_2am_2$), 0.5 equiv, measured immediately after the mixing.

Addition of 0.5 equiv of *cis*-$PtBr_2(NH_3)_2$ did not lead to any immediate change in the CD spectrum (Figure 4). However, after incubation at 22°C for 72 h, the spectrum changed showing clear differences on the whole wavelength range (Figure 5). In particular, both CD bands at 280 and 250 nm increased in intensity, the first by about 15%.

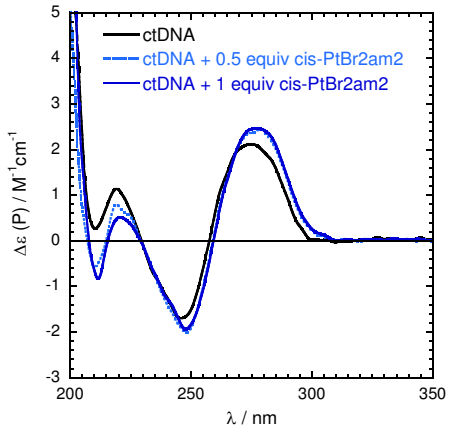

Figure 5 CD spectra of CT DNA without and with *cis*-$PtBr_2(NH_3)_2$ (cis-$PtBr_2am_2$) , 0.5 and 1 equiv, after 72 h incubation.

From inspection of CD we can state that spectra measured after addition of 0.5 or 1 equivalents of *cis*-$PtBr_2(NH_3)_2$ were consistent and no significant changes in the spectral profiles were detected. Evidences that

cis-$PtBr_2(NH_3)_2$ interacts with CT DNA very similarly to cisplatin derive from the comparative analysis of the CD spectra of CT DNA after incubation with 1 equivalent of *cis*-$PtBr_2(NH_3)_2$ or cisplatin (Figure 6).

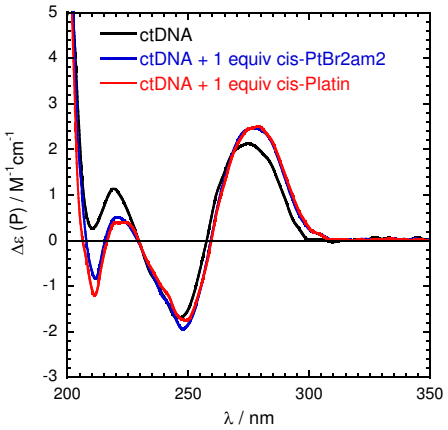

Figure 6 CD spectra of CT DNA with *cis*-$PtBr_2(NH_3)_2$ (cis-$PtBr_2am_2$) and cisplatin, 1 equivalent, after 72 h incubation.

Cellular effects

Then, we investigated the response of a small panel of human cancer cell lines, to *cis*-$PtBr_2(NH_3)_2$ treatment in terms of cell proliferation inhibition according to the method described in the experimental section (see below). The cancer cell panel included the following lines: A549 (human lung cancer), HCT116 (human colon cancer), IGROV-1 (human ovarian cancer) and FLG 29.1 (human acute myeloid leukaemia). These cells were exposed to increasing concentrations of the drug in the 0–200 μM range and treated for 24 hours; then IC_{50} values were determined (calculated through the Trypan blue exclusion test) (Table 1). From data collected it is evident that *cis*-$PtBr_2(NH_3)_2$, in the four cancer cell lines, produces, on the whole, cytotoxic effects almost superimposable to those of cisplatin. Quite peculiar is just the case of the leukaemia cell line FLG 29.1 where the cytotoxicity of *cis*-$PtBr_2(NH_3)_2$ is significantly greater than cisplatin (the IC_{50} is roughly halved).

These encouraging results led us to deepen our investigation. The effects of *cis*-$PtBr_2(NH_3)_2$ on cell cycle and apoptosis were further evaluated in the FLG 29.1 cell line, emerging as the most sensitive to this compound in comparison to cisplatin. Upon treatment with *cis*-$PtBr_2(NH_3)_2$ we

noticed a strong reduction in the percentage of cells in the G0/G1 phase accompanied by an increase in G2/M more pronounced than for cisplatin (see Figure 7). We next evaluated the effect of *cis*-$PtBr_2(NH_3)_2$ in the induction of apoptosis by Annexin/PI test. As reported in figure 8 the treatment with *cis*-$PtBr_2(NH_3)_2$ for 24 hours determined in FLG 29.1 an induction of apoptosis more evident than for cisplatin with a percentage of Annexin+/PI- cells of 51.85±4.5 versus 41.15±2.75 in the case of cisplatin.

	IC_{50} Cisplatin (μM) mean±SEM	**IC_{50} *cis-*$PtBr_2(NH_3)_2$ (μM)** mean±SEM
A549	8.61±0.73	10.08±0.73
FLG 29.1	24.33±0.75	14.66±0.63
HCT-116	20.04±0.95	28.28±3.11
IGROV-1	24.12±0.49	25.63±0.25

Table 1 Evaluation of IC_{50} on a panel of tumor cell lines. A549,FLG,HCT-116 and IGROV-1 cell lines were exposed to IC_{50} concentrations of Cisplatin and *cis*-$PtBr_2(NH_3)_2$ for 24 hours and cell viability was evaluated via Trypan Blue exclusion assay. Means and SEMs are relative to one experiment mounted in triplicate.

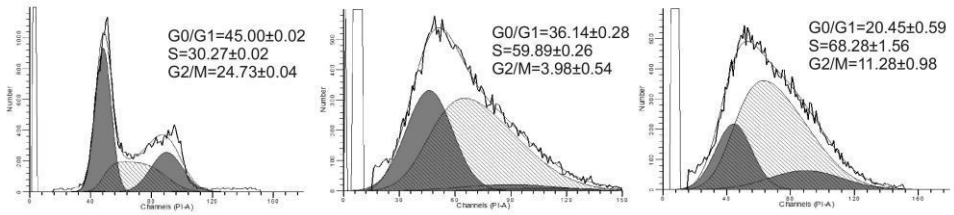

Figure 7 effect of cisplatin and *cis*-$PtBr_2(NH_3)_2$ on cell cycle of FLG cells. Effect of Cisplatin and of *cis*-$PtBr_2(NH_3)_2$ given at their IC_{50}s on cell cycle of FLG cells after 24h of treatment. A=control, B=treated with cisplatin C=treated with *cis*-$PtBr_2(NH_3)_2$. The means and SEMs relative to two independent experiments are reported next to each representative panel.

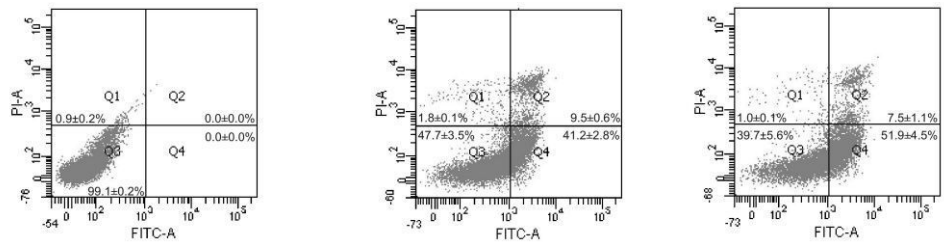

A B C

Figure 8 effect of cisplatin and *cis*-$PtBr_2(NH_3)_2$ on apoptosis of FLG cells. Effect of Cisplatin and of *cis*-$PtBr_2(NH_3)_2$ given at their IC_{50}s on the induction of apoptosis on FLG cells after 24h of treatment. The means and SEMs relative to two independent experiments are reported in each representative panel. A=control, B=treated with cisplatin C=treated with *cis*-$PtBr_2(NH_3)_2$.

5.1.1.3 Discussion and conclusions

Very recently (see chapter 4) we have studied the behaviour of the diiodido analogue of cisplatin that turned out to show very attractive chemical and biological features.[1] Notably the diiodido analogue manifests conspicuous cytotoxic effects *in vitro* and is able to overcome to a large extent resistance to cisplatin. Some peculiarities in the nature of the reaction of *cis*-$PtI_2(NH_3)_2$ with model proteins were also highlighted. Here we have extended our investigation to the dibromido analogue in such a way to gain a more complete description of this issue.

cis-$PtBr_2(NH_3)_2$ could be prepared quite easily according to the classical synthetic procedure of Dhara with slight modifications. Its solution chemistry was explored in a standard physiological buffer and a behaviour very close to cisplatin emerged, indeed, activation *cis*-$PtBr_2(NH_3)_2$ occurs through bromide release.

When reacted with the model protein lysozyme a platination pattern similar to cisplatin was again detected with protein coordination of $[cisPt(NH_3)_2]^{2+}$ fragments. Even the process of platination of standard CT DNA (800 bp) is highly reminiscent of that of cisplatin and CD spectroscopy clearly proves the interaction. One equivalent of ligand (per base pair, 0.5 equiv per base) is enough to achieve full binding. The binding is similar for *cis*-$PtBr_2(NH_3)_2$ and cisplatin. Using our fragmented ctDNA, the effects of cisplatin are different from those reported in the literature for non-sonicated CT DNA. [6,7]

Cellular studies were conducted on four distinct cancer cell lines. In general, i.e. in 3 out of 4 cancer cell lines, antiproliferative effects nearly superimposable to those caused by cisplatin were measured. More remarkable effects were observed only in the case of FLG cells where our platinum complex displayed an activity significantly greater than cisplatin (by about a factor 2). In the latter FLG cells *cis*-$PtBr_2(NH_3)_2$ was also found to be more effective than cisplatin in producing apoptosis and in perturbing the cell cycle distribution.
We believe that these differences, though quite small, might be exploited for further preclinical studies of this analogue and for a full assessment of its pharmacological profile with respect to cisplatin. Indeed, as the two compounds are very similar in their chemical and biological profile slight differences might translate into an effective therapeutic advantage and/or in a somewhat modified spectrum of anticancer actions for *cis*-$PtBr_2(NH_3)_2$ compared to cisplatin.

5.1.1.4 Experimental section

Chemistry of *cis*-$PtBr_2(NH_3)_2$, synthesis and characterisation

The synthesis of this Pt complex was performed through a slight modification of Dhara's synthesis for cisplatin.[8] A solution of 400 mg (2.4 mmol) of KI in 3 mL of water was added to an aqueous solution (5 mL) of 250 mg of $K_2[PtCl_4]$ (0.6 mmol) which was quantitatively converted into a dark solution containing $K_2[PtI_4]$ after five minutes of stirring at room temperature. Then the addition of two equivalents of ammonium hydroxide as a 40% solution results in the separation of *cis*-$PtI_2(NH_3)_2$ as a bright yellow compound, leaving behind a colorless solution. The solid was filtered off and thoroughly washed with water. (Yield 90%).
A suspension of 200 mg of *cis*-$PtI_2(NH_3)_2$ (0.41 mmol) in water (5mL) was mixed with a solution of $AgNO_3$ (0.82 mmol) in water (1,5 mL) and stirred in the dark (40ºC) until a pale yellow solution was formed over the suspension. The AgI formed was then filter off using neutral celite over a solution of two equivalents of KBr in 7 mL of water. The colorless solution was stored until orange crystalline precipitation was observed. The bright orange crystals of *cis*-$PtBr_2(NH_3)_2$ were filtered off and washed with water and dried in air. Yield was 25%. Purity of the product was assessed through elemental analysis of C, N and H [calculated C: 0%, H: 1.45%, N: 7.20%, experimental: C: 0,54%, H: 1.45%, N: 7.18%], ^{1}H, ^{195}Pt NMR and

IR analysis (see supplementary material). Cis geometry checked as describe in the literature.[9] Solution behaviour of *cis*-$PtBr_2(NH_3)_2$ was assessed through spectrophotometric experiments performed with a Varian Cary 50 Bio UV-Vis spectrophotometer in buffered solutions without the use of DMSO and of NaCl. A solution of the complex (10^{-4} M) was prepared in 50 mM phosphate buffer at pH = 7.4. The absorbance was monitored in the wavelength range between 200 and 800 nm for 72 h at 25° C.

ESI-MS experiments

A solution of *cis*-$PtBr_2(NH_3)_2$ (10^{-4} M) was incubated with lysozyme (3:1 metal/protein ratio) for 72 h at 37° C in 20 mmol L^{-1} ammonium acetate at pH=6.8. ESI-MS spectra were recorded after 24 and 72 h. After a 20-fold dilution with water, ESI MS spectra have been recorded by direct introduction at 5 µl min^{-1} flow rate in an Orbitrap high-resolution mass spectrometer (Thermo, San Jose, CA, USA), equipped with a conventional ESI source. The working conditions were the following: spray voltage 3.1 kV, capillary voltage 45 V, capillary temperature 220°C, tube lens voltage 230 V. The sheath and the auxiliary gases were set, respectively, at 17 (arbitrary units) and 1 (arbitrary units). For acquisition, Xcalibur 2.0. software (Thermo) was used and monoisotopic and average deconvoluted masses were obtained by using the integrated -Xtract tool. For spectrum acquisition, a nominal resolution (at m/z 400) of 100,000 was used.

Circular Dichroism experiments, interaction with CT DNA

Sample: CT DNA 52.0 µM (per base, P) in phosphate buffer 50 mM, pH=7.4; additioned with *cis*-$PtBr_2(NH_3)_2$ 2.3 mM in H_2O or cisplatin 1.0 mM in H_2O, to 0.5:1 and 1:1 molar ratio (indicated per base); 1-cm quartz cylindrical cell, volume ca. 2.5 ml; all samples (except one, see results) incubated at room temperature (22°C) for 72h before measurement. The CT DNA has a base-pair length of ca. 800, obtained with a standardized procedure by sonication.[10] The DNA concentration was checked by absorbance measurement at 260 nm (0.34 u.A., 1 cm cell). Phosphate buffer was used in all case to measure the blank spectrum.

Measurements: CD spectra measured with Jasco J-715 spectropolarimeter with the following conditions: scan speed 50 nm/min; response 1 sec; data pitch 0.1 nm; bandwidth 2.0 nm; 8 accumulations.
Cell cultures: A549 and HDF cell lines were cultured in DMEM High glucose (Euroclone; Milan, Italy) with 10% Fetal Bovine Serum (FBS) (Euroclone Defined; Euroclone; Milan, Italy). HCT-116, FLG 29.1 and IGROV-1 were cultured in RPMI 1640 (Euroclone; Milan, Italy) with 10% Fetal Bovine Serum (FBS) (Euroclone Defined; Euroclone; Milan, Italy). HCT116 cells were kindly provided by Dr R. Falcioni (Regina Elena Cancer Institute, Roma). We cultured the cell lines at 37 °C under a humidified atmosphere in 5% CO2 in air.

Pharmacology experiments: cells were seeded in a 96-well flat-bottomed plate (Corning-Costar, Corning, NY, USA) at a cell density of 1×10^4 cells per well in either RPMI or DMEM complete medium. Drugs were used, after solubilisation in water, without using DMSO, in range of concentration of 0-200 µM. After 24 h, viable cells (determined by Trypan blue exclusion) were counted in triplicate using a haemocytometer. Each experimental point represents the mean of a single experiments carried out in triplicate.

Trypan blue assay: cells viability was assessed by the Trypan blue exclusion assay. In brief, 10 µL of 0.4% trypan blue solution was added to 10 µL cell suspensions in culture medium. The suspension was gently mixed and transferred to a haemocytometer. Viable and dead cells were identified and counted under a light microscope. Blue cells failing to exclude the dyes were considered nonviable, and transparent cells were considered viable. The percentage of viable cells was calculated on the basis of the total number of cells (viable plus nonviable). The IC_{50} value (i.e., the dose that caused apoptosis of 50% of cells) was calculated by fitting the data points (after 24 h of incubation) with a sigmoidal curve using Calcusyn software (Biosoft, Cambridge, UK).

Cell cycle analysis: the effect of cisplatin and cis$Pt(NH_3)_2Br_2$ on cell cycle distribution was assessed by flow cytometry after staining the cells with propidium iodide (PI). Briefly, the cells (5 × 105 cells per mL) were analyzed prior to and after treatment with IC_{50}s of both drugs for 24 h. The cells were harvested, washed with PBS and resuspended in 300 µL 1× propidium iodide staining solution and incubated at 4 °C in the dark for 20

minutes. DNA content of the cells was measured by BD FACSCanto (Becton Dickinson, Franklin Lakes, NJ, USA) Flow Cytometer and the population of each phase was determined using ModFit LT 3.0 analysis software (Verity Software House, Topsham, ME USA).

Annexin/PI assay: The effects of the different drugs on our cell line panel was investigated through annexin V/propidium iodide (Annexin-VFLUOS staining kit; Roche Diagnostics, Mennheim, Germany). Cells were seeded at $2*10^5$/well in 6-well plates and incubated with different drugs for 24 hours. Cells were then harvested, washed with PBS, re-suspended in 100 µL of binding buffer and incubated with FITC-conjugated annexin V and propidium iodide for 15 min. Flow cytometric analysis were performed with BD FACSCanto (Becton Dickinson, Franklin Lakes, NJ, USA) and analysed with BD FACSDiva Software 6.1.3. Each experiment was performed in triplicate.

References

[1] Marzo T., Pillozzi S., Hrabina O., Kasparkova J., Brabec V., Arcangeli A., Bartoli G., Severi M., Lunghi A., Totti F., Gabbiani C., Quiroga A.G. and Messori L. Dalton Trans., **2015**, 44, 14896-14905.
[2] Casini A., Mastrobuoni G., Temperini C., Gabbiani C., Francese S., Moneti G., Supuran C.T., Scozzafava A., Messori L. Chem. Commun., **2007,** 2, 156-158.
[3] Messori L., Marzo T., Gabbiani C., Valdes A.A., Quiroga A.G. and Merlino A. Inorg. Chem., **2013**, 52, 13827-13829.
[4] Siddik Z.H. Oncogene, **2003**, 22**,** 7265-7279.
[5] Dorraji P.S. and Jalali F. J. Braz. Chem. Soc., **2013**, 24, 939-945.
[6] Tamburro A.M., Celotti L, Furlan D., Guantieri D. Chem. Biol. Interactions,**1977**, 16, 1-11.
[7] Sristava, R.C., FroehlichJ., Eichhorn G.L., Biochimie, **1978**, 60, 879-891.
[8] Dhara S.C. Indian J. Chem., **1970**,8, 193-194.
[9] Nakamoto K. (**1997**) Infrared and Raman Spectra of Inorganic and Coordination Compounds, Part B. Application in Coordination, Organometallic and Bioinorganic Chemistry. 5th Edition. Wiley Interscience, John Wiley and Sons, Inc. New York.
[10] Biver T., Secco F., Tinè M.R., Venturini M. Arch. Biochjem. Biophys., **2003**, 418, 63-70.

6

PRELIMINARY ASSESSMENTS OF cis-$PtI_2(NH_3)_2$ *IN VIVO*

6. PRELIMINARY ASSESSMENTS OF *cis*-$PtI_2(NH_3)_2$ *IN VIVO*

The results presented in this chapter are unpublished and have not been submitted to any journal to date.

6.1 Introduction

In vivo toxicity experiments are preclinical safety tests allowing the evaluation of the effects produced on the animals by the drugs, in order to observe the reactions produced on models that simulate the complexity of human organism. This allows an evaluation of correlated risk.
Two main methods are commonly used to assess drug toxicity: acute toxicity test and chronic toxicity test (repeated doses).
Acute toxicity test allows to evaluate the effects associated with a single administration on the animal, for which the effects are monitored for 14 days. In case of death of the animal during the treatment, deep analysis are carried out to find biochemical, histological, pathological and morphological alterations on the animal itself. With this methodology it is possible to estimate the effects of the drug through determination of the median lethal dose (LD_{50}). This determination implies a large group of animals and high mortality. This aspect led to the application of alternative methodologies that are more correct from an ethical point of view: FDP (Fixed Dose Procedure), ATC (Acute Toxic Category method) and UDP (Up and Down method).
In the protocol for chronic toxicity assessment, a multiple administration strategy is used for a prolonged time (depending on the time are divided in chronic or sub-chronic). The drug is daily administered and the administration is repeated regularly over a period of time (at least 14 days).
In this type of determination mice have a weight almost uniform (± 20%).
The group of animals should be divided in two sub-groups:

1. control, i.e. mice as reference models for the standard behavior of the subject;
2. treated mice that receive drug administration and undergo the effect of treatments

During the experiment, a series of parameters (both behavioral and biochemical) should be monitored to assess the percentage of change

determined by the drug. Results are finally associated to the control of immunotoxicity (observed through determination of Delayed Type Hypersensitivity, DTH; antibody response to T-dependent antigens and other parameters).

6.2 Experimental Protocol

A solution o *cis*-$PtI_2(NH_3)_2$ in water, with final concentration (0,9 mg/mL) was prepared and divided in aliquots (volume= 0,5 mL). Single-dose aliquots were store at -20°C until their use. At variance with cisplatin (administered as a solution containing NaCl in clinical protocols), *cis*-$PtI_2(NH_3)_2$ was solubilised in pure water without NaCl to avoid any interference. Also, storage at -20°C allowed to avoid hydrolysis before injection (see chapter 4).
In the experiment reported in this thesis, 6 (two control) 5-week-old, female athymic mice (Fox1nu), have been treated with *cis*-$PtI_2(NH_3)_2$ to assess chronic toxicity of this potential anticancer Pt-based drug. The protocol was the following: intraperitoneal injections (3.5 mg/Kg)[1] 2 time/week (3 weeks treatment). Injection were made in correspondence of the lower right quadrant. During injection a series of data on the animal were collected to evaluate possible symptoms or evidence of sufferance induced by stress and/or drug cytotoxicity, but no evidences were found. Sacrifice of mice was made at the end of the protocol through preliminary injection of anesthetic (Avertin). The efficacy of the anesthetic was properly tested and verified. Afterward, dissection of mice and collection of organs (i.e. liver, kidneys, spleen) and pheripheral blood (PB) was carried out.

6.3 Results, discussion and conclusions

Obtained results highlight as *in vivo* chronic toxicity test carried out in a murine model, for the treatment with the anticancer drug *cis*-$PtI_2(NH_3)_2$ does not show any particular problem.
The weight of mice was monitored during all the treatment. The first control was made before the first administration and the last control after the last administration and there was no evidence for weight loss in the treated mice. Remarkably, neither microscopic or macroscopic alteration were found in liver, kidneys and spleen.
Furthermore, analysis of a series of serum parameters were made to find eventual biochemical alterations in the treated animals (Table 1).

	controls	**treated**
AST*	69±4 IU/L	67±5 IU/L
ALT**	30±2 IU/L	32±4 IU/L
Creatinine***	0.5±0.06 mg/dl	0.51±0.08 mg/dl

*Aspartate transaminase (hepatic function)
**Alanine transaminase (hepatic function)
*** Renal function

Table 1 AST, ALT and creatinine value for treated and untreated mice.

Beyond the absence of lesions in liver, kidneys and spleen, comparing analytical values for hepatic and renal function (i.e. AST, ALT and creatinine respectively) for treated and untreated mice, it emerges as treated animals maintain both functions, being this confirmation that treatment does not present any particular side effect.

Overall, the treatment with *cis*-$PtI_2(NH_3)_2$ has been well tolerated in murine models. This evidence is of great significance and strongly warrants for further preclinical assessments that hopefully will confirm this complex as very promising antineoplastic agent in those cancers resistant to the conventional chemotherapeutic drugs.

References

[1] Shishido S.N., Nguyen T.A. PLoS One, **2012**, 7(9):e44963.

7

CONCLUSIONS

7. CONCLUSIONS

In this work we have investigated and characterised some important aspect of the structure-function relationships in a panel of Pt-based anticancer drugs, both in widespread clinical use (i.e. cisplatin, carboplatin and oxaliplatin), or some promising analogues that may become interesting drug candidates (i.e. diiodido and dibromido analogues of cisplatin).
Particular attention has been paid to the reaction of these complexes with the model proteins lysozyme and RNase. In fact, though it is today widely recognised that reaction of Pt based drugs with proteins, is of central importance in relation to overall pharmacological and toxicological impact of cisplatin and its analogues; yet, the structural information concerning platination of protein, and the characterization of the resulting adducts, is limited.

In the first part of this thesis we have characterized at molecular level, and comparatively, the interaction of established platinum drugs cisplatin, carboplatin and oxaliplatin with the model proteins lysozyme and RNase, mainly through ESI-MS and x-ray crystallography.
Valuable structural and functional information on these adducts was derived. In fact these two physicochemical techniques, in combination with other methods, allow, at least in selected cases, to describe in details and with an high accuracy the reaction of metallodrugs with protein targets.
Overall, on the ground of the obtained results, a rather satisfactory and comprehensive description of the reactivity of cisplatin, carboplatin and oxaliplatin with proteins can be inferred that might be of broader validity.
The main aspects of such reactivity are summarised below.
All these drugs are prodrugs, i.e. they undergo an activation step before binding to the proteins. In particular, this step involves the detachment of one or more labile ligands (chloride for cisplatin, oxalate for oxaliplatin and CBD for carboplatin). Notably through ESI-MS analysis it is possible to show that the kinetic of this process may be very different for the mentioned drugs. This is the case of cisplatin and carboplatin for instance, that, despite having a very similar behavior in the binding to proteins, it must be stressed that cisplatin shows a rapid kinetic in the binding, and a greater reactivity than carboplatin in terms of amounts of formed derivatives.

From our comparative analysis it emerges that adduct formation occurs in a few positions, although a rather large number of potential donors, implying a certain selectivity in metal binding. In addition, the two drugs having similar pharmacological profiles (i.e. cisplatin and carboplatin), exert their coordination to the protein through the same residues. Conversely, oxaliplatin, showing a rather different pharmacological profile, either in the reaction with lysozyme as well as in the reaction with Rnase, coordinates to the proteins in a different fashion (i.e. through a different bound fragment in different positions).
From this latter consideration, a quite clear picture results, from which important consequences may be outlined.
In fact we can suggest that differences in reactivity and adduct formation may have a more general significance and may be at the basis of the different pharmacological and toxicological profile of these three drugs. Altogether these data support previous hypotheses that metal ligands play a key role in the protein-metallodrug interactions, driving the drug-biological target recognition and stabilizing the structure of the final adduct.
It appears also very interesting, the coordination of cisplatin, carboplatin and oxaliplatin to the S-donor of amminoacidic residues, since coordination to sulfur atoms of glutathione or methionine is today recognized to have a central role in terms of toxicity as well as in drug transportation.
Mechanistic hypothesis for the binding of Pt-drugs to proteins can be formulated as in the case of oxaliplatin; it emerges quite clearly that oxaliplatin binds to the proteins through a two-step process, primarily involving a monodentate adduct formation, followed by ring opening allowing the replacement of oxalate with the carboxylate from an Asp residue. Noteworthy, the finding that cisplatin and oxaliplatin, bind to lysozyme in different sites. At least in principle, this result reflects the real possibility (already experimented in clinical trials) to administrate in combination these two drugs to overcome resistance and improve the efficiency of anticancer treatments.

In the second part of this work we have focused our attention on two strict cisplatin analogues and comparatively we have considered their solution behaviour, their reactivity with biomolecules and the cellular effects. In particular the two compounds *cis*-$PtI_2(NH_3)_2$ and *cis*-$PtBr_2(NH_3)_2$ have been synthesised.

First of all, as reported above for established platinum anticancer drugs, *cis*-$PtI_2(NH_3)_2$ has been subjected to an extensive investigation of its reactions with HEWL by X-ray crystallography and ESI-MS spectrometry. With these studies, we have provided unambiguous evidence that the diiodido analogue of cisplatin forms stable protein adducts containing a different type of protein bound metal fragment. While cisplatin typically affords protein platination through coordination of a $[Pt(NH_3)_2]^{2+}$ fragment to selected protein side-chains, *cis*-$PtI_2(NH_3)_2$ preferentially gives rise to a protein bound $[PtI_2NH_3]$ fragment with full retention of the two halide ligands. This finding is of great interest implying that the diiodido analogue produces a type of biomolecular metalation remarkably distinct from that inferred by cisplatin.

To assess whether the differences in the reactivity toward model proteins, in comparison with cisplatin, lead to some different pharmacological profile, we have deeply investigated *cis*-$PtI_2(NH_3)_2$ under chemical and biological point of view. From our studies it emerges that in contrast to the expectations and to old claims of inactivity, replacement of chloride with iodide ligands doesn't imply the loss of anticancer activity; producing cytotoxic effects comparable and often greater than those caused by cisplatin, at least in four representative cancer cell lines. Also, this complex is capable to overcome to a large extent resistance to cisplatin in a cancer cell line showing acquired resistance to cisplatin, being taken up in a far greater amount. This implies that the recognition processes for the two Pt complexes are distinct.

After these promising results we started *in vivo* studies on murine model to assess the chronic toxicity of complex. From these preclinical studies it emerges that *cis*-$PtI_2(NH_3)_2$, is well tolerated at the dose of 3.5 mg/Kg administered intraperitoneally and no evidences for lesions to spleen, liver and kidneys as well as alteration in hepatic and renal function were found. This finding, despite just a preliminary *in vivo* assessment, strongly warrants for further investigations on this complex, being now ongoing to determine crucial parameters such as CI (combination index) and others.

At variance, *cis*-$PtBr_2(NH_3)_2$ manifests a behaviour rather similar to cisplatin in terms of chemical features as well as in term of protein metalation. Cellular studies have underlined as its cytotoxic effects *in vitro* are superimposable to those of cisplatin except for leukemia FLG line where dibromido analogue is two times more effective than cisplatin. This represents an indirect confirmation that very small changes in the structures of these drugs may have an important impact in the final pharmacological effect.

In conclusion, the results here reported strongly support further investigations on iodido and dibromido derivatives drugs and their full re-evaluations as potential antineoplastic agents.
Furthermore, we can state that the approach used in this study is very efficient since permits a detailed and accurate characterisation of the interaction of metal-based anticancer drugs with model proteins. The informations derived are of great interest in order to give a full description of the adducts under structural and functional point of view. Of course, when carrying out these experiments one should never forget that just very simplified systems are analysed. Real system are profoundly different and more complicated due to the thousands of different hypothetical targets. Beside it is also necessary to consider that obtainment of important information in a cell free system, is a task of great significance and a real advantage, since the intrinsic simplicity of the system itself, make it rapid and convenient despite a full prediction of the behaviour of a drug in cell systems as well as *in vivo* is impossible.

SUPPLEMENTARY MATERIAL

SUPPLEMENTARY MATERIAL

3.1.3 Oxaliplatin vs Cisplatin: competition experiments in the binding to Lysozyme

Figure S1 Superposition of bis-adduct (brown) and atomic resolution structure of HEWL (PDB code 2VB1, yellow).

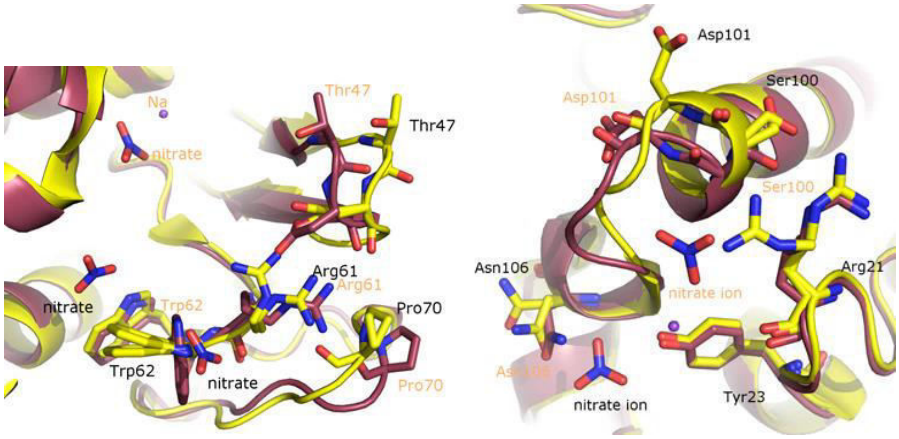

A B

Figure S2 Details of the comparison of the HEWL structure in the bis-adduct (brown) and in the and atomic resolution structure (yellow, PDB code 2VB1). Major differences are observed at the end of helix constituted by residues 88-101 and in the loop regions corresponding to residues 44-51 and 69-73. These structural variations are probably related to the differences in the position of nitrate ions on the protein surface.

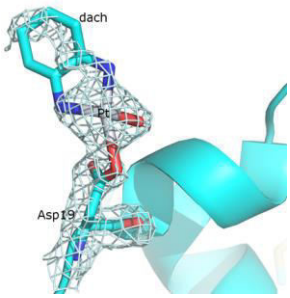

Figure S3 Oxaliplatin binding site in the second structure of bis-adduct (PDB code 4ZEE). 2Fo-Fc electron density maps are contoured at 1σ (grey) level.

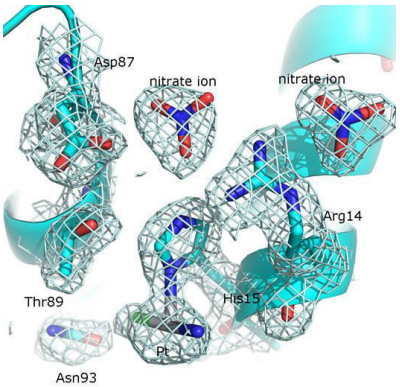

Figure S4 Cisplatin binding site in the second structure of bis-adduct (PDB code 4ZEE). 2Fo-Fc electron density maps are contoured at 1σ (grey) level.

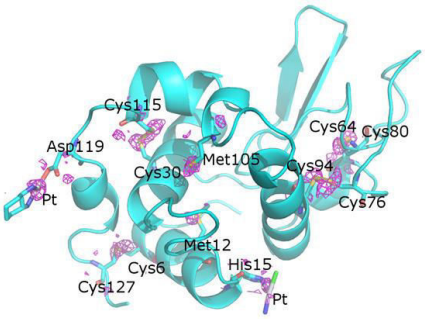

Figure S5 Anomalous difference map calculated from anomalous data collected for the second bis-adduct crystal (PDB code 4ZEE). The anomalous map is rendered in violet and contoured at 2.0 σ. The inspection of the map allows the identification of the positions of Pt and of sulphur atoms of Cys6, Met12, Cys30, Cys64, Cys76, Cys80, Cys94, Met105, Cys115 and Cys127.

Surface plasmon resonance (SPR) experiments. Real time binding assays were performed at 25 °C on a Biacore 3000 Surface Plasmon Resonance (SPR) instrument (GE Healthcare). HEWL was immobilized at 940 RU, on a CM5 Biacore sensor chip in 10 mM sodium acetate pH 5.5, by using the EDC/NHS chemistry, with a flow rate of 5 µL x min^{-1} and an injection time of 7 min. Binding assays were carried out by injecting 90 µL of analyte, at 20 µL x min^{-1}, with 20 mM sodium citrate at pH 4.4 as running-buffers. Experiments have been also carried out at pH 7.4 using HBS (10 mM Hepes, 150 mM NaCl, 3 mM EDTA, pH 7.4) as running buffer. The association phase (k_{on}) was followed for 270 s, whereas the dissociation phase (k_{off}) was followed for 300 s. The reference chip sensorgrams were opportunely subtracted to sample sensorgrams. Kinetic parameters were estimated assuming a 1:1 binding model and using version 4.1 Evaluation Software (GE Healthcare). A sequential injection experiment (by injecting first 30 µL of Oxaliplatin and then 30 µL of cisplatin at 1 mM) has been also performed using exactly the same experimental conditions of the single injection experiments. The inverse experiment where Oxaliplatin is injected after Cisplatin shows that in the short time of the experiment Oxaliplatin does not bind the preformed HEWL-Cisplatin adduct.

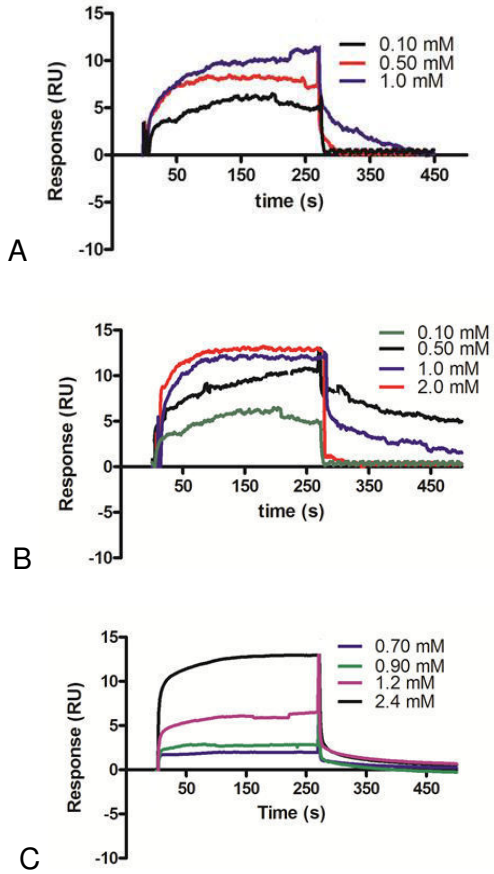

Figure S6 Overlay of sensorgrams for the interaction between Oxaliplatin (A) and Cisplatin (B) and HEWL. Experiments have been carried out at room temperature using

20 mM sodium citrate at pH 4.4 as running-buffers. In panel C, the interaction between HEWL and Cisplatin has been evaluated at room temperature using HBS (10 mM Hepes, 150 mM NaCl, 3 mM EDTA, pH 7.4) as running buffer.

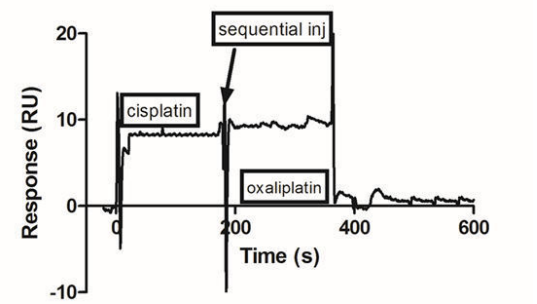

Figure S7 SPR Sensorgram for the sequential injection of Cisplatin and (then) Oxaliplatin, both at 1 mM, to immobilized HEWL in the presence of 20 mM sodium citrate buffer at pH 4.4. In the time of this experiment Oxaliplatin does not bind the preformed HEWL-Cisplatin adduct.

Circular dichroism thermal denaturation experiments. Protein thermal denaturation experiments were performed by following the circular dichroism (CD) signal at 222 nm as function of temperature for HEWL, HEWL/Cisplatin, HEWL/Oxaliplatin (protein sample was pre-incubated in the presence of the metallodrug for 24 h at room temperature) and for the bis-adduct that forms when a) HEWL is concomitantly incubated for 24 h in the presence of equal amount of Cisplatin and Oxaliplatin (HEWL/Cisplatin+Oxaliplatin), b) HEWL is first incubated for 24 h with Cisplatin and then for 24 h with Oxaliplatin (HEWL/Cisplatin then Oxaliplatin) and c) viceversa, i.e. HEWL is first incubated for 24 h with Oxaliplatin and then for 24 h with Cisplatin (HEWL/Oxaliplatin then Cisplatin). In all cases, final protein:metal ratio is 1:10 for each complex and protein concentration is about 20 µM. The experiments have been carried out at pH 4.4 (10 mM sodium acetate buffer). A Peltier temperature controller was used to set up the temperature of the sample, with a slope of 20 °C/1 hour.

4.1.1 Peculiar features in the crystal structure of the adduct between lysozyme and *cis*-$PtI_2(NH_3)_2$

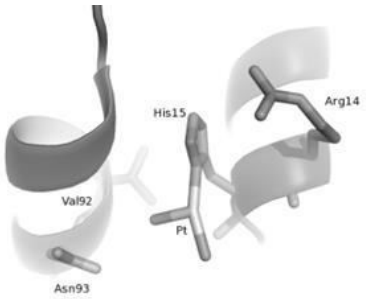

Figure S8 Scheme of cisplatin binding to HEWL at the right-handed site, as observed by Casini et al. Pt(II) has an occupancy equal to 0.3 and is bound to the nitrogens of two ammonia molecules in cisplatin.

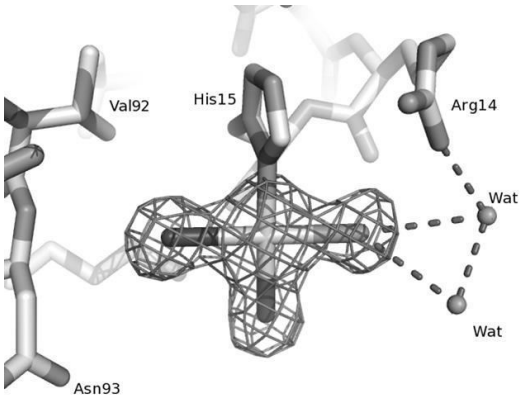

Figure S9 Anomalous electron density maps contoured at 4.0 σ in the Pt binding site, i.e. close to His15. The presence of three peaks of anomalous electron density close to Pt atom suggests the presence of two alternative mode of binding of $[PtI_2NH_3]$ moiety. For sake of clarity just one of the two different modes of binding of *cis*-$PtI_2(NH_3)_2$ to HEWL is shown.

4.1.2 Further insight into antineoplastic properties of *cis*-$PtI_2(NH_3)_2$

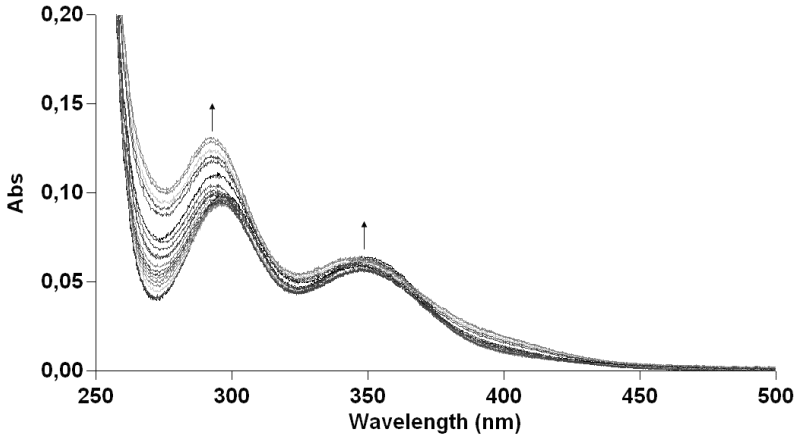

Figure S10 UV-Vis spectrum of complex cis-$Pt(NH_3)_2I_2$ 10^{-4} M with 10^{-3} M KI in 50 mM phosphate buffer (pH=7.4) followed for 72 h.

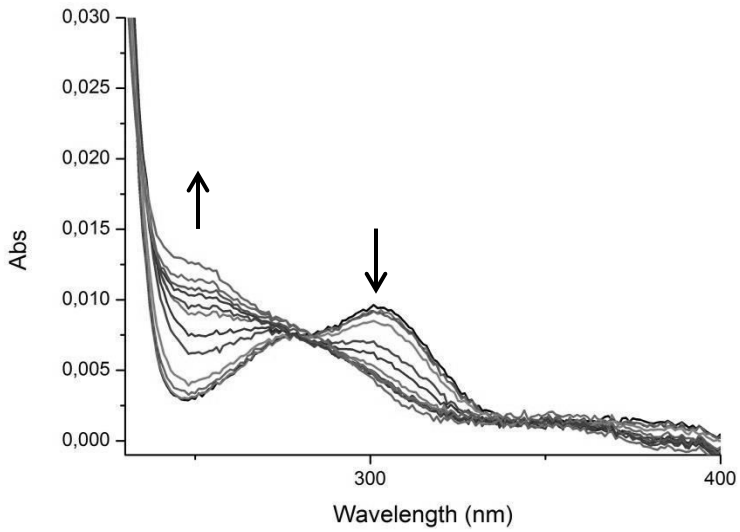

Figure S11 Time dependent UV-Vis spectrum of cisplatin 10^{-4} M buffer phosphate 50 mM pH=7.4 recorded for 72 h at RT.

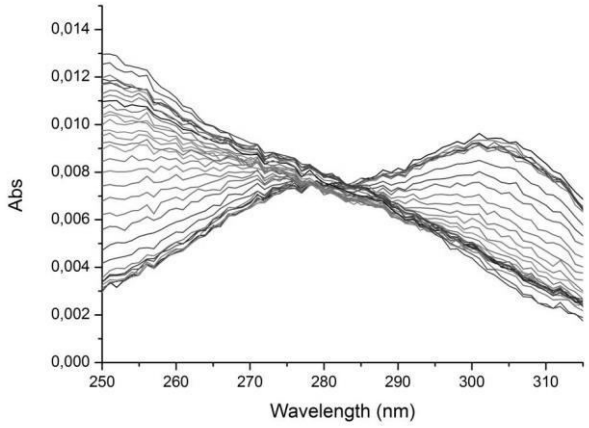

Figure S12 Time dependent UV-Vis spectrum of cisplatin 10^{-4} M buffer phosphate 50 mM pH=7.4 recorded for 72 h at RT. isosbestic points of the two complexes (285 nm for cisplatin and 284 $cisPtI_2$), drift during the analysis, this is the evidence that allows us to hypothesize a biphasic reaction with two very close rate constants.[1]

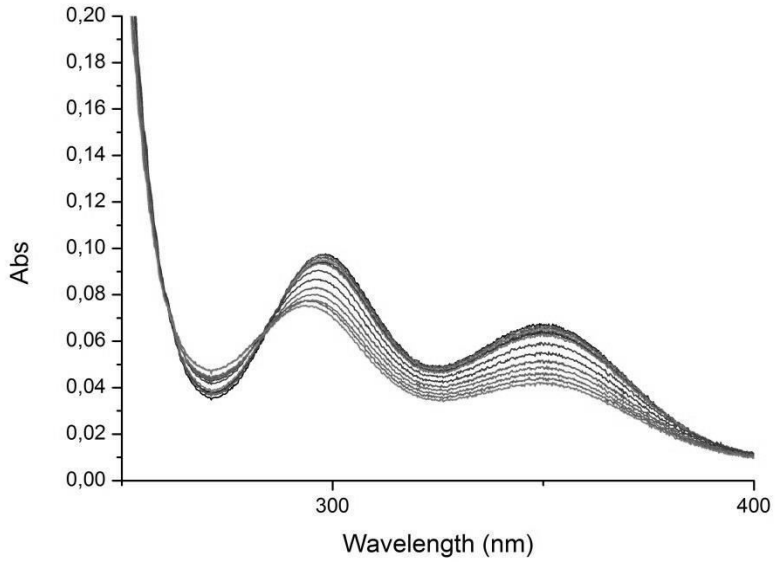

Figure S13 Detail on isosbestic point for time dependent UV-Vis spectrum of $cisPtI_2$ 10^{-4}M buffer phosphate 50 mM pH=7.4 recorded for 72 h at RT.

Final products analysis. we have considered as final UV-Vis spectrum the spectral profile recorded after 72 h, since after this time there are no evidences for changes in absorbance within the investigated range (200-800 nm). For both complexes, there are evidences of existence of the same species characterised by two absorption bands at 285 and 350 nm, as result from deconvoluted spectral profiles. The relative differences existing between DFT calculation and experimental spectral profiles may be assignable to various equilibria determined by pH value. Acid dissociation constants for coordinated water molecules in products cis-$[PtCl(H_2O)(NH_3)]^+$, cis-$[Pt(H_2O)_2(NH_3)_2]^{2+}$ and cis-$[Pt(H_2O)(OH)(NH_3)_2]^+$ are 6.41; 5.37; 7.21 and using buffered solution at pH=7.4 it is reasonable to hypothesise a series of equilibria that produce different species (i.e. hydroxo species) in different ratio.[2] In a similar manner same process are likely involved in the hydrolysis of cisPtI_2.

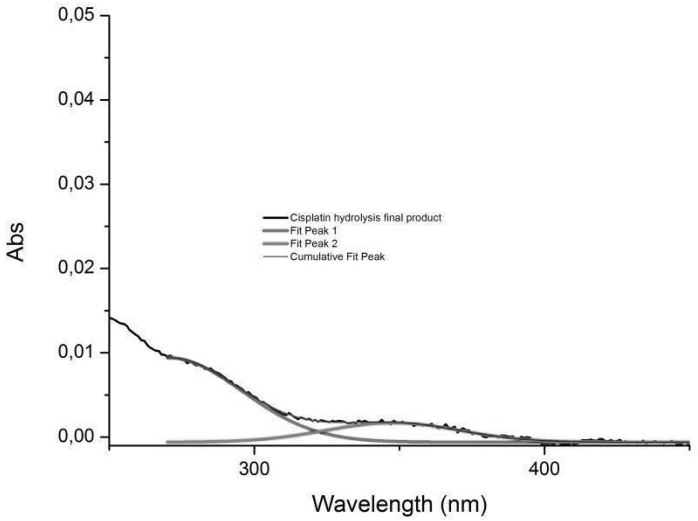

Figure S14 Detail on deconvolution of final product spectral profile for time dependent UV-Vis spectrum of cisplatin 10^{-4}M buffer phosphate 50 mM pH=7.4 recorded for 72 h at RT.

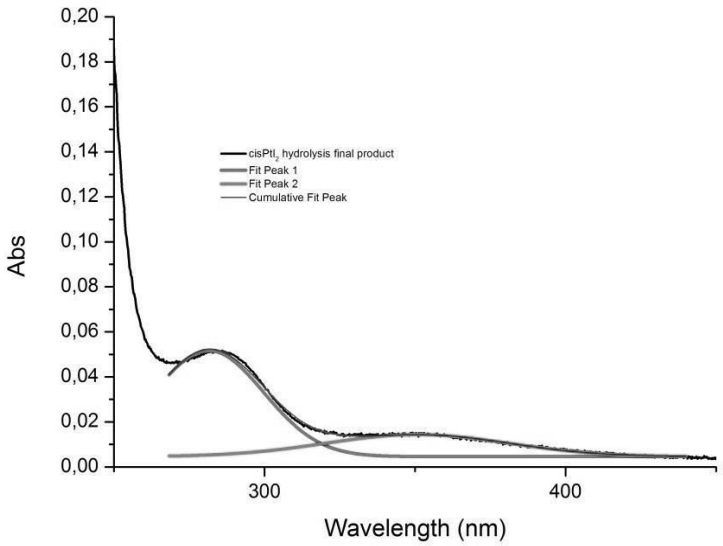

Figure S15 Detail on deconvolution of final product spectral profile for time dependent UV-Vis spectrum of $cisPtI_2$ 10^{-4}M buffer phosphate 50 mM pH=7.4 recorded for 72 h at RT.

Pseudo first-order rate constant calculation. According to Miller et al.,[1] it is possible to analyse these experimental time dependent spectral profiles treating the hydrolysis process as a pseudo-first order reaction. Calculations were done plotting the variation of absorbance as function of time for both $cisPtI_2$ and cisplatin respectively monitoring the maxima at 350 and 305 nm.

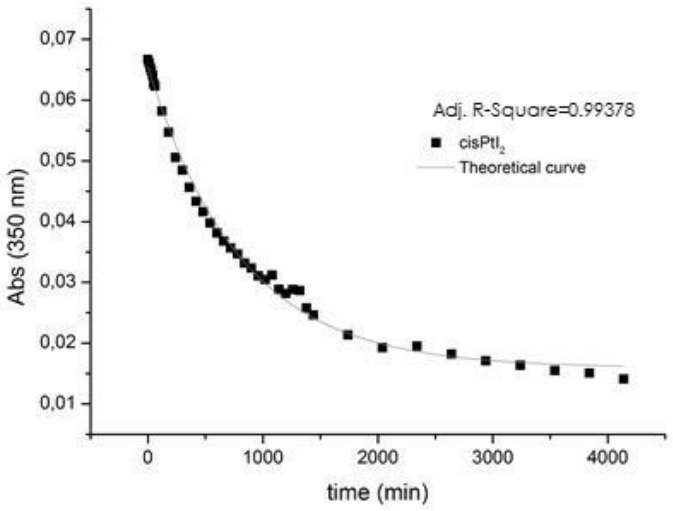

Figure S16 Experimental kinetic traces and calculated theoretical curve for the hydrolysis of $cisPtI_2$. k_{obs} were calculated fitting with a single exponential function.

	k_{obs} (s^{-1}) [1/t]	$t_{1/2}$ (min) [t*ln(2)]
cisplatin	**$2,96*10^{-5}$**	**395±66**
***cis*PtI_2**	**$1,77*10^{-5}$**	**639±11**

Table S1 K_{obs} and $t_{1/2}$ values determined fitting with a single exponential function.

ESI-MS experiment. cis-$Pt(NH_3)_2I_2$ was solubilized in ammonium acetate buffer pH= 4.5, and ESI-MS spectra were recorded by direct introduction at 5 µl/min flow rate in an Orbitrap high-resolution mass spectrometer (Thermo, San Jose, CA, USA), equipped with a conventional ESI source. The working conditions were the following: spray voltage 3.1 kV, capillary voltage 45 V, capillary temperature 220°C, tube lens voltage 230 V. The sheath and the auxiliary gases were set, respectively, at 17 (arbitrary units) and 1 (arbitrary units). For acquisition, Xcalibur 2.0. software (Thermo) was used and monoisotopic and average deconvoluted masses were obtained by using the integrated Xtract tool. For spectrum acquisition a nominal resolution (at m/z 400) of 100,000 was used.

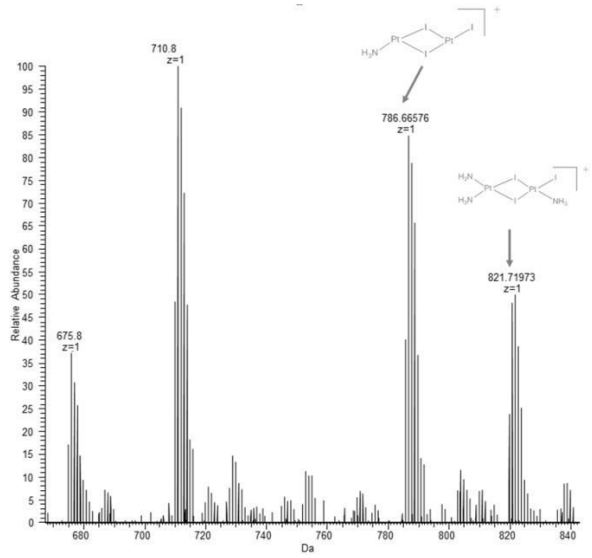

Figure S17 ESI-MS spectrum of complex cis-$Pt(NH_3)_2I_2$ 10^{-4} M in 20 mM ammonium acetate buffer (pH=4.5).

DNA interstrand cross-linking in the linear pUC19 DNA (linearized with EcoRI restriction enzyme). In order to quantitate the interstrand cross-linking efficiency of cis-$PtI_2(NH_3)_2$ the above reported linearized plasmid DNA was 3´-end-labeled and modified by the cis-$PtI_2(NH_3)$ or cisplatin at various r_b values. The samples were analyzed for the interstrand cross-links (CLs) by agarose gel electrophoresis under denaturing conditions.[3] Upon electrophoresis, 3′-end labeled strands of the linear fragment containing no interstrand CLs migrate as a 2686-base single strand, whereas the interstrand cross-linked strands migrate more slowly as a higher molecular mass species (Figure S18). The intensity of the more slowly migrating band increased with the growing level of the modification. The radioactivity associated with the individual bands in each lane was measured to obtain estimates of the fraction of noncross-linked or cross-linked DNA under each condition. The frequency of interstrand CLs was calculated using the Poisson distribution from the fraction of interstrand cross-linked DNA in combination with the r_b values and the fragment size.[4]

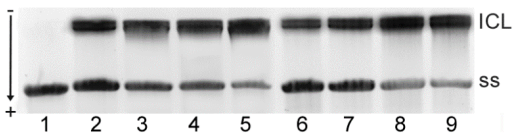

Figure S18 Formation of interstrand cross-links. Interstrand cross-linking by cis-$PtI_2(NH_3)_2$ and cisplatin in the linear pUC19 plasmid DNA. Autoradiogram of denaturing 1% agarose gels of linearized DNA which was 3′-end labeled. The interstrand cross-linked DNA appears as the top bands migrating on the gel more slowly than the single-stranded DNA (contained in the bottom bands). Lanes: 1, control, unplatinated DNA; 2-5, DNA modified

by cisplatin; 6-9, DNA modified by cis-$PtI_2(NH_3)_2$. r_b values: 0.0003 (lanes 2 and 6); 0.0005 (lanes 3 and 7); 0.0007(lanes 4 and 8); 0.001 (lanes 5 and 9).

DNA unwinding. Native agarose electrophoresis is used to determine the unwinding induced in negatively supercoiled plasmid DNA by monitoring the degree of supercoiling.[5] A compound that unwinds the DNA duplex reduces the number of supercoils in closed circular DNA. This decrease causes a decrease in the rate of migration through agarose gel, which makes it possible to observe and quantify the mean value of unwinding per adduct. Figure S19 shows electrophoresis gels from experiments in which different amount of *cis*-[$PtI_2(NH_3)_2$] was bound to a mixture of relaxed and negatively supercoiled pSP73KB. Interestingly, both complexes increased the mobility of the relaxed form similarly as does cisplatin, whose bifunctional binding to DNA shortens and condenses the DNA helix.[6,7] The mean unwinding angle is given by $\Phi = -18\sigma/r_b(c)$, where σ is the superhelical density and $r_b(c)$ is the value of r_b at which the supercoiled and nicked forms comigrate.[5] Under the present experimental conditions, the value for σ of plasmid DNA used in these experiments was calculated to be -0.072 on the basis of the data of cisplatin for which the $r_b(c)$ was determined in this study and $\Phi = 13°$ was assumed.[5]

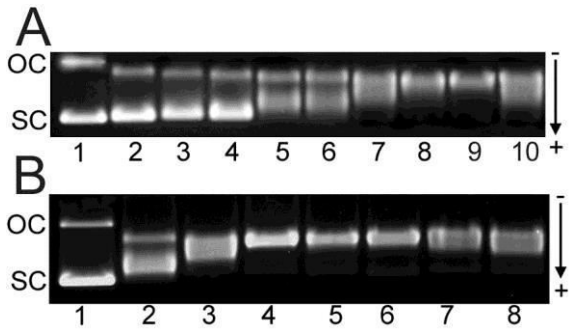

Figure S19 Unwinding of negatively supercoiled pSP73KB plasmid DNA by platinum complexes. The top bands (oc) correspond to nicked plasmid and the bottom bands (sc) correspond to the closed, negatively supercoiled plasmid. A) Cisplatin. Lanes: 1, control, nonmodified DNA, 2–10 rb = 0.03, 0.04, 0.05, 0.06, 0.07, 0.08, 0.09,0.11, respectively. B) *cis*-PtI2(NH3)2. Lanes: 1, control, nonmodified DNA, 2–8 rb = 0.05, 0.07, 0.09, 0.1, 0.12, 0.14, 0.16, respectively.

5.1.1 Cisplatin and its dibromido analogue: a comparison of chemical and biological profiles

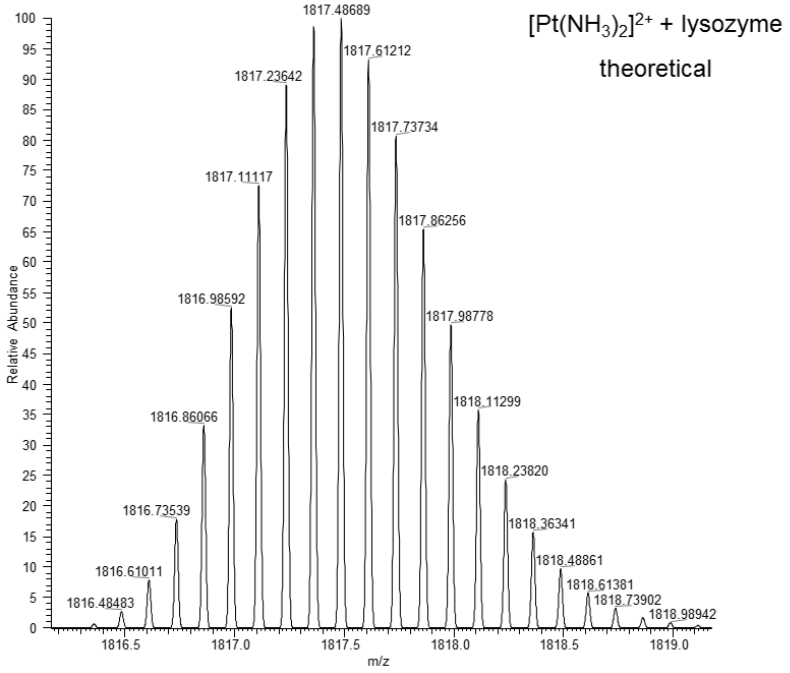

A

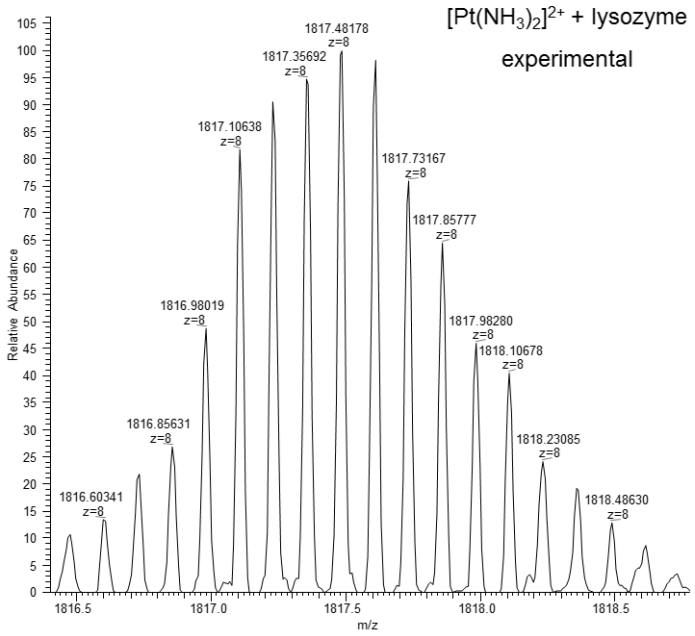

A

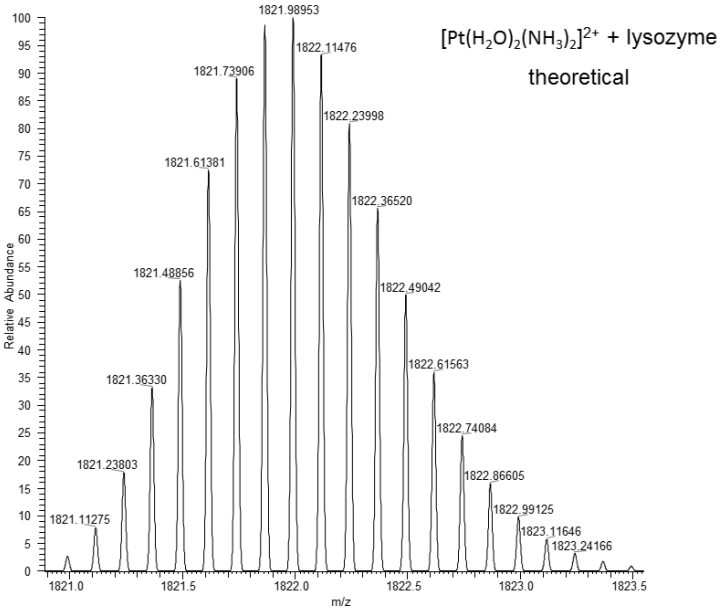
$[Pt(H_2O)_2(NH_3)_2]^{2+}$ + lysozyme
theoretical
1821.98953
1822.11476
1821.73906
1822.23998
1821.61381
1822.36520
1821.48856
1822.49042
1822.61563
1821.36330
1822.74084
1821.23803
1822.86605
1822.99125
1821.11275
1823.11646
1823.24166
Relative Abundance
m/z
1821.0
1821.5
1822.0
1822.5
1823.0
1823.5

B

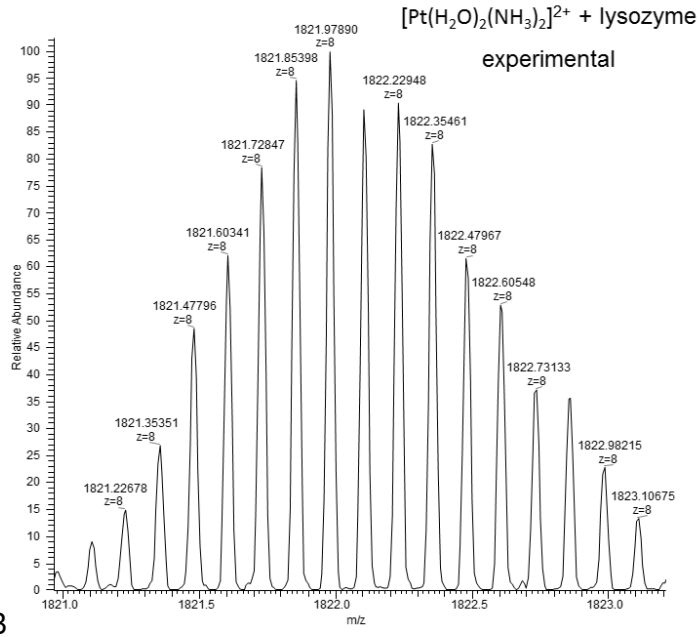
$[Pt(H_2O)_2(NH_3)_2]^{2+}$ + lysozyme
experimental
1821.97890 z=8
1821.85398 z=8
1822.22948 z=8
1822.35461 z=8
1821.72847 z=8
1821.60341 z=8
1822.47967 z=8
1822.60548 z=8
1821.47796 z=8
1822.73133 z=8
1821.35351 z=8
1822.98215 z=8
1821.22678 z=8
1823.10675 z=8
Relative Abundance
m/z
1821.0
1821.5
1822.0
1822.5
1823.0

B

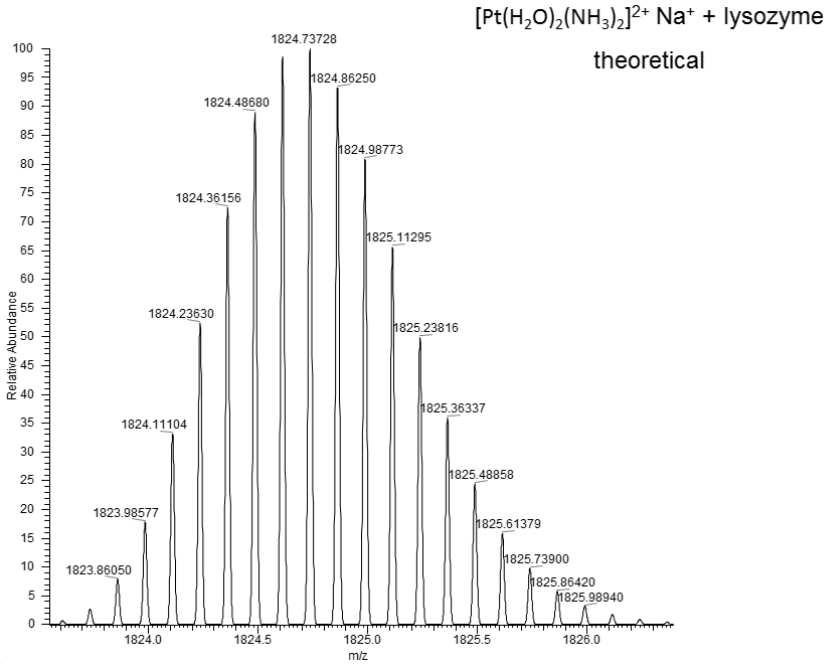
$[Pt(H_2O)_2(NH_3)_2]^{2+}$ Na^+ + lysozyme
theoretical
1824.73728
1824.86250
1824.48680
1824.98773
1824.36156
1825.11295
1824.23630
1825.23816
1825.36337
1824.11104
1825.48858
1823.98577
1825.61379
1825.73900
1823.86050
1825.86420
1825.98940
Relative Abundance
m/z

C

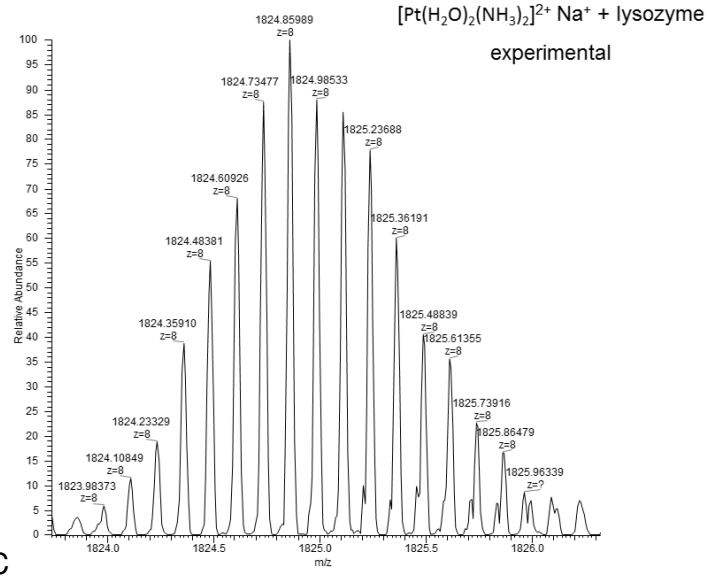
$[Pt(H_2O)_2(NH_3)_2]^{2+}$ Na^+ + lysozyme
experimental
1824.85989 z=8
1824.73477 z=8
1824.98533 z=8
1825.23688 z=8
1824.60926 z=8
1825.36191 z=8
1824.48381 z=8
1825.48839 z=8
1824.35910 z=8
1825.61355 z=8
1825.73916 z=8
1824.23329 z=8
1825.86479 z=8
1824.10849 z=8
1825.96339 z=?
1823.98373 z=8
Relative Abundance
m/z

C

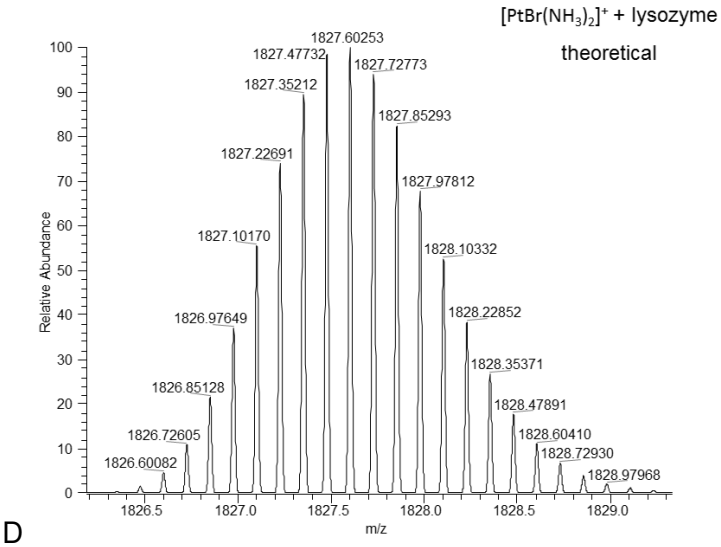

D

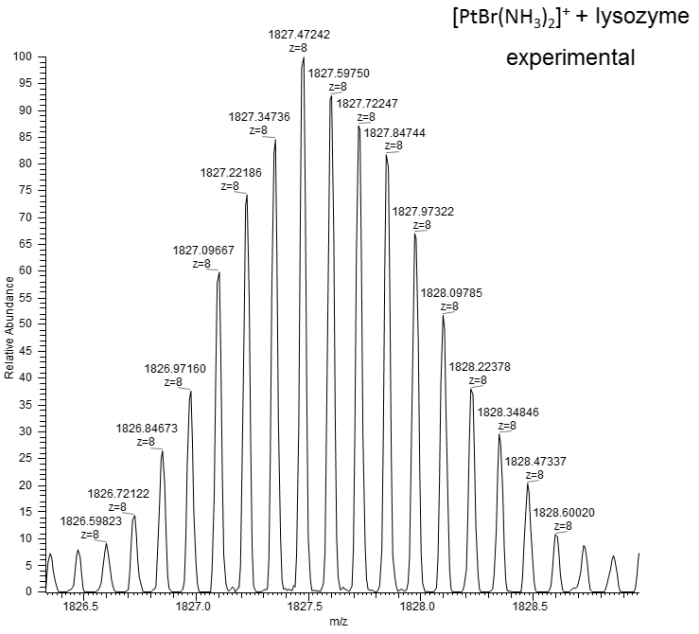

D

Figure S20 Comparison between experimental and theoretical peaks for the main adducts.

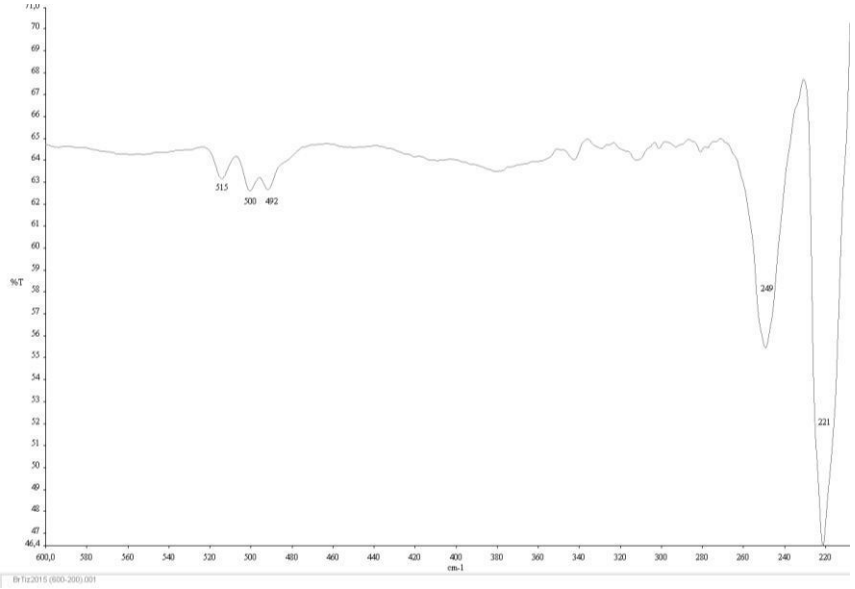

Figure S21 IR of the compound cis-$PtBr_2(NH_3)_2$ from 600 to 200 cm^{-1}.

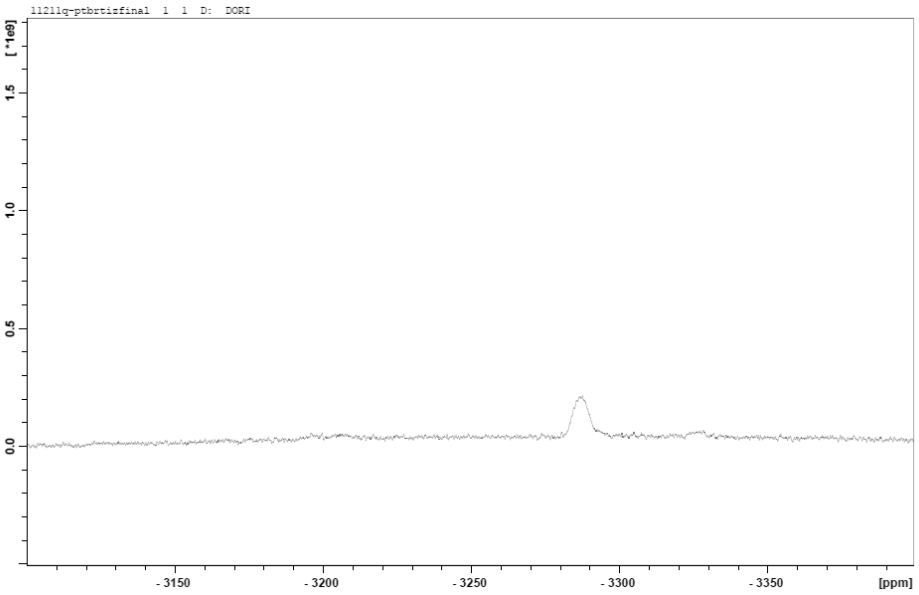

Figure S22 ^{195}Pt NMR of the compound cis-$PtBr_2(NH_3)_2$ in DMSO.

.

References

[1] Miller S.E., House D.A. *ICA,***1989**, *166, 189-197*.
[2] Berners-Price S.J., Appleton T.G. (**2000**) *The chemistry of Cisplatin in Aqueous solution*. In Platinum-based drugs in cancer therapy, Humana Press Inc., Totowa, NJ,pp. 3-35.
[3] Brabec V., Leng M., Proc. Natl. Acad. Sci USA, **1993**, 90, 5345-5349.
[4] Farrel N., Qu Y., Feng L., Van Houten B. Biochemistry, **1990**, 29, 9522-9531.
[5] Keck M.V., Lippard S.J. JACS, **1992**, 114, 3386-3390.
[6] Cohen G. L., Bauer W. R., Barton J. K. and Lippard S. J. Science,**1979**, *203*, 1014-1016.
[7] Scovell W. M., and Collart F. Nucleic Acids Res., **1985**, *13*, 2881-2895.